ERDC/CRREL TR-19-17

Cold Regions Research and Engineering Laboratory

US Army Corps of Engineers®
Engineer Research and Development Center

ERDC
ENGINEER RESEARCH & DEVELOPMENT CENTER

ERDC 6.2 Boreal Aspects of Ensured Maneuver (BAEM)

Assessment of Field Methods for Measuring Mechanical Properties of Snow

Sally A. Shoop, Wendy L. Wieder, Bruce C. Elder,
Samuel A. Beal, and Elias J. Deeb

August 2019



Approved for public release; distribution is unlimited.

The U.S. Army Engineer Research and Development Center (ERDC) solves the nation's toughest engineering and environmental challenges. ERDC develops innovative solutions in civil and military engineering, geospatial sciences, water resources, and environmental sciences for the Army, the Department of Defense, civilian agencies, and our nation's public good. Find out more at www.erdc.usace.army.mil.

To search for other technical reports published by ERDC, visit the ERDC online library at http://acwc.sdp.sirsi.net/client/default.

ERDC/CRREL TR-19-17
August 2019

Assessment of Field Methods for Measuring Mechanical Properties of Snow

Sally A. Shoop, Wendy L. Wieder, Bruce C. Elder, Samuel A. Beal, and Elias J. Deeb

U.S. Army Engineer Research and Development Center (ERDC)
Cold Regions Research and Engineering Laboratory (CRREL)
72 Lyme Road
Hanover, NH 03755-1290

Final Report

Approved for public release; distribution is unlimited.

Prepared for Assistant Secretary of the Army for Acquisition, Logistics, and Technology
103 Army Pentagon
Washington, DC 20314-1000

Under Project 465395, ERDC 6.2 “Boreal Aspects of Ensured Maneuver (BAEM)” and Project 471941, “Remote Assessment of Snow Mechanical Properties” and “Mobility in Peat and Northern Soils”

Abstract

Winter climates present a variety of surfaces that challenge vehicle mobility. Surfaces range from soft, virgin snow, to groomed snow and ice. This study evaluated the capabilities of various testing devices to measure the mechanical properties of winter surfaces. Concurrent satellite imagery supplemented in situ physical testing. The goals were (1) to find tests that most practically evaluate these winter surfaces for vehicle mobility and (2) to determine if imagery analysis correlates with mechanical properties, thus potentially allowing remote assessment of snow physical and mechanical characteristics.

The test methods were typically useful for either virgin snow or groomed snow; no method worked well on all surfaces. Correlations between test devices were generally poor, but there were some important trends identified between (1) tests that measure the near-surface snow strength, (2) tests best suited for stronger snow, (3) the Clegg Impact Hammers and California Bearing Ratio, and (4) the optical imagery and surface drop cones. This study provides a rich dataset for assessing the current state of the art and future research needs for measurement and remote assessment of snow mechanical properties for vehicle mobility prediction.

DISCLAIMER: The contents of this report are not to be used for advertising, publication, or promotional purposes. Citation of trade names does not constitute an official endorsement or approval of the use of such commercial products. All product names and trademarks cited are the property of their respective owners. The findings of this report are not to be construed as an official Department of the Army position unless so designated by other authorized documents.

DESTROY THIS REPORT WHEN NO LONGER NEEDED. DO NOT RETURN IT TO THE ORIGINATOR.

Contents

Abstract ii

Figures and Tables v

Preface x

Acronyms and Abbreviations xi

Unit Conversion Factors xiii

1 Introduction 1

1.1 Background 1
1.2 Objectives 1
1.3 Approach 1

2 Field Sites 3

2.1 Montana 3
2.2 Michigan 4
2.3 Test-point discussion 5

3 Data Collection 15

3.1 Mechanical measurements for groomed snow 16
3.1.1 Field California Bearing Ratio (CBR) 16
3.1.2 Cleggs 18
3.1.3 Light Weight Deflectometer (LWD) 19
3.1.4 Russian Snow Penetrometer 20
3.1.5 CTI 21
3.1.6 Micro tools 22
3.2 Mechanical measurement for soft snow 23
3.2.1 Rammsonde 23
3.2.2 SnowMicroPenetrometer 25
3.2.3 Yamaha drop cone 25
3.2.4 MagnaProbe 26
3.2.5 Plate sinkage 27
3.3 Additional physical and optical measurements 28
3.3.1 Air and snow temperatures 28
3.3.2 Snow density 28
3.3.3 Denoth meter 30
3.3.4 Finnish snow fork 30
3.3.5 NIR photography 30
3.3.6 GPR 30
3.3.7 Nadir spectral reflectance 31
3.3.8 Satellite imagery 32
3.4 Data analysis 33

4 Results and Discussion 35
4.1 General site conditions 35
4.2 Snow-strength measurement techniques 37
4.2.1 Snow-strength profile data 43
4.2.2 Strength of groomed snow surfaces 44
4.2.3 Correlation between strength measurements 47
4.3 Spectral measurements 50
4.3.1 WV2 and WV3 satellite imagery 50
4.3.2 Satellite TSX imagery 54
4.3.3 ASD field-measured reflectance 54
4.4 Comparison of strength measurements with spectra data 59

5 Conclusions and Recommendations for Future Work 60

References 64

Appendix A: Additional Site Imagery 68

Appendix B: Michigan Ground-Surface Photos 73

Appendix C: Snow Pit and Weather Data 88

Appendix D: Summary of Snow Measurements by Site 104

Appendix E: Comparison of Snow Moisture and Density Measurement Techniques (Student Intern Poster) 118

Appendix F: WV2 and WV3 Data Concurrent with Michigan Field Campaign 120

Appendix G: Surface-Condition Photos and Michigan Cloud-Cover Photos for Field Spectrometer (ASD) Data Collection 124

Report Documentation Page

Figures and Tables

Figures

1 Montana test site at West Yellowstone Airport 10
2 Montana test points superimposed over winter imagery taken during the field campaign 11
3 Schematic of the Michigan test site 12
4 Michigan test points superimposed on imagery from summer to show to show ground surfaces 13
5 Michigan test points superimposed on winter imagery 14
6 Field CBR test setup in Michigan 17
7 The 0.5 kg Clegg 18
8 The LWD 20
9 RSP in use in Michigan 21
10 CTI test in Michigan 22
11 Ram testing in Michigan 24
12 Yamaha drop cone in use in Michigan 26
13 Yamaha drop cone schematic and specifications 26
14 Snow MagnaProbe 27
15 Plate sinkage test in Michigan 28
16 Snow-density-sample extraction in a snow pit 29
17 Snow-density test using the aluminum cylinder in Michigan 29
18 ASD taking a datum measurement in Michigan 31
19 Snow depth and type by site in Michigan 35
20 Snow depth by site in Montana 35
21 Finnish fork density and moisture compared to sample density and Denoth moisture in different snow pits 36
22 NIR photo (*top*) and standard photo (*bottom*) of Montana snow pits walls 37
23 Boxplots of each snow-strength measurement technique by study area for the Michigan site 39
24 Boxplots of each snow-strength measurement technique by study area at the Montana site 40
25 Boxplots of each snow-strength measurement technique by surface type in Michigan. The *p*-values are for Kruskal-Wallis analysis of variance 41
26 Boxplots of each snow-strength measurement technique by surface type for Montana. The *p*-values are for Kruskal-Wallis analysis of variance 41
27 RSP hardness profiles from Michigan 43
28 SMP profile from virgin snow in Montana 44
29 Measured CBR by site in Michigan 45
30 Measured CBR by site in Montana 45
31 Mean site surface CBR calculated from 2.25 kg Clegg Impact Values in

Michigan. Error bars are ± one standard deviation 46
32 Mean site surface CBR calculated from 2.25 kg Clegg Impact Values in Montana. Error bars are ± one standard deviation....46
33 Spearman correlation matrix of measured snow properties with $n > 1$ comparative observations. LWD ISM values listed are representative (averages are nearly identical). The p-values are indicated as * < 0.1, ** < 0.05, and *** < 0.01....48
34 CIV versus field CBR 49
35 CTI versus 0.5 kg Clegg CIV 49
36 RSP versus 2.25 kg Clegg CIV....50
37 WV2/WV3 reflectance spectra for each Michigan study area. Each line represents a site. The colors relate to the type of surface....52
38 Michigan WorldView reflectance spectra averaged by surface type 54
39 ASD field spectrometer reflectance subsampled into the eight WV2 bands for asphalt, groomed snow, ice, and virgin snow surfaces in Michigan 55
40 Michigan ASD field spectrometer reflectance subsampled into the WV3 bands. *Red lines* are for asphalt, *purple* for ice, *blue* for groomed snow, and *green* for virgin snow. The panchromatic band is 450 to 800 nm....56
41 Full spectra of the Michigan ASD reflectance from the virgin snow measurements....57
42 Michigan ASD field spectrometer reflectance values for asphalt (*red*), ice (*purple*), groomed snow (*blue*), and virgin snow (*green*) surfaces....58
43 Michigan ASD field spectrometer reflectance values for 800–1200 nm, for asphalt (*red*), ice (*purple*), groomed snow (*blue*), and virgin snow (*green*) surfaces....58
44 Michigan groomed snow (*red*) falls within the scatter of the undisturbed snow (*various greens*) 59
45 Plots of significant ($p < 0.01$) Spearman correlations between Michigan WV2 MS1 spectral band (400–450 nm) and snow strength measured with the CTI and Yamaha drop cone 59
A-1 West Yellowstone Airport central runway, taxiway, and ice lane test points as they relate to the airport pavement surfaces 68
A-2 Michigan Spin Up Pads 1 and 2 test points....68
A-3 Michigan Spin Up Pads 1 and 2 test points winter imagery....69
A-4 Michigan Spin Up Pad 3, Loop 1, Vehicle Dynamics Area 2, and the 900 and 300 ft circles test points 69
A-5 Michigan Spin Up Pad 3, Loop 1, Vehicle Dynamics Area 2, and the 900 and 300 ft circles test points winter imagery 70
A-6 Michigan Ice Rink and Sweeper parking pad test points....70
A-7 Michigan Ice Rink and Sweeper parking pad test points winter imagery....71
A-8 Michigan Loop 3, Stability Area, and Loop 4 test points....71
A-9 Michigan Loop 3, Stability Area, and Loop 4 test points winter imagery....72
B-1 Spin Up Pad 2 (points 19SU2_A through F, 21SU2, 22SU2). Note that the *bottom* photo looks out into the wooded area of points 19SU2VS_A through E....73

B-2 Loop 1 washed gravel road (points 20LP1WG_1 through 3) 74
B-3 Loop 1 grass-surfaced road (points 20LP1GS_4 through 6) 75
B-4 Gravel pad (points 20GPVS and 21GPVS) 76
B-5 Sweeper parking pad (points 21SPW_1 through 3) 77
B-6 Ice slope: entire slope (*top*), steep slope area (*middle*) (point 21IS_S), and lower slope area (*bottom*) (point 21IS_L) 78
B-7 Spin Up Pad 1 (points 21SU1_1 and 2) 79
B-8 Gravel road adjacent to the gravel pad, part of Loop 1 (point 22GPRD_1 and 2) 80
B-9 Spin Up Pad 3 (points SU3_1 through 3) 81
B-10 Terrain north of Spin Up Pad 3 (points 22SU3VS_1 through 6) 82
B-11 Ice Rink area (points 22IR_S and 22IR_I) 83
B-12 Stability Test Area (points 22STAB_S and 22SATB_GI) 84
B-13 Vehicle Dynamics Area 2 (points 22VDA2_1 and 2) 85
B-14 Loop 4 (point 22LP4) 86
B-15 Terrain off Loop 4 (point 22LP4VS) 87
C-1 Snow-pit density, temperature, and snow moisture profiles for the two snow pits at Montana test point 27RWYS, 27 January 2018 89
C-2 Snow-pit density, temperature, and snow moisture profiles for the snow pit at Montana test point 27TWYS, 27 January 2018 90
C-3 Snow-pit density, temperature, and snow moisture profiles for the snow pit at Montana test point 28MLPW, 28 January 2018 90
C-4 Snow-pit density, temperature, and snow moisture profiles for the snow pit at Montana test point 27TWYS, 29 January 2018 91
C-5 Snow-pit density, temperature, and snow moisture profiles for the snow pit at Montana test point 27RWYS, 29 January 2018 91
C-6 Snow-pit density, temperature, and snow moisture profiles for the snow pit at Montana test point 27RWYS, 30 January 2018 92
C-7 Snow-pit density, temperature, and snow moisture profiles for the snow pit at Montana test point 30MLPN, 30 January 2018 92
C-8 Snow-pit density, temperature, and snow moisture profiles for the snow pit at Montana test point 27RWYS, 31 January 2018 93
C-9 Snow-pit density, temperature, and snow moisture profiles for the snow pit at Michigan test point 19SU2VS_A, 19 February 2018 93
C-10 Snow-pit density, temperature, and snow moisture profiles for the snow pit at Michigan test point 19SU2VS_E, 19 February 2018 94
C-11 Snow-pit density, temperature, and snow moisture profiles for the snow pit at Michigan test point 20GPVS, 20 February 2018 94
C-12 Snow-pit density, temperature, and snow moisture profiles for the snow pit at Michigan test point 21IS_S, 21 February 2018 95
C-13 Snow-pit density, temperature, and snow moisture profiles for the snow pit at Michigan test point 21IS_L, 21 February 2018 95
C-14 Snow-pit density, temperature, and snow moisture profiles for the snow pit at Michigan test point 22SU3VS, 21 February 2018 96

C-15 Snow-pit density, temperature, and snow moisture profiles for the snow pit at Michigan test point 23HQP, 23 February 2018 96
C-16 Montana meteorological data for 24 January 2018 97
C-17 Montana meteorological data for 25 January 2018 97
C-18 Montana meteorological data for 26 January 2018 98
C-19 Montana meteorological data for 27 January 2018 98
C-20 Montana meteorological data for 28 January 2018 99
C-21 Montana meteorological data for 29 January 2018 99
C-22 Montana meteorological data for 30 January 2018 100
C-23 Montana meteorological data for 31 January 2018 100
C-24 Michigan meteorological data for 18 February 2018 101
C-25 Michigan meteorological data for 19 February 2018 101
C-26 Michigan meteorological data for 20 February 2018 102
C-27 Michigan meteorological data for 21 February 2018 102
C-28 Michigan meteorological data for 22 February 2018 103
C-29 Michigan meteorological data for 23 February 2018 103
F-1 WorldView-2 reflectance spectra averaged by study area 120
F-2 WorldView-2 reflectance spectra averaged by subgrade 120
F-3 WorldView-3 reflectance spectra averaged by study area 121
F-4 WorldView-3 reflectance spectra averaged by snow surface type 121
F-5 WorldView-3 reflectance spectra averaged by subgrade 121
F-6 Plots of significant ($p < 0.01$) Spearman correlations between WorldView-2 multispectral bands (MS1–MS8) and snow strength measurements, with linear regression models (Michigan data set) 123
G-1 Montana ice lane (Montana point 28IL) 124
G-2 Asphalt concrete pavement at Ice Rink (Michigan point 22IR_AC) both wet and dry conditions 125
G-3 Michigan groomed snow points 22SU3 (*top*) and 22SU2 (*bottom*) 126
G-4 Michigan smooth ice surface point 22IR_I (*top*) and grooved ice surface point 22STAB_GI (*bottom*) 127
G-5 Michigan rutted snow surface point 22900C (*top*) and tracked snow surface point 22LP3NW (*bottom*) 128
G-6 Michigan virgin snow points 22SU3VS (*top*) and 22300CVS (*bottom*) 129
G-7 Cirrostratus cloud cover at the beginning of ASD testing (9:43 local time) 130
G-8 Cirrostratus and altostratus cloud cover at noon during ASD testing 130
G-9 Altocumulus cloud cover at the end ASD testing (~16:30 local time) 131

Tables

1 Testing times 4
2 Summary of Montana BAEM test points from winter 2018 6
3 Summary of Michigan BAEM test points from winter 2018 7
4 WV3 sensing bandwidths (DigitalGlobe 2012, 2014) 32

5 List of snow characterization parameters used in this study 34
6 Effectiveness matrix of field tests as rated by operators (1 = good, 5 = bad) 42
D-1 Montana snow data summary 105
D-2 Michigan snow data summary 106
D-3 Montana Clegg data 108
D-4 Michigan Clegg data 109
D-5 Montana Rammsonde data 112
D-6 Michigan Rammsonde data 113
D-7 Additional Michigan Rammsonde data 114
D-8 Montana Russian Snow Penetrometer data 115
D-9 Michigan Russian Snow Penetrometer data 115
D-10 Additional Michigan Russian Snow Penetrometer data 116
D-11 Further Michigan Russian Snow Penetrometer data 117
F-1 Spearman correlations between WorldView-2 multispectral bands and snow mechanical measurements (Michigan). The *p*-values are indicated as * <0.05, ** <0.01, and *** <0.001 122

Preface

This study was conducted for the Assistant Secretary of the Army for Acquisition, Logistics, and Technology under project number 465395, "Boreal Aspects of Ensured Maneuver (BAEM)," which is part of the U.S. Army Engineer Research and Development Center (ERDC) 6.2 Remote Assessment of Infrastructure for Ensured Maneuver (RAFTER) Program managed by Ms. Danielle Whitlow, ERDC Geotechnical and Structures Laboratory (GSL). This work is continuing under project number 471941, "Remote Assessment of Snow Mechanical Properties" and "Mobility in Peat and Northern Soils," under the Entry and Sustainment in Complex Contested Environments Program managed by Dr. John Rushing, GSL.

The work was performed by Force Projection and Sustainment Branch (CEERD-RRH), the Terrestrial and Cryospheric Sciences Branch (CEERD-RRG), and the Biogeochemical Sciences Branch (CEERD-RRN) of the Research and Engineering Division (CEERD-RR) and the Lidar and Wetlands Group of the Remote Sensing / Geographic Information Systems Center of Expertise (CEERD-RS), U.S. Army Engineer Research and Development Center, Cold Regions Research and Engineering Laboratory (ERDC-CRREL). At the time of publication, Mr. Justin Putnam was Acting Chief, CEERD-RRH; Dr. John Weatherly was Chief, CEERD-RRG; Dr. Justin Berman was Chief, CEERD-RRN; Dr. Elias Deeb was lead for the Lidar and Wetlands Group; Mr. Jared Oren was Acting Chief, CEERD-RR; and Mr. David Finnegan was Chief, CEERD-RS. The Deputy Director of ERDC-CRREL was Mr. David B. Ringelberg, and the Director was Dr. Joseph L. Corriveau.

The authors acknowledge the following people for field support: Mr. Charlie Smith, Mr. Andrew Bernier, Mr. Jason Olivier, Mr. Mike Ekegren, Dr. Susan Frankenstein, and Dr. Carrie Vuyovich of CRREL; Mr. Tate Meehan of Boise State University; and Dr. Russ Alger of the Michigan Technical University. Dr. John Fegyveresi, CRREL, analyzed and plotted the snow pit data; and Ms. Michelle Michaels, CRREL, helped with analysis of the field spectrometer data. Ms. Kathleen Jones, CRREL, and Dr. H.P. Marshall, Boise State University, provided manuscript review comments. Assistance was also provided by the staff of the Nevada Automotive Test Center during testing at West Yellowstone, Montana, and the staff of the Keweenaw Research Center during testing in Calumet, Michigan.

COL Ivan P. Beckman was Commander of ERDC, and Dr. David W. Pittman was the Director.

Acronyms and Abbreviations

ASD	Analytic Spectral Devices Field-Spec4 Hi-Res Spectroradiometer
AWS	Automated Weather Station
BAEM	Boreal Aspects of Ensured Maneuver
CAVIS	Clouds, Aerosols, Vapors, Ice, and Snow
CBR	California Bearing Ratio
CIV	Clegg Impact Value
Clegg	Clegg Impact Hammer
CRREL	Cold Regions Research and Engineering Laboratory
ERDC	U.S. Army Engineer Research and Development Center
FM	Field Manual
FWD	Falling Weight Deflectometer
FY	Fiscal Year
GPR	Ground-Penetrating Radar
GPS	Global Positioning System
GSL	Geotechnical and Structures Laboratory
ISM	Impulse Stiffness Modulus
KRC	Keweenaw Research Center
LL	Load Level
LWD	Light Weight Deflectometer
MS	Multispectral
NASA	National Air and Space Administration
NATC	Nevada Automotive Test Center

NDVI	Normalized Difference Vegetation Index
NIR	Near-Infrared
RAFTER	Remote Assessment of Infrastructure for Ensured Maneuver
ram	Rammsonde
RSP	Russian Snow Penetrometer
SMP	SnowMicroPenetrometer
SWIR	Shortwave Infrared
TACOM	Tank Automotive Command
TSX	TerraSAR-X
USACE	U.S. Army Corps of Engineers
WV2	WorldView-2
WV3	WorldView-3

Unit Conversion Factors

Multiply	By	To Obtain
acres	4,046.873	square meters
cubic feet	0.02831685	cubic meters
cubic inches	1.6387064 E-05	cubic meters
degrees (angle)	0.01745329	radians
degrees Fahrenheit	(F-32)/1.8	degrees Celsius
feet	0.3048	meters
inches	0.0254	meters
kips	4448.22	newtons
microinches	0.0254	micrometers
miles (U.S. statute)	1,609.347	meters
mils	0.0254	millimeters
pounds (force)	4.448222	newtons
pounds (force) per square inch	6.894757	kilopascals
pounds (mass)	0.45359237	kilograms
pounds (mass) per cubic foot	16.01846	kilograms per cubic meter
pounds (mass) per cubic inch	2.757990 E+04	kilograms per cubic meter
square feet	0.09290304	square meters
square inches	6.4516 E-04	square meters
square miles	2.589998 E+06	square meters

1 Introduction

1.1 Background

The U.S. military has been fighting in the desert for the last 20 years and is therefore ill-prepared to apply new technologies to cold regions environments consisting of freeze and thaw, heavily organic and vegetated terrain, and snow and ice cover. To address this issue, a one-year pilot study in Fiscal Year (FY) 2018, Boreal Aspects of Ensured Maneuver (BAEM), assessed terrain in boreal terrestrial lands, specifically those unique to the far north, such as snow, ice, freezing and thawing soils, and peat and organic soils. These investigations will inform future in-depth research into maneuver in Arctic and boreal terrestrial lands of concern in military conflict. These boreal terrains are typically saturated and weak during thaw and summer rainy seasons but can be strong when frozen. Additionally, characterization for trafficability during winter, when the snow cover is ubiquitous, is of prime importance to military ground operations.

Several efforts were part of the larger BAEM study. This report documents specifically efforts to characterize winter terrain with various mechanical testing methods and spectral imaging.

1.2 Objectives

The objectives of this portion of the larger BAEM project were twofold:

1. Determine methods to measure and classify the mechanical behavior of unique northern terrain important to entry and maneuver, specifically snow-covered terrain.
2. Assess the accuracy of current capabilities and evaluate enhancements to physics algorithms and satellite-based sensing techniques focusing on physical and mechanical properties of snow.

1.3 Approach

To accomplish these objectives, the U.S. Army Engineer Research and Development Center's Cold Regions Research and Engineering Laboratory (ERDC-CRREL) team collected data on snow and ice physical and optical characteristics with concurrent satellite data collections at two sites: the Nevada Automotive Test Center's (NATC) Winter Test Facility located at

the West Yellowstone Airport, West Yellowstone, Montana, and the Keweenaw Research Center (KRC), Calumet, Michigan.

Both facilities run a wide range of winter vehicle testing over a multitude of surfaces with many types of vehicles, both military and commercial. Testing during our field experiments included a variety of measurements to characterize snow in the virgin snowpack and on numerous groomed or trafficked snow surfaces. The specific testing during the two field campaigns varied based on availability of equipment and personnel. Section 3 discusses this further.

We performed various mechanical tests to characterize the basic properties of the groomed and virgin snow surfaces. They included a range of strength tests, some more suited to one snow surface than the other. Several of the tests (i.e., California Bearing Ratio [CBR] and Clegg Impact Hammer [Clegg]) are commonly used for pavement materials and soils testing. Our study evaluated the effectiveness of these tools on snow surfaces, as well as tools specifically designed for use on snow, such as the Rammsonde (ram) and Russian Snow Penetrometer (RSP). Additional testing and measurements documented the snow depth, density, moisture content, and temperature to investigate possible correlations with snow strength.

Lastly ground-based measurements of spectral reflectance were made using an Analytical Spectral Devices (ASD) Field-Spec4 Hi-Res spectroradiometer (which we refer to as the ASD), and satellite acquisitions from WorldView-3 (WV3) multispectral optical imagery and TerraSAR-X (TSX) radar imagery that were obtained concurrently with the field campaigns.

This report documents the field methods and assesses the mechanical measurement techniques and the multispectral optical measurements based on the snow surface type. Further mechanical measurements took place in conjunction with vehicle testing and will be analyzed in a separate report.

2 Field Sites

Both the NATC and KRC test sites were large facilities with several other functions and testing programs happening concurrently with our efforts. This sometimes resulted in undocumented vehicle traffic, especially on the snow road surfaces used for durability and handling testing unrelated to the BAEM study.

2.1 Montana

NATC maintains approximately 20 hectares (49 acres) of groomed test surfaces. Test surfaces are maintained at medium pack (70–80 CTI*), soft pack (50–70 CTI), and hard pack (80–90 CTI), with virgin snow and ice surfaces also available. The vehicle test areas include, but are not limited to, the following:

- Airport terminal apron, groomed snow over asphalt pavement (677 m × 76 m [2220 ft × 250 ft])
- Taxiway, groomed snow over asphalt pavement (2560 m × 23 m [8400 ft × 75 ft])
- Runway, groomed snow over asphalt pavement (2560 m × 46 m [8400 ft × 150 ft])
- Vehicle mobility loop, through snowpack over unsurfaced terrain
- Virgin snow

We conducted the field experiments at West Yellowstone, Montana, from 24 January to 2 February 2018. They included vehicle mobility testing, on-site snow assessment, and concurrent satellite collections. CRREL collaborated with the U.S. Marine Corps, NATC, and Boise State University to perform these experiments.

On 24 January, a section of bare asphalt concrete pavement was still uncovered by snow at the south end of the taxiway. After this day, a new snowfall buried the bare pavement and provided three basic snow surfaces: snow over asphalt concrete runway, snow over asphalt concrete taxiway, and virgin snow over the grass fields adjacent to the airport's paved surfaces.

* CTI is a measure of snow-surface compaction discussed further in section 3.1.5

Testing in Montana occurred during various hours (the hours are significant because some of the electronic test equipment changed dates during night shifts). The times in Table 1 are local time.

Table 1. Testing times.

Day	Time
25 Jan. 2018	19:00–4:30 (the next day)
26 Jan. 2018	19:00–1:30
27 Jan. 2018	15:00–22:30
28 Jan. 2018	12:30–20:00
29 Jan. 2018	8:00–17:00
30 Jan. 2018	5:30–15:00
31 Jan. 2018	4:30–12:30

These work hours were chosen to reduce thermal changes in the snow surfaces and to accommodate other testing at the site.

2.2 Michigan

The second field campaign was completed at KRC in Calumet, Michigan, from 19 to 23 February 2018. KRC is a research agency of Michigan Technological University. Its goal is to generate and conduct externally funded research that supports the university's overall education mission.

The site is located in the Upper Peninsula of Michigan adjacent to the Houghton Memorial Airport, 11 km (7 miles) north of the main Michigan Tech campus. KRC is the former test site of the U.S. Army Tank Automotive Command (TACOM), and TACOM continues to sponsor research and testing at KRC.

The test course consists of over 365 hectares (900 acres) of test areas, such as handling loops, a circular track, and slopes. The variety of terrain, combined with northern Michigan's wide-ranging weather conditions, allows for realistic field evaluations. The course is used year-round for acceleration and braking, slope climbing, noise, vibration, obstacle crossing, and endurance tests. Every winter, special ice and snow areas are constructed for ride and handling studies, antilock brake tests, and tire traction evaluations.

The KRC Winter Test Facility includes several prepared snow and ice surfaces:

- Three vehicle handling loops
- Several packed-snow vehicle dynamics pads
- Packed-snow slopes of 7, 10, 15, 20, 25, and 30 percent grade
- A 61 m × 366 m (200 ft × 1200 ft) ice rink with cleared asphalt, ice, and snow lanes
- Packed-snow/ice circles with 91, 183, and 274 m (300, 600, and 900 ft) inside diameters
- Naturally vegetated terrain with virgin snow cover adjacent to the prepared surfaces

Testing in Michigan was during standard daylight work hours.

2.3 Test-point discussion

The BAEM test points, such as 19RWY0, are labeled as follows. The first two numbers indicate the testing date, such as 19 January. The next three or four letters indicate the surface type or location, such as runway. The final numbers or letters are a descriptor of the point on the surface. During the actual testing, different names may have been given to test points. The naming was normalized during the data transcription and preanalysis processing to ensure the correct data were attributed to the correct test point.

Tables 2 and 3 list the test points with the date of testing; approximate local time; and a description of the test point, ground surface, and snow-surface conditions at the time of each test. The time spent at a specific location depended on the number of points in the vicinity, the number of tests applicable to that area's snow conditions, and the number of team members working in the area. Some points, such as 27RWYSVS and 27TWYSVS, had additional testing in the same vicinity later in the test program. Figures 1–5 show the test points used in this study. Appendix A provides additional views of the test areas, and Appendix B provides photos of the various ground surfaces in Michigan without snow cover.

In Montana, again, some testing days stared at 22:00 and went into the morning of the next day. For these points, the two-digit date designator was the date that testing started. Therefore, some points with designator "25" actually may have been tested during the early morning hours of 26 January.

Table 2. Summary of Montana BAEM test points from winter 2018.

Test Point	Date	Approximate local time	Longitude (Degrees)	Latitude (Degrees North)	Description	Snow Surface	Ground Surface
25RWY0	1/25/2018	21:45–23:00	−111.115	44.693	Runway, north end—point 0	Fresh over groomed snow	Asphalt concrete pavement
25RWY50	1/25/2018	22:00–23:00	−111.115	44.693	Runway, north end—point 50	Fresh over groomed snow	Asphalt concrete pavement
25RWY100	1/25/2018	22:00–23:00	−111.115	44.692	Runway, north end—point 100	Fresh over groomed snow	Asphalt concrete pavement
25TWY0	1/26/2018	2:45–3:45	−111.114	44.691	Taxiway, north end—point 0	Fresh over groomed snow	Asphalt concrete pavement
25TWY50	1/26/2018	2:45–3:45	−111.114	44.691	Taxiway, north end—point 50	Fresh over groomed snow	Asphalt concrete pavement
25TWY100	1/26/2018	2:45–3:45	−111.114	44.691	Taxiway, north end—point 100	Fresh over groomed snow	Asphalt concrete pavement
27RWYSVS	1/27/2018	17:50–18:50	−111.125	44.679	Off south end of runway to the west, also tested on other days as 29RWYSVS, 30RWYSVS, and 31RSWVS	Virgin snow	Minimally maintained, leveled terrain over sandy soil
27TWYSVS	1/27/2018	19:00–20:00	−111.123	44.677	Off south end of taxiway, also tested as 29TWYSVS	Virgin snow	Minimally maintained, leveled terrain over sandy soil
28MLPW	1/28/2018	15:20–17:00	−111.117	44.692	Mobility Loop, west straightaway	Rutted snowpack	Minimally maintained, leveled terrain over sandy soil
29RWYC	1/29/2018	10:45–11:30	−111.116	44.691	Runway, center	Groomed snow	Minimally maintained, leveled terrain over sandy soil
30MLPN	1/30/2018	7:00–11:00	−111.109	44.699	Mobility Loop, entrance at north end of the taxiway	Rutted snowpack	Minimally maintained, leveled terrain over sandy soil
31RWYC	1/31/2018	5:45–6:30	−111.116	44.691	Runway, center	Groomed snow	Minimally maintained, leveled terrain over sandy soil

Table 3. Summary of Michigan BAEM test points from winter 2018.

Test Point	Date	Approximate Local Time	Longitude (Degrees)	Latitude (Degrees North)	Description	Snow Surface	Ground Surface
19SU2_A	2/19/2018	10:00–15:30	−88.509	47.164	Spin Up Pad 2—point A	Fresh over groomed snow	Grass over brown silty sand with gravel
19SU2_B	2/19/2018	10:00–15:30	−88.509	47.164	Spin Up Pad 2—point B	Fresh over groomed snow	Grass over brown silty sand with gravel
19SU2_C	2/19/2018	10:00–15:30	−88.509	47.164	Spin Up Pad 2—point C	Fresh over groomed snow	Grass over brown silty sand with gravel
19SU2_D	2/19/2018	10:00–15:30	−88.509	47.164	Spin Up Pad 2—point D	Fresh over groomed snow	Grass over brown silty sand with gravel
19SU2_E	2/19/2018	10:00–15:30	−88.509	47.163	Spin Up Pad 2—point E	Fresh over groomed snow	Grass over brown silty sand with gravel
19SU2_F	2/19/2018	10:00–15:30	−88.509	47.164	Spin Up Pad 2—point F	Fresh over groomed snow	Grass over brown silty sand with gravel
19SU2VS_A	2/19/2018	14:30–16:00	−88.510	47.164	Spin Up Pad 2, old road virgin snow—point A	Virgin snow	Natural terrain—glacial loamy silts and sands
19SU2VS_B	2/19/2018	14:30–16:00	−88.510	47.164	Spin Up Pad 2, old road virgin snow—point B	Virgin snow	Natural terrain—glacial loamy silts and sands
19SU2VS_C	2/19/2018	14:30–16:00	−88.510	47.164	Spin Up Pad 2, old road virgin snow—point C	Virgin snow	Natural terrain—glacial loamy silts and sands
19SU2VS_D	2/19/2018	14:30–16:00	−88.510	47.164	Spin Up Pad 2, old road virgin snow—point D	Virgin snow	Natural terrain—glacial loamy silts and sands
19SU2VS_E	2/19/2018	14:30–16:00	−88.510	47.164	Spin Up Pad 2, old road virgin snow—point E	Virgin snow	Natural terrain—glacial loamy silts and sands
20LP1WG_1	2/20/2018	10:00–11:30	−88.505	47.160	Loop 1, washed gravel subgrade—point 1	Freezing rain and fresh snow over groomed snow	Compacted road gravel
20LP1WG_2	2/20/2018	10:00–11:30	−88.506	47.160	Loop 1, washed gravel subgrade—point 2	Freezing rain and fresh snow over groomed snow	Compacted road gravel
20LP1WG_3	2/20/2018	10:00–11:30	−88.506	47.160	Loop 1, washed gravel subgrade—point 3	Freezing rain fresh snow over groomed snow	Compacted road gravel
20LP1GS_4	2/20/2018	12:30–15:00	−88.505	47.159	Loop 1, grass subgrade—point 4	Freezing rain fresh snow over groomed snow	Grass over brown silty sand with gravel
20LP1GS_5	2/20/2018	12:30–15:00	−88.505	47.159	Loop 1, grass subgrade—point 5	Freezing rain fresh snow over groomed snow	Grass over brown silty sand with gravel
20LP1GS_6	2/20/2018	12:30–15:00	−88.505	47.159	Loop 1, grass subgrade—point 6	Freezing rain fresh snow over groomed snow	Grass over brown silty sand with gravel
20GPVS	2/20/2018	15:10–15:45	−88.508	47.157	Gravel pad virgin snow next to Loop 1	Virgin snow	Compacted road gravel
21SWP_1	2/21/2018	8:00–9:30	−88.494	47.159	Sweeper parking pad—point 1	Fresh over groomed snow	Grass over brown silty sand with gravel
21SWP_2	2/21/2018	8:00–9:30	−88.495	47.159	Sweeper parking pad—point 2	Fresh over groomed snow	Grass over brown silty sand with gravel

Table 3 (cont.). Summary of Michigan BAEM test points from winter 2018.

Test Point	Date	Approximate Local Time	Longitude (Degrees)	Latitude (Degrees North)	Description	Snow Surface	Ground Surface
21SWP_3	2/21/2018	8:00–9:30	−88.495	47.159	Sweeper parking pad—point 3	Fresh over groomed snow	Grass over brown silty sand with gravel
21IS_S	2/21/2018	9:40–11:00	−88.495	47.159	Ice slopes next to sweeper pad, steep	Virgin snow over ice	Compacted road gravel
21IS_L	2/21/2018	9:40–11:00	−88.495	47.159	Ice slopes next to sweeper pad, lower	Virgin snow over ice	Grass over brown silty sand with gravel
21SU1_1	2/21/2018	13:00–13:45	−88.502	47.166	Spin Up Pad 1—point 1	Groomed snow	Compacted road gravel
21SU1_2	2/21/2018	13:00–13:45	−88.502	47.166	Spin Up Pad 1—point 2	Groomed snow	Compacted road gravel
21GPRD_1	2/21/2018	14:00–14;45	−88.508	47.158	Loop 1 road adjacent to 21GPVS—point 1	Groomed snow	Compacted road gravel
21GPRD_2	2/21/2018	14:00–14;45	−88.508	47.158	Loop 1 road adjacent to 21GPVS—point 2	Groomed snow	Compacted road gravel
21GPVS	2/21/2018	14:00–14;45	−88.508	47.157	Gravel pad virgin snow next to Loop 1	Virgin snow	Compacted road gravel
21SU2_A2	2/21/2018	15:00–16:00	−88.508	47.163	Spin Up Pad 2—point A2 (further west of original 2/19 point A)	Groomed snow	Grass over brown silty sand with gravel
21SU2_B2	2/21/2018	15:00–16:00	−88.507	47.163	Spin Up Pad 2—point B2 (different from original 2/19 point B)	Groomed snow	Grass over brown silty sand with gravel
22SU3_1	2/22/2018	8:00–9:00	−88.507	47.160	Spin Up Pad 3—point 1	Groomed snow	Compacted road gravel
22SU3_2	2/22/2018	8:00–9:00	−88.507	47.160	Spin Up Pad 3—point 2	Groomed snow	Compacted road gravel
22SU3_3	2/22/2018	8:00–9:40	−88.506	47.160	Spin Up Pad 3—point 3	Groomed snow	Compacted road gravel
22SU3VS	2/22/2018	9:40–11:00	−88.507	47.160	Spin Up Pad 3, virgin snow to north	Virgin snow	Grass over brown silty sand with gravel
22SU3VS_1	2/22/2018	9:40–11:00	−88.507	47.160	Spin Up Pad 3, virgin snow to north	Virgin snow	Grass over brown silty sand with gravel
22SU3VS_3	2/22/2018	9:40–11:00	−88.507	47.160	Spin Up Pad 3, virgin snow to north	Virgin snow	Grass over brown silty sand with gravel
22SU3VS_4	2/22/2018	9:40–11:00	−88.507	47.160	Spin Up Pad 3, virgin snow to north	Virgin snow	Grass over brown silty sand with gravel
22SU3VS_5	2/22/2018	9:40–11:00	−88.507	47.160	Spin Up Pad 3, virgin snow to north	Virgin snow	Grass over brown silty sand with gravel
22SU3VS_6	2/22/2018	9:40–11:00	−88.507	47.160	Spin Up Pad 3, virgin snow to north	Virgin snow	Grass over brown silty sand with gravel
22SU2	2/22/2018	11:30–11:45	−88.507	47.163	Spin Up Pad 2, near 21SU2_B2 (furthest west)	Groomed snow	Grass over brown silty sand with gravel
22SU3	2/22/2018	11:50–12:05	−88.505	47.160	Spin Up Pad 3 at the top of the sloped roads	Groomed snow	Compacted road gravel
22SU3_7D	2/22/2018	11:50–12:05	−88.505	47.160	Spin Up Pad 3, sloped access roads, 7 degree	Groomed snow	Compacted road gravel
22SU3_10D	2/22/2018	11:50–12:05	−88.505	47.160	Spin Up Pad 3, sloped access roads, 10 degree	Groomed snow	Compacted road gravel

Table 3 (cont.). Summary of Michigan BAEM test points from winter 2018.

Test Point	Date	Approximate Local Time	Longitude (Degrees)	Latitude (Degrees North)	Description	Snow Surface	Ground Surface
22SU3_15D	2/22/2018	11:50–12:05	−88.505	47.160	Spin Up Pad 3, sloped access roads, 15 degree	Groomed snow	Compacted road gravel
22SU3_20D	2/22/2018	11:50–12:05	−88.505	47.160	Spin Up Pad 3, sloped access roads, 20 degree	Groomed snow	Compacted road gravel
22LP3E	2/22/2018	12:10*	−88.484	47.162	Loop 3 east	Groomed snow	Compacted road gravel
22LP3EVS	2/22/2018	12:10*	−88.484	47.162	Loop 3 east, adjacent virgin snow	Virgin snow	Compacted road gravel
22IR_I	2/22/2018	12:25*	−88.496	47.159	Ice rink, ice surface	Ice	Grass over brown silty sand with gravel
22IR_S	2/22/2018	12:25*	−88.496	47.159	Ice rink, snow surface	Groomed snow	Grass over brown silty sand with gravel
22IR_AC	2/22/2018	12:25*	−88.496	47.159	Ice rink, asphalt concrete surface	Asphalt	Asphalt concrete pavement
22STAB_S	2/22/2018	12:35*	−88.488	47.158	Stability Test Area, snow	Groomed snow	Grass over well-graded sand/silt sand
22STAB_GI	2/22/2018	12:40*	−88.487	47.158	Stability Test Area, grooved ice	Grooved ice	Grass over well-graded sand/silt sand
22VDA2_1	2/22/2018	12:50*	−88.501	47.160	Vehicle Dynamics Area 2	Groomed snow	Grass over brown silty sand with gravel
22VDA2_2	2/22/2018	12:50*	−88.501	47.159	Vehicle Dynamics Area 2	Groomed snow	Grass over brown silty sand with gravel
22900C	2/22/2018	12:55*	−88.504	47.160	900 ft circle	Groomed snow	Compacted road gravel
22300C	2/22/2018	13:00*	−88.503	47.159	300 ft circle	Groomed snow	Compacted road gravel
22300CVS	2/22/2018	13:10*	−88.503	47.159	300 ft circle, center virgin snow	Virgin snow	Grass over brown silty sand with gravel
22LP4	2/22/2018	14:30*	−88.489	47.156	Loop 4	Groomed snow	Well-graded sand/silt sand
22LP4VS	2/22/2018	14:30*	−88.489	47.156	Loop 4, adjacent virgin snow	Virgin snow	Grass over well-graded sand/silt sand
22LP3NW	2/22/2018	14:50*	−88.492	47.163	Loop 3 northwest	Groomed snow	Compacted road gravel
22LP3NWVS	2/22/2018	14:50*	−88.492	47.163	Loop 3 northwest, adjacent virgin snow	Virgin snow	Natural terrain—glacial loamy silts and sands
22STAB_GI2	2/22/2018	15:00*	−88.487	47.158	Stability Test Area, grooved ice, additional LWD with outer geophones	Groomed snow	Grass over well-graded sand/silt sand
23HQP	2/23/2018	10:00–10:45	−88.504	47.170	Headquarters parking lot	New snow	Grass over brown silty sand with gravel

* These points were tested in less than 10 minutes per site if possible.

Figure 1. Montana test site at West Yellowstone Airport.



Figure 2. Montana test points superimposed over winter imagery taken during the field campaign.



Figure 3. Schematic of the Michigan test site.

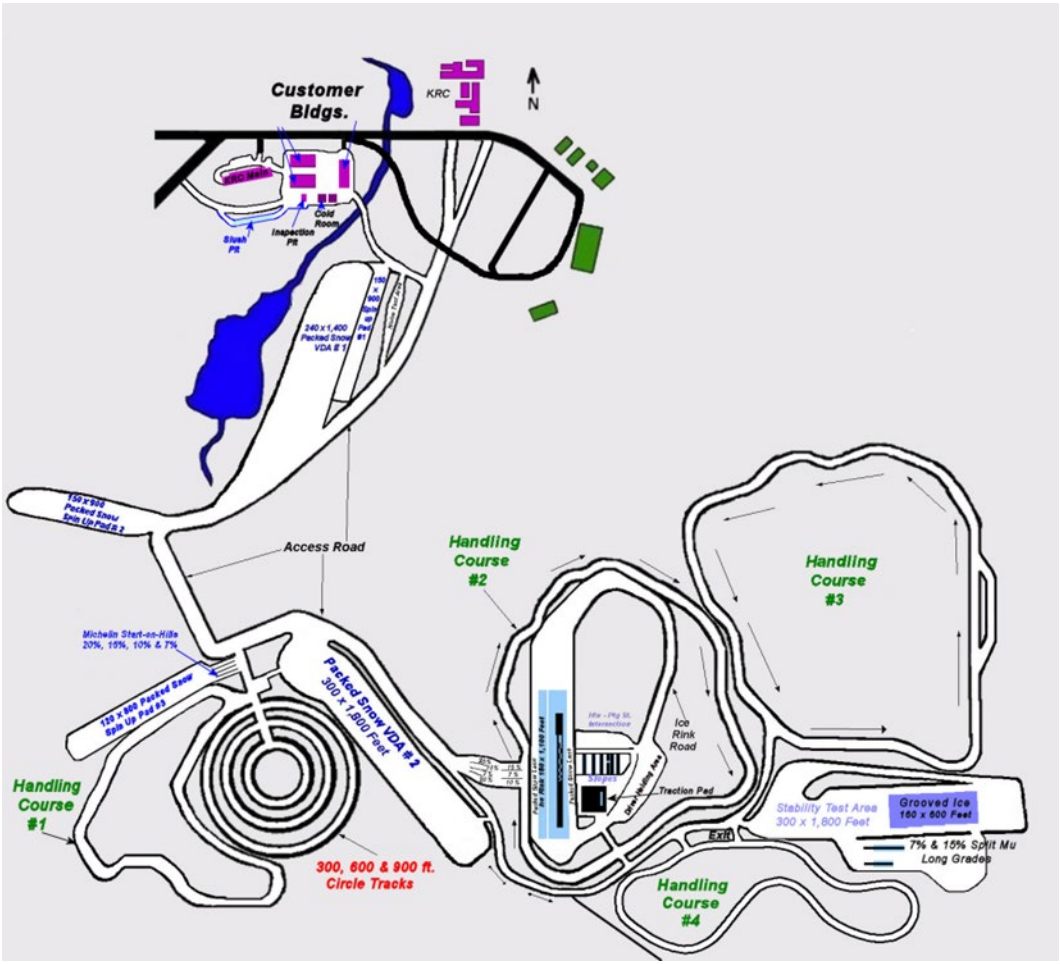
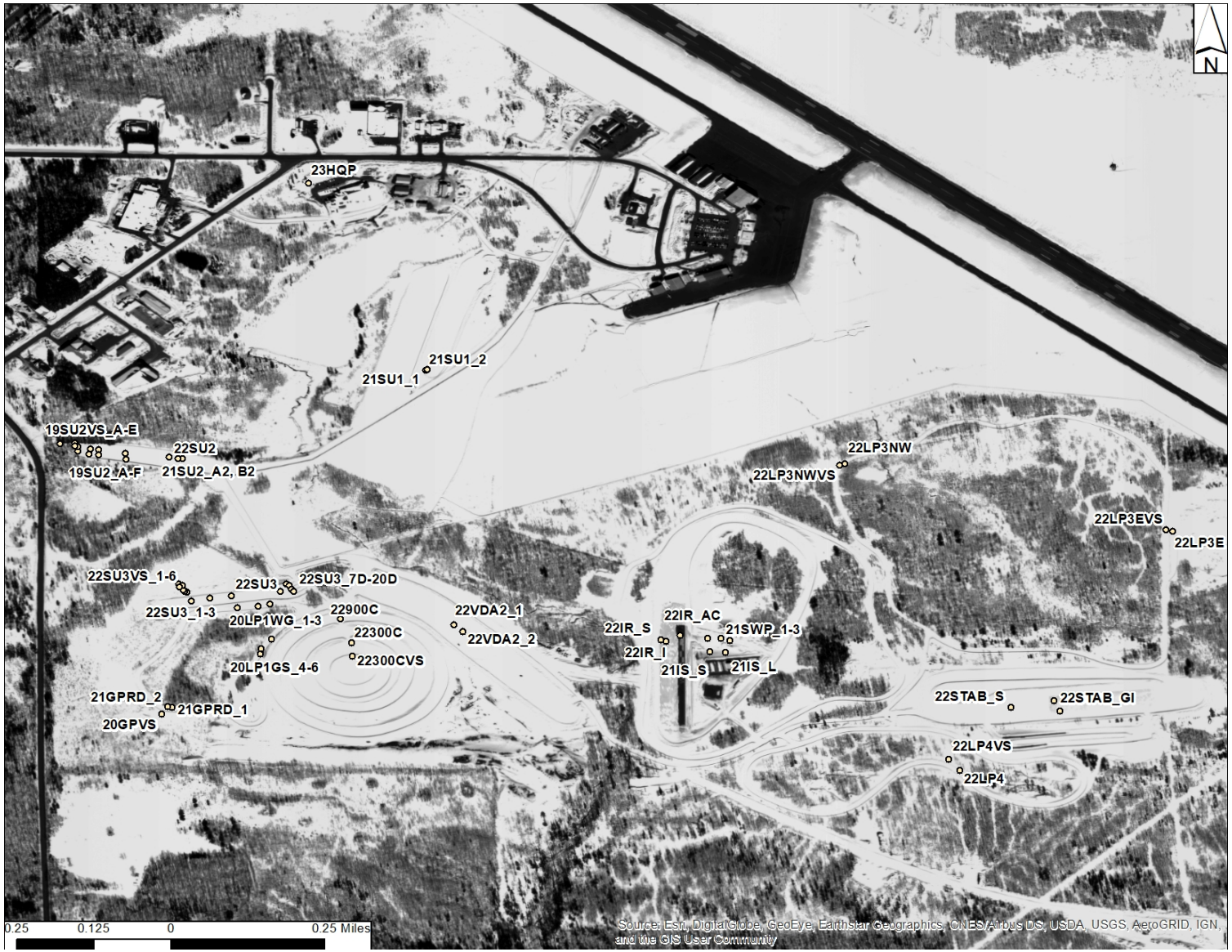


Figure 4. Michigan test points superimposed on imagery from summer to show to show ground surfaces.



Figure 5. Michigan test points superimposed on winter imagery.



3 Data Collection

The capabilities, or measurement range, of each particular piece of testing equipment tended to fall in one of two categories: (1) soft snow and (2) hard or groomed snow. Soft snow was accumulated virgin snow, undisturbed by vehicles or any other activity except natural weather activity (i.e., wind, sun, and precipitation). Groomed snow had been prepared by plows, drags, or other grooming equipment or by vehicle traffic. The basic physical and optical properties measurements, however, were applicable both to groomed and soft snow surfaces: air and snow temperatures, snow density, reflectance, and WV3 and TSX satellite imagery.

The following lists summarize the test methods evaluated in this study, and the following sections fully describe each specific method. Not all equipment was used at every sampling location.

Mechanical measurements for groomed snow:

- Field CBR (Montana and Michigan)
- 0.5 and 2.25 kg (1.1 and 5 lb) Clegg (Montana and Michigan)
- Light Weight Deflectometer (LWD) (Montana and Michigan)
- RSP (Montana and Michigan)
- CTI snow compaction gauge (Michigan)
- Micro tools—assorted small shear vanes and hardness penetrometers (Montana and Michigan)

Mechanical measurements for soft snow:

- Rammsonde penetrometer (ram) (Montana and Michigan)
- SnowMicroPenetrometer (SMP) (Montana)
- Yamaha drop cone (Michigan)
- MagnaProbe (Michigan)
- Plate sinkage (Montana and Michigan)
- Micro tools—assorted small shear vanes and hardness penetrometers (Montana and Michigan)

Additional physical and optical measurements and tests:

- Air temperature (Montana and Michigan)
- Snow temperature, at surface and with depth, where possible (Montana and Michigan)
- Weight-based snow density (soft snow Montana, soft and groomed snow Michigan)
- Finnish fork snow moisture and density (Montana and Michigan)
- Denoth meter snow moisture (Montana and Michigan)
- Near-infrared (NIR) Photography
- 500 MHz and 1 GHz ground-penetrating radar (GPR) (Montana)
- Spectral reflectance from 350 to 2500 nm (Montana and Michigan)
- WV2/WV3 satellite imagery (Montana and Michigan)
- TSX satellite imagery (Montana and Michigan)

Several of the measurements were accomplished by digging snow pits. Snow pits allowed snow samples to be taken throughout the depth of virgin snow for direct measurement of snow density; depth profiling of moisture content (using the Finnish fork and Denoth meter) and temperature measurements were taken in the walls of each pit. We also used some of the smaller mechanical measurements, grouped together and called micro tools, in the walls of snow pits to obtain strength profiles.

3.1 Mechanical measurements for groomed snow

3.1.1 Field California Bearing Ratio (CBR)

CBR is a load-deformation test performed in the field or laboratory. The results are used with empirical design charts to determine the thickness of flexible pavement, base, and other layers for a given vehicle loading and number of passes. The U.S. Army Corps of Engineers (USACE) adopted the CBR method of design for flexible airfield pavements in the 1940s; and today the USACE, U.S. Navy, and U.S. Air Force design practice for surfaced and unsurfaced airfields is still based on CBR (U.S. Army and Air Force 1994).

The field CBR test procedure is described in ASTM International D4429-09a, *Standard Test Method for CBR (California Bearing Ratio) of Soils in Place* (ASTM 2010) and in Army Field Manual (FM) 5-530, *Materials Testing* (U.S. Army et al. 1987). The CBR test is performed by measuring the penetration resistance of a 1.954 in. (5.0 cm) diameter (3 in.^{2} [19 cm^2] end area) cylindrical steel piston advanced into the soil at a rate of 0.05 in./min (1.27 mm/min). CBR test parameters are in English units as

the equipment was developed in the 1940s. The reaction force is measured by means of a calibrated proving ring at increments of 0.025 in. (0.635 mm) until reaching a total penetration of 0.500 in. (12.7 mm). Using field CBR on groomed snow surfaces (Figure 6) is an uncommon application of the test.

Figure 6. Field CBR test setup in Michigan.



The CBR is reported as a percentage from 0 to 100 where standard stress values are based on crushed, well-graded (passing through a ¾ in. [19.0 mm] sieve) limestone serving as the 100% (CBR = 100) material. The stress penetration curves are calculated using the force divided by the piston area. The corrected stress values for 0.10 in. and 0.20 in. (2.54 mm and 5.08 mm) penetration taken from stress-penetration curves are divided by 1000 psi and 1500 psi (6.9 MPa and 10.3 MPa), respectively, the reference value for limestone, and then multiplied by 100 to determine the CBR values. The bearing ratio that is reported for the soil is the ratio determined from the 0.10 in. (2.54 mm) penetration; however, if the bearing ratio measured at 0.20 in. (5.08 mm) penetration is greater than that of the

0.10 in. (2.54 mm) penetration, the test must be rerun. If the ratio determined using the 0.20 in. (5.08 mm) penetration is still greater again in the second test, the bearing ratio at 0.20 in. (5.08 mm) penetration should be used as the CBR value (ASTM 2010).

3.1.2 Cleggs

The Clegg Impact Hammer consists of a cylindrical mass hammer that is dropped within a guide tube from a set height (Clegg 1980; ASTM 2016a). The hammer is equipped with an accelerometer that measures the peak deceleration on impact in gravity units. The hammer is dropped four times at each location, and deceleration readings are recorded for each drop (Figure 7). The readings are reported in 1/10 g-forces. Typically, both the 2.25 kg (5.0 lb) and the 0.5 kg (1.1 lb) size Cleggs are typically used to measure natural ground or uncompacted soil surfaces. Shoop et al. (2012) provides a good summary and background on the different Clegg sizes, their use for snow-strength measurement, and conversion to other strength parameters.

Figure 7. The 0.5 kg Clegg.



Clegg measurements were taken at each site using both the 2.25 kg (5.0 lb) and the 0.5 kg (1.1 lb) weight hammers. If a groomed snow site had received fresh snow, two sets of measurements were taken; one on top of the fresh snow and one on the underlying groomed surface after brushing off the surface.

Clegg Impact Values (CIVs) for each site were taken as the average measurement of the third drop for the 2.25 kg (5.0 lb) Clegg and the fourth drop for the 0.5 kg (1.1 lb) Clegg. CIV values were converted to CBR following equation (1) for the 2.25 kg (5.0 lb) Clegg data and equation (2) for the 0.5 kg (1.1 lb) Clegg data (Shoop et al. 2012; Millar 1977):

$$CBR\ (\%) = e^{\frac{10\ CIV_{2.25kg} - 14.936}{79.523}}. \quad (1)$$

$$CBR\ (\%) = 0.55\ CIV_{0.5kg} - 1. \quad (2)$$

3.1.3 Light Weight Deflectometer (LWD)

The LWD is a portable version of the larger, typically trailer-mounted, falling weight deflectometer (FWD). It was developed to estimate the in situ stiffness modulus of soils and is often used for quality control/quality assurance and structural evaluation of mechanically compacted earthwork and pavement construction (Senseney and Mooney 2010). With its proprietary software, the LWD may be used to backcalculate the soil elastic modulus for known one- and two-layer stratigraphy by using the deflection data measured by three geophones (seismic transducers), one at the center of the loading plate and two offset radially beyond the edge of the plate. It can also be used in single geophone mode to calculate an Impulse Stiffness Modulus (ISM).

The Dynatest 3031 LWD device consists of a weight dropped from increasing heights along a guide rod. The weight makes contact with a rubber buffer, and the load is transferred to the soil surface via a 300 mm (11.8 in.) diameter loading plate. The surface response from the load impact generates a vertical deflection response measured (through integration of velocity) with one or three geophones. One geophone was centrally located on the loading plate; the other two are external and were not used on snow for this project as they did not register a signal on the groomed snow surfaces. The geophone response is reported as deflection in mils

(1/1000 in.). The LWD tests performed for this program typically had 16 drops per test point (Figure 8). More information of the procedures developed under BAEM for using the LWD on winter surfaces is presented in Wieder et al. (2019) and Menke et al. (2019).

Figure 8. The LWD.



3.1.4 Russian Snow Penetrometer

Though similar to the ram in operation, the RSP (Figure 9), was designed for testing compacted snow (Blaisdell et al. 1995). The RSP has a 30° cone tip with a maximum diameter of 1.15 cm (0.45 in.) and uses a 1.75 kg (3.9 lb) hammer dropped from a height of 50 cm (19.7 in.) to drive a 1.421 kg (3.1 lb) penetrometer (with tip). In this study, RSP penetration depth was noted every 1–2 hammer blows and ranged from a 0 to 320 mm (0 to 12.6 in.) penetration depth per reading, depending on the strength of the

snow. RSP hardness is calculated using the same equations as the one developed for the ram, discussed in section 3.2.1

Figure 9. RSP in use in Michigan.



3.1.5 CTI

The CTI snow compaction gauge (Figure 10), manufactured by Smithers Rapra, is shaped like a surveyor's plumb bob (cone) except that the point is rounded with a 1.6 mm (1/16 in.) radius. Each gauge is adjusted in the laboratory to have a weight of 220 ± 1 g (0.485 ± 0.002 lb), including the knurled nut on top of the drop rod. The drop height is set to 218.9 ± 0.25 mm (8.92 ± 0.01 in.).

In use, the mass of the cone and rod is dropped a preset distance through a guide tube. The kinetic energy is expended in both vertical penetration and side compression.

The penetration distance is measured using a calibrated scale to directly read the hardness of the snow surface as a standardized index with values ranging from 50–100 CTI (ASTM 2016b).

Figure 10. CTI test in Michigan.



3.1.6 Micro tools

3.1.6.1 Pocket penetrometer

The Geotester dial penetrometer (henceforth pocket penetrometer) is designed for use on cohesive soils. It estimates the unconfined compressive strength of the soil surface in kilograms per square centimeter when used with the standard 6.35 mm (0.25 in.) diameter plunger. Four larger plungers of 10, 15, 20, and 25 mm (0.39, 0.59, 0.79, and 0.98 in.) in diameter can provide strengths over a wide range of soil types.

The plunger of the pocket penetrometer was pressed into the snow until the snow collapsed or to the depth of the calibration notch. The penetrometer was withdrawn from the snow with the test value, in kilograms, retained on the dial. Dial readings were manually recorded and later

converted to bearing capacity by using calibration charts provided by the manufacturer (AMS 2018). As snow strength varied considerably between sites, different plunger sizes were used. After selecting an appropriate plunger size, three measurements, or more if readings were inconsistent, were taken at each site and were averaged.

3.1.6.2 Shear vane

Measurements of surface shear strength were made using a Geonor H-60 handheld vane tester (henceforth shear vane). The shear vane has an orthogonal, cross-shaped blade. The vane blade comes in three standard sizes, and the size is chosen based on the snow strength. Custom vane sizes may also be used when snow conditions are either too hard or too soft for the standard vanes. The vane is inserted into the snow to a depth covering the entire vane, and then a steady turning force is applied until the snow shears. The maximum shear force is recorded as kilopascals. The shear strength values for each site are the average of three measurements. ASTM D2573–18 (ASTM 2018) covers the use of the shear vane in soils.

3.1.6.3 Snow hardness plates

Plates of various sizes can be used to assess snow hardness. This tool was most useful on horizontal surfaces, such as the snow surface, and for characterizing the hardness of interspersed snow or ice layers.

3.2 Mechanical measurement for soft snow

3.2.1 Rammsonde

The Rammsonde is used to measure the penetration resistance of the snow, called a ram hardness. The ram hardness of snow is an indication of the resistance of snow to vertical penetration by a cone tip driven by the force of a weight dropped from a known height (Abele 1990). Ram hardness is significantly correlated with unconfined compressive strength (Abele 1963) and with shear strength (Abele 1968), and ram hardness is linearly correlated with CBR (Abele 1990). Successive drops and notation of penetration distance can provide a profile of ram hardness through the snowpack.

The ram used in this study (Figure 11) was equipped with a 30° cone tip (2.4 cm [0.9 in.] diameter, 3.9 cm [1.5 in.] height, and 5 cm [2.0 in.] total length), typically used on groomed snow surfaces (snow roads and airfields). A 0.5, 1.0, or 3.00 kg (1.1, 2.2, or 6.6 lb) weight was dropped from a

height of 10 to 50 cm (3.9 to 19.7 in.) above the snow surface to drive the 1.02 kg (2.2 lb) penetrometer. Drop weights and heights were adjusted to achieve penetrations less than 2 cm (0.8 in.) for each recorded interval, although this was usually not possible for virgin snow.

Figure 11. Ram testing in Michigan.



The ram hardness (R, kgf) is calculated as

$$R = \frac{Whn}{x} + W + Q, \tag{3}$$

where

W = the mass of the drop hammer,
h = the height of the drop,
n = the number of blows,
x = the penetration after n blows, and
Q = the mass of the penetrometer.

Calculated R is multiplied by a factor of 1.56 to convert to R values using the standard 60° cone tip, more commonly used in avalanche studies (Abele 1990). Further, to correct for the conical tip and proximity of a free surface, R values are corrected by a factor of 4.0 from a 0 to 5 cm (0 to

2.0 in.) depth and by a factor of 1.6 from a 5 to 10 cm (2.0 to 3.9 in.) depth (Abele 1990).

3.2.2 SnowMicroPenetrometer

The SMP is a mechanically driven sonde penetrometer used to measure the hardness of the snowpack as a multimodal penetration force. The SMP has a 60° cone with a base diameter of 5 mm (0.2 in.). This instrument samples the penetration force 250 times per millimeter and drives through the snowpack with a strain rate above 10^{-3} such that the snow behaves nearly linear elastically with brittle failure (Marshall and Johnson 2009). Thus, in theory, the SMP is capable of measuring the individual ruptures of snow crystals that are in contact with the penetrometer tip. The SMP was designed to operate in light alpine snowpacks and to be sensitive to structural weaknesses within the snowpack to assess avalanche hazard (Schneebeli and Johnson 1998).

The standard SMP sensor is sensitive to a range of forces between 0 and 42 N (9.4 lbf) (Pielmeier and Schneebeli 2003). For the Montana campaign, the SMP was equipped with an alternative force sensor, enabling the SMP to measure forces up to 250 N (56.2 lbf). The increased dynamic force range comes at a cost in force resolution as the instrument's discrete quantization levels were not increased when the sensor capacity was increased. Meehan et al. (2019a, 2019b) document and analyze the SMP, its use, and results. While this instrument worked very well in the soft snow conditions it was designed for, future experiments would benefit from an SMP that could measure larger forces as many of the groomed surfaces were too hard for this instrument even with the larger force sensor.

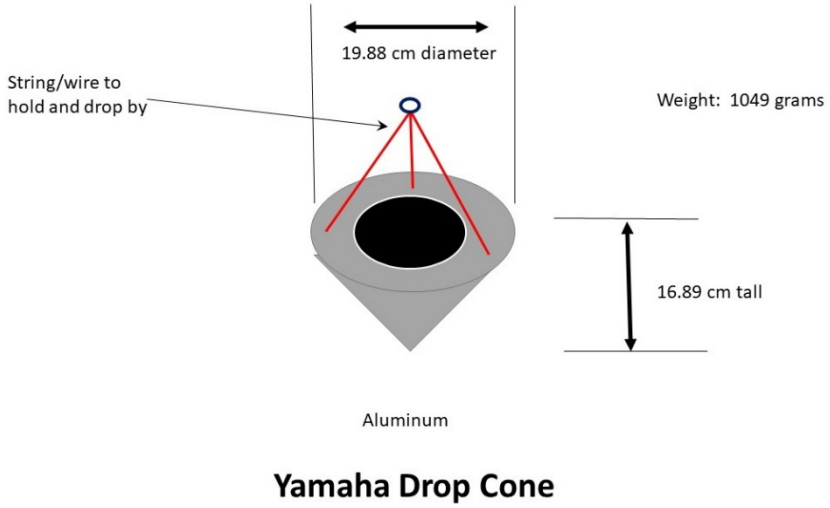
3.2.3 Yamaha drop cone

The Yamaha drop cone (Figure 12) is an aluminum cone that is dropped from a specific height onto ungroomed snow. The resulting depth of penetration into the snow is then measured. Figure 13 provides a schematic for the Yamaha drop cone.

Figure 12. Yamaha drop cone in use in Michigan.



Figure 13. Yamaha drop cone schematic and specifications.



3.2.4 MagnaProbe

The MagnaProbe (Figure 14), manufactured by Snow-Hydro, is a self-recording snow-depth probe that interfaces with a GPS (global positioning system) for geolocation (Sturm and Holmgren 1999). The MagnaProbe consists of a rod that is approximately 1.5 m (5 ft) in length, and at the end of the probe is a white basket that will ride on the top of the snowpack. The control button at the top of the probe is pushed to record the snow-depth

measurement and GPS location. Data are recorded by a Campbell Scientific datalogger. Accuracy of the GPS is ±10 m (33 ft) absolute and ±2 m (6.5 ft) relative on repeated surveys. Using this probe, an operator can walk across a snow-covered landscape and in several hours produce a detailed transect of snow depths.

Figure 14. Snow MagnaProbe.



3.2.5 Plate sinkage

Prior to deployment for the 2018 BAEM field campaign, CRREL engineers manufactured a prototype plate sinkage device (Figure 15). The intent of the device was to characterize virgin snow strength by measuring the force required to drive, by hand, plates of different diameters through the snow.

Figure 15. Plate sinkage test in Michigan.



3.3 Additional physical and optical measurements

3.3.1 Air and snow temperatures

Weather data from nearby weather stations were collected (Appendix C). In addition, temperatures at 15 cm (6 in.) above the surface, at the surface, and 2.5 cm (1 in.) below the surface were also recorded. In the fresh and virgin snowpacks, temperatures within the snow were recoded every 10 cm (4 in.) in the walls of each snow pit.

3.3.2 Snow density

Two different methods of snow-density measurements were required for the soft and groomed snow surfaces encountered in both Montana and Michigan.

For virgin snow, density was measured by taking samples of the snow using a cutting tool (Conger and McClung 2009; Carroll 1977). This was done by shoveling a pit in the snow down to the ground surface. The pit walls were shoveled as neatly and as near vertical as possible. At regular intervals, a 100 cm^3 stainless steel cutter was inserted horizontally and a rec-

tangular block of snow extracted (Figure 16). The rectangular block of snow was weighed to calculate the density of that layer.

Figure 16. Snow-density-sample extraction in a snow pit.



For the denser snow surfaces, when the snow was too hard to take a sample without damaging the cutter (densities greater than approximately 0.5 g/cm^3 [0.018 lb/in^3]), another method was needed. For these surfaces, we drove a 5.8 cm (2.28 in.) diameter cylinder into the surface of the snow down to depths of 2.5, 5.0, and 7.6 cm (1, 2, and 3 in.), Figure 17, and carefully removed the sample. This sample was weighed, the volume calculated, and the resultant density recorded. This technique, developed by Russ Alger at KRC, was used at the Michigan site only.

Figure 17. Snow-density test using the aluminum cylinder in Michigan.



3.3.3 Denoth meter

The Denoth snow moisture meter is an electronic dielectric device that measures the real part of the dielectric constant of snow at 20 MHz by using a capacitance plate. Empirical relationships with snow moisture and density, which must be measured separately, allow the calculation of snow-volume wetness (Denoth 1989). These measurements were taken in snow pit walls at a 10 cm (4.0 in.) spacing. On the surface of the snow, the unit can be used to make a half-space measurement. Measurements within 5 cm (2.0 in.) of the ground are affected by the dielectric properties of the underlying ground surface and should be interpreted with caution.

3.3.4 Finnish snow fork

The Toikka Oy snow fork, commonly referred to as the Finnish snow fork, measures the real and imaginary components of the dielectric constant of snow by using microwave resonance in the range of 500 to 900 MHz. The dielectric constant can be related to snow density and liquid water content through semiempirical relationships (Tiuri and Sihvola 1986). We used the snow fork to measure density and liquid water content (wetness) at 5 cm (2.0 in.) depth intervals in the sidewall of the pits dug through the snow down to the terrain surface. Note that, unlike the Denoth meter, the snow fork does not require an additional density observation. However, similar to the Denoth meter, observations within 5 cm (2.0 in.) of the ground will be influence by the ground conditions and should be interpreted with caution.

3.3.5 NIR photography

NIR photographs were taken with a Canon DSLR camera that was modified to capture broadband light and was outfitted with an 800–1100 nm filter on the lens. At these wavelengths, the snow's reflectance significantly depends on grain size and microstructure (Matzl and Schneebeli 2006). This technique allows mapping of the stratigraphic layers identified in snow pits.

3.3.6 GPR

A Sensors & Software Inc. 1 GHz GPR was operated in the virgin snow, vehicle belly drags, and tire ruts during the Montana field work. A broadband wave pulse is transmitted by the GPR into the snow and echoes from stratigraphic layers within the snow and the snow-ground interface. The reflected energy (echoes) are sensed by the receiving antenna and digitized to create the GPR image. The transmitting and receiving antennas are

housed independently such that the horizontal separation (offset) between them can be varied. The antennas were placed on the snow surface, and their offset was expanded incrementally to a maximum separation of 2 m. The travel times associated with the GPR wave reflection off of the snow-ground interface measured at the various offsets are used to estimate the dielectric constant of the snow. Similar to the function of the Finnish snow fork, the dielectric permittivity is related to the snow density, which can be used as a proxy for snow strength. We have not fully evaluated data from the GPR at this time.

3.3.7 Nadir spectral reflectance

We took field spectral measurements using an ASD manufactured by Malvern Panalytical Ltd (Figure 18). Reflectance measurements from 350 to 2500 nm with 3–8 nm of spectral resolution were collected at target locations on a variety of surfaces, including asphalt, ice, packed snow, and fresh natural snow. A 5-degree field of view foreoptic was used. The spectral signature from a given surface at nadir (i.e., the ASD probe pointed vertically down at the surface) and the spectral signature at nadir from a white Spectralon reference plate were measured at each site. The spectral reflectance was calculated by dividing the surface measurement by the reference standard measurement.

Figure 18. ASD taking a datum measurement in Michigan.



3.3.8 Satellite imagery

This project used Digital Globe's WorldView-2 and -3 (WV2 and WV3) satellite imagery to study the different winter surfaces. WV2's 8 multispectral bands range from 0.4 to 1.04 μm and are typically used for vegetation, coastal, and land-use mapping (Kruse 2015). WV3 senses the same 8 multispectral (MS) bands as WV2 plus 8 shortwave infrared (SWIR) bands ranging from 1195 to 2365 nm and 12 clouds, aerosols, vapors, ice, and snow (CAVIS) bands ranging from 405 to 2245 nm (Table 4).

Table 4. WV3 sensing bandwidths (DigitalGlobe 2012, 2014).

Band	Description	Wavelength (nm)
Panchromatic*		450–800
MS1*	Coastal	400–450
MS2*	Blue	450–510
MS3*	Green	510–580
MS4*	Yellow	585–625
MS5*	Red	630–690
MS6*	Red Edge	705–745
MS7*	NIR1	770–895
MS8*	NIR2	860–1040
SWIR1		1195–1225
SWIR2		1550–1590
SWIR3		1640–1680
SWIR4		1710-1750
SWIR5		2145–2185
SWIR6		2185–2225
SWIR7		2235–2285
SWIR8		2295–2365
CAVIS1	Desert Clouds	405–420
CAVIS2	Aerosol 1	459–509
CAVIS3	Green	525–585
CAVIS4	Aerosol 2	635–685
CAVIS5	Water 1	845–885
CAVIS6	Water 2	897–927
CAVIS7	Water 3	930–965
CAVIS8	NDVI SWIR†	1220–1252
CAVIS9	Cirrus	1365–1405
CAVIS10	Snow	1620–1680
CAVIS11	Aerosol 1	2105–2245

* Indicates bands included in WV2. WV2 has a panchromatic band (~0.46 m resolution at nadir) and 8 multispectral bands (~1.85 m resolution at nadir). WV3 has a panchromatic band (~0.31 m resolution at nadir), 8 multispectral bands (~1.24 m resolution at nadir), 8 SWIR bands (~3.70 m resolution at nadir), and 12 CAVIS bands (~30 m resolution at nadir).

† NDVI = Normalized Difference Vegetation Index; SWIR = Short Wave Infrared

These CAVIS bands help to mitigate effects caused by the atmosphere, and the SWIR bands allow for a closer look at surface materials that present unique reflectance and absorption features (Longbotham et al. 2014). WV3 also has higher spatial resolution than WV2, as indicated in the footnote of Table 4 (Digital Globe 2014).

TSX is not optical imagery but is an X-band radar imaging system. TSX satellite acquisitions were collected at the highest spatial resolution (~0.25 cm [~0.98 in.]), resulting in a single horizontally polarized backscatter image.

CRREL requested remote imagery for both WV3 and TSX during the on-site collections. Over the course of this study, one WV2 and two WV3 collections were acquired from Digital Globe. The WV2/WV3 collections took place on 24 February 2018 (Montana) and 26 February and 16 March 2018 (Michigan). TSX satellite imagery collections took place on 27 January 2018 (Montana) and on 21 February 2018 (Michigan). All satellite imagery was geographically referenced, and the WorldView images were atmospherically corrected.

3.4 Data analysis

We analyzed the mechanical and physical properties and the WorldView data for correlations, analysis of variance, and statistical tests by using R 3.4 (R Core Team 2017). Nonparametric statistical methods were used due to the nonnormality of data typical of some measurement techniques. These include Spearman rank correlation, Kruskal-Wallis one-way analysis of variance, and the Conover-Iman test (Conover and Iman 1979). Linear regression models were built for some log-transformed measurements. Table 5 lists the snow measurements and their units. Appendix D provides tabular summaries of the data.

Table 5. List of snow characterization parameters used in this study.

Parameter	Units	Description
CBR	%	Field California Bearing Ratio
CBR 2.25 kg	%	California Bearing Ratio from 2.25 kg Clegg
CBR 0.5 kg	%	California Bearing Ratio from 0.5 kg Clegg
Clegg 2.25 kg	CIV	Clegg Impact Value from 2.25 kg Clegg
Clegg 0.5 kg	CIV	Clegg Impact Value from 0.5 kg Clegg
Ram	kgf	Ram Index (*R*)
RSP	kgf	RSP Index (*R*)
Pocket Pen.	kg cm^{-2}	Pressure from pocket penetrometer
LWD ISM	kips/in.	LWD ISM at four load levels (LL): LL1, LL2, LL3, and LL4
Shear Vane	kPa	Shear stress at the surface and in virgin snow profiles
CTI	CTI	CTI snow compaction gauge
Reflectance Value		The fraction of incident light reflected by a surface, a unitless number (Shaw and Burke 2003)
Snow Density	g/cm^3	Snow density for the top 5 cm and/or average for the depth of snow at the site
Air Temperature	°C	Ambient air temperature at the time of testing
Snow Temperature	°C	Temperature of the snow at various depths
Snow Moisture	%	Percent by volume
Snow Depth	cm	Depth of the snow layer
Yamaha Drop Cone	cm	Penetration into snow when dropped from 10 in. height

4 Results and Discussion

4.1 General site conditions

Numerous statistics were calculated to generate information on the general site conditions and to determine which strength measures correlated to standard techniques and to concurrent satellite data. The MagnaProbe was easy to use and produced transects of virgin snow depth across the sites quickly to give an indication of how the snow depth varied. The data were naturally scattered as snow is a highly variable material. Snow depth and snow-surface type are given in Figure 19 for Michigan and in Figure 20 for Montana. Appendix C includes graphs of the temperature and density profiles (and liquid moisture, if any) for each of the sites.

Figure 19. Snow depth and type by site in Michigan.

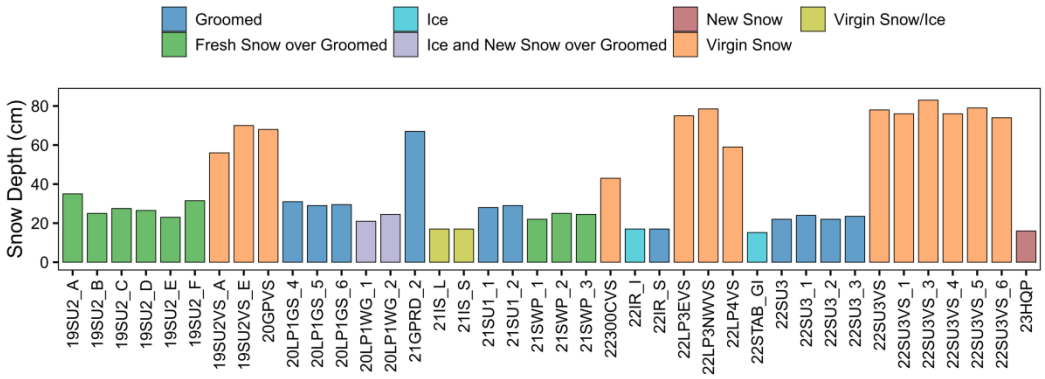
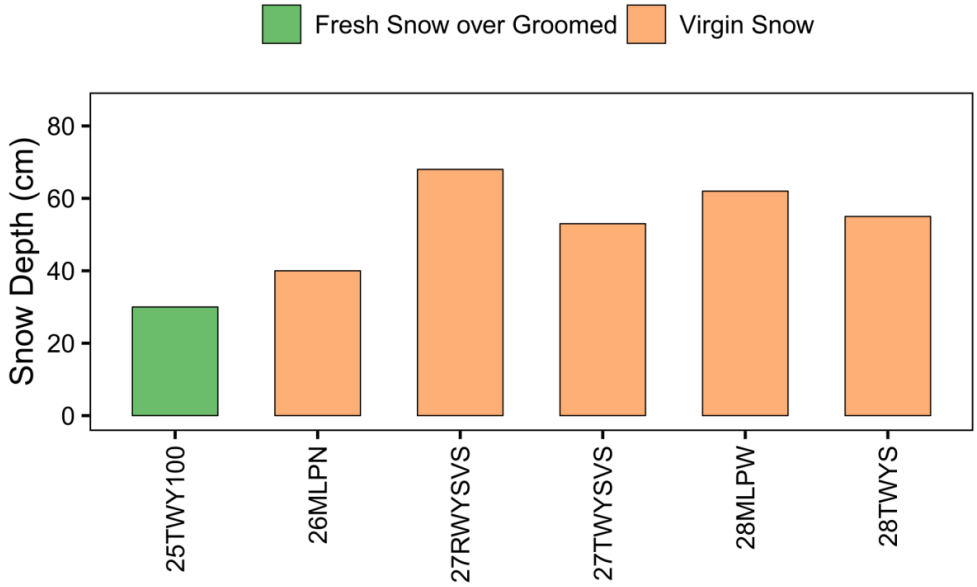
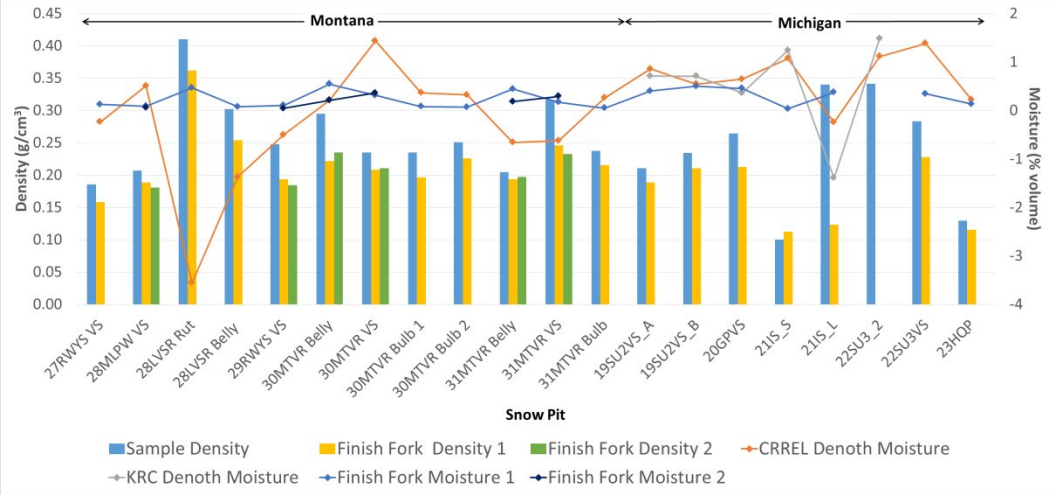


Figure 20. Snow depth by site in Montana.



Snow moisture and density were measured in side-by-side measurements by using the Finnish fork, the Denoth meter, and densities from samples collected in numerous snow pits in both Montana and Michigan. We also performed a laboratory experiment for side-by-side measurements of several Denoth meters with the Finnish fork and sample measurements. Figure 21 shows a sample of the comparison of the density and moisture measurements for a variety of snow pits in both Montana and Michigan.

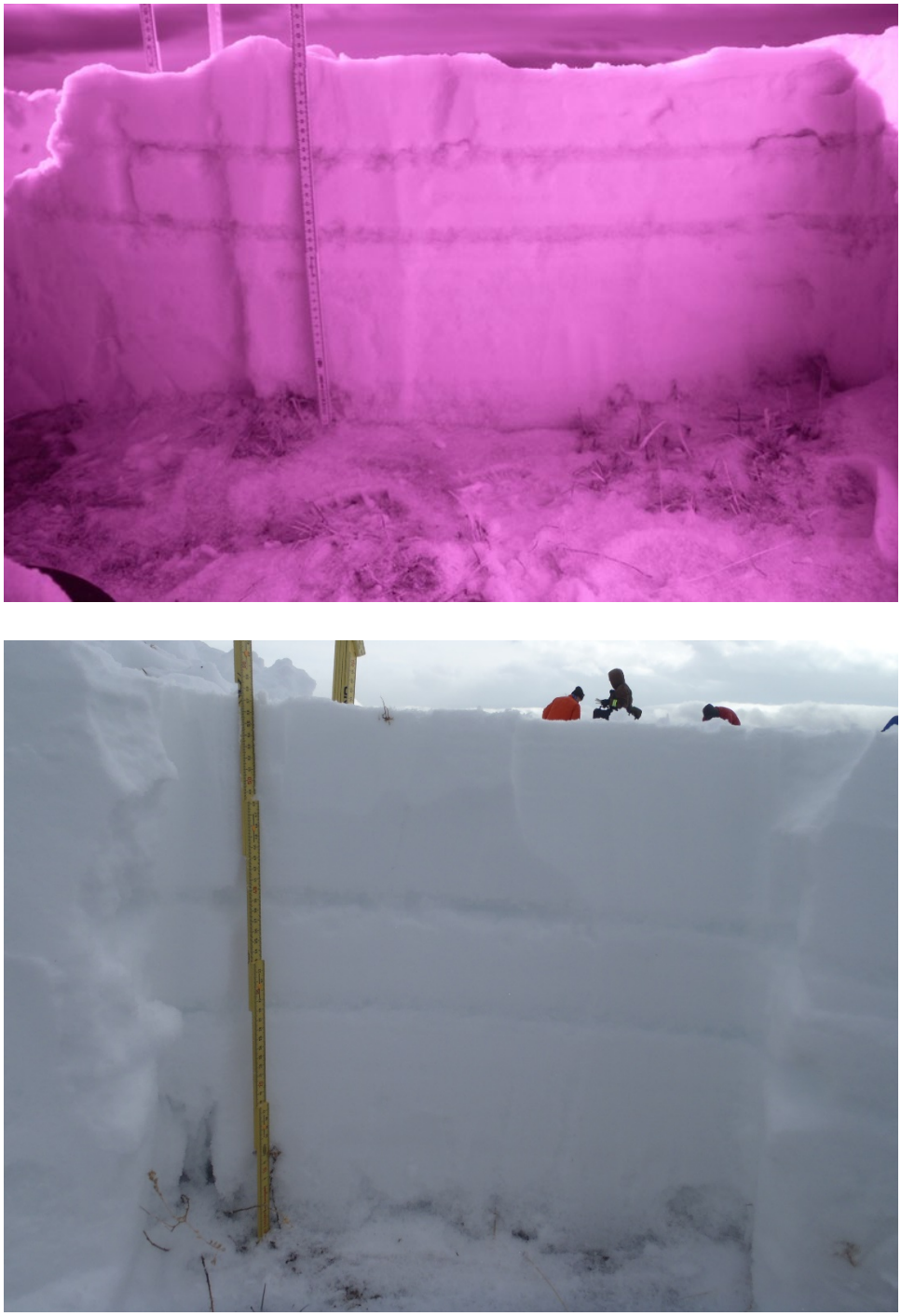
Figure 21. Finnish fork density and moisture compared to sample density and Denoth moisture in different snow pits.



In general, we found good consistency between the snow moisture (liquid water content) measured with the Finish fork and the Denoth meters and consistency between different Denoth meters. We also found that the density measured with the Finish fork tended to be lower than density from collected samples but was unreliable when the snow was wet. Feyrer et al. (2018) completed a preliminary analysis of the full field data set and associated laboratory experiments, reported in the poster in Appendix E. Elder et al. (2019) presents a more thorough analysis.

Figure 22 illustrates NIR photos of a snow pit wall. These photos demonstrate the ability of NIR photography to show different layers within the snow. NIR is sensitive to snow grain size and can be used to estimate snow's specific surface area and to document stratigraphy.

Figure 22. NIR photo (*top*) and standard photo (*bottom*) of Montana snow pits walls.



4.2 Snow-strength measurement techniques

Many types of strength measurements were used at each site. Some were better suited for soft snow and others for groomed snow, so not all techniques were used at each site. In addition, some are profile measurements that characterize the snow strength with depth. These are not necessarily

well suited for reducing to a single number as the benefit of the information is to capture the details of the entire snow profile. Figure 23 and Figure 24 compile the strength measurements for the sites at Michigan and Montana, respectively. These plots illustrate the variability at each site and how the strength may be further explored by snow-surface type, as shown in Figure 25 and Figure 26.

Where measurements were collected from multiple surface covers, some differences in strength emerged. In Michigan, there were significant strength differences detected ($p < 0.05$) between surface covers when using the 2.25 kg Clegg, CTI, ISM load levels 2 and 4, and Rammsonde (ram) (Figure 25). In Montana, only the 0.5 kg Clegg could distinguish significant strength differences between the surface types (Figure 25). Statistical power was largely limited by the low sample size between surface cover types. Increasing the sample size using strength measurements that function well across different surface types would likely reveal more robust strength relationships.

This type of information, along with further analysis of the data collected in this study, will allow us to optimize the data collections to better suit the snow cover and to tune the strength collection equipment for use in snow (see also Shoop et al. 2019a).

It was apparent that the strength measurement techniques could be grouped based on their suitability to certain snow types.

Table 6 provides an initial assessment of the effectiveness of each of the techniques for use on different types of snow and ice covers. In some cases, a particular instrument was neither good nor bad but completely unsuited to a particular snow type. For example, the RSP usually dropped through virgin snow without a single reading until it hit the underlying ground surface. Other instruments would specifically benefit from modifications for use in snow: plate sinkage, which requires sturdier construction and less complicated wiring, and shear vanes, which would benefit from modified vane sizes tailored to varied snow surfaces.

Figure 23. Boxplots of each snow-strength measurement technique by study area for the Michigan site.



Figure 24. Boxplots of each snow-strength measurement technique by study area at the Montana site.

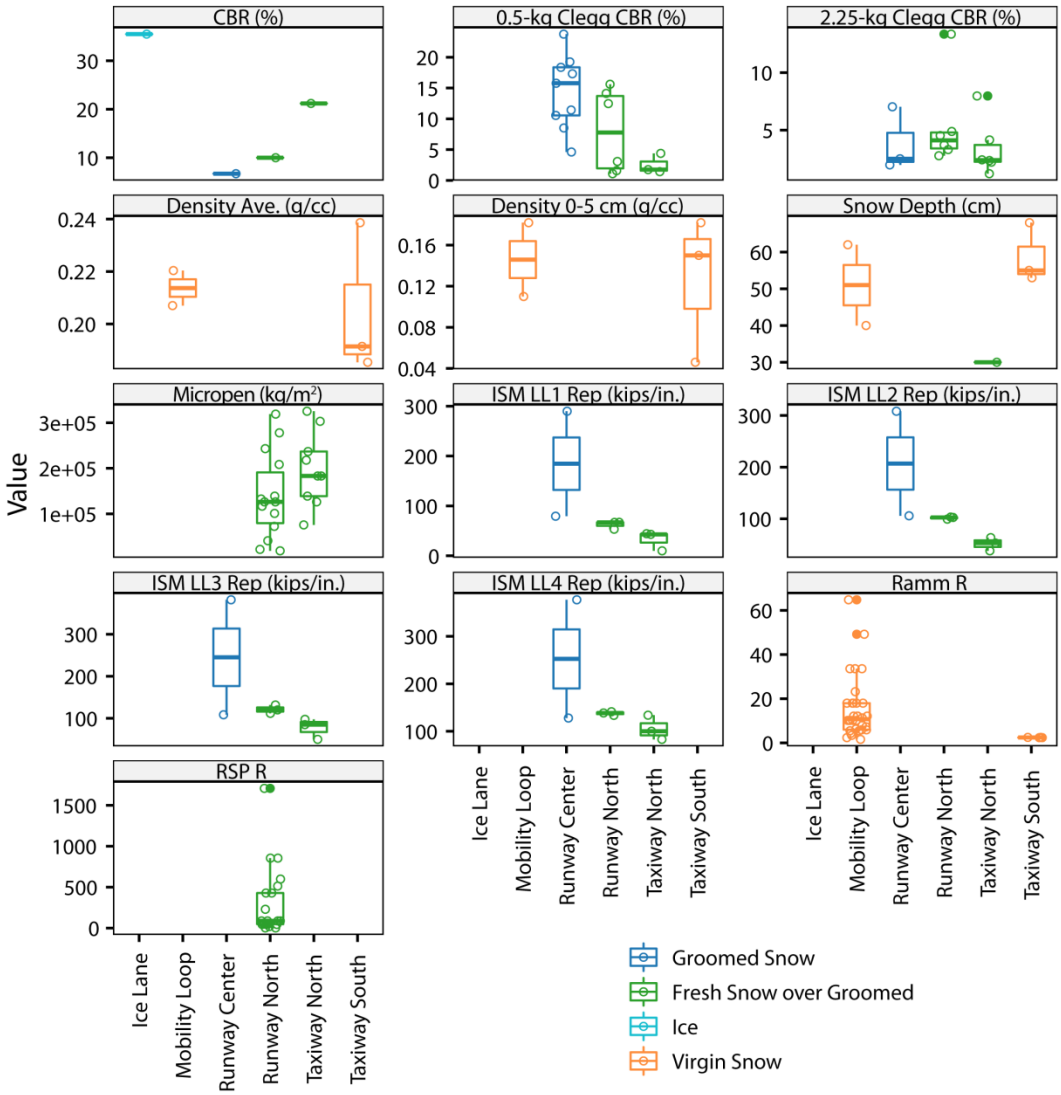


Figure 25. Boxplots of each snow-strength measurement technique by surface type in Michigan. The *p*-values are for Kruskal-Wallis analysis of variance.

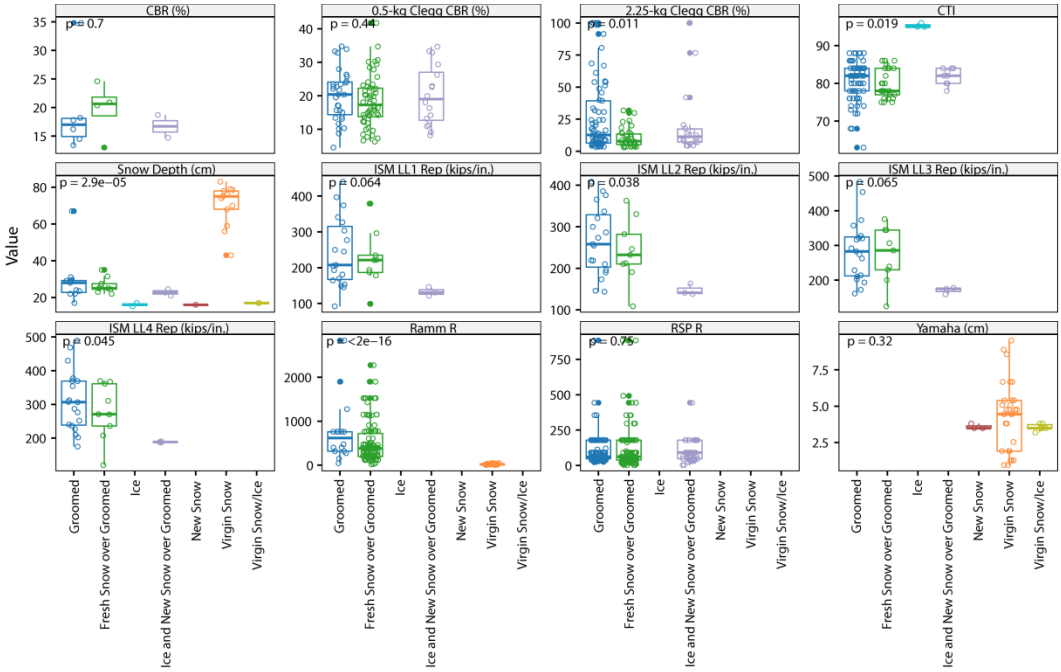


Figure 26. Boxplots of each snow-strength measurement technique by surface type for Montana. The *p*-values are for Kruskal-Wallis analysis of variance.

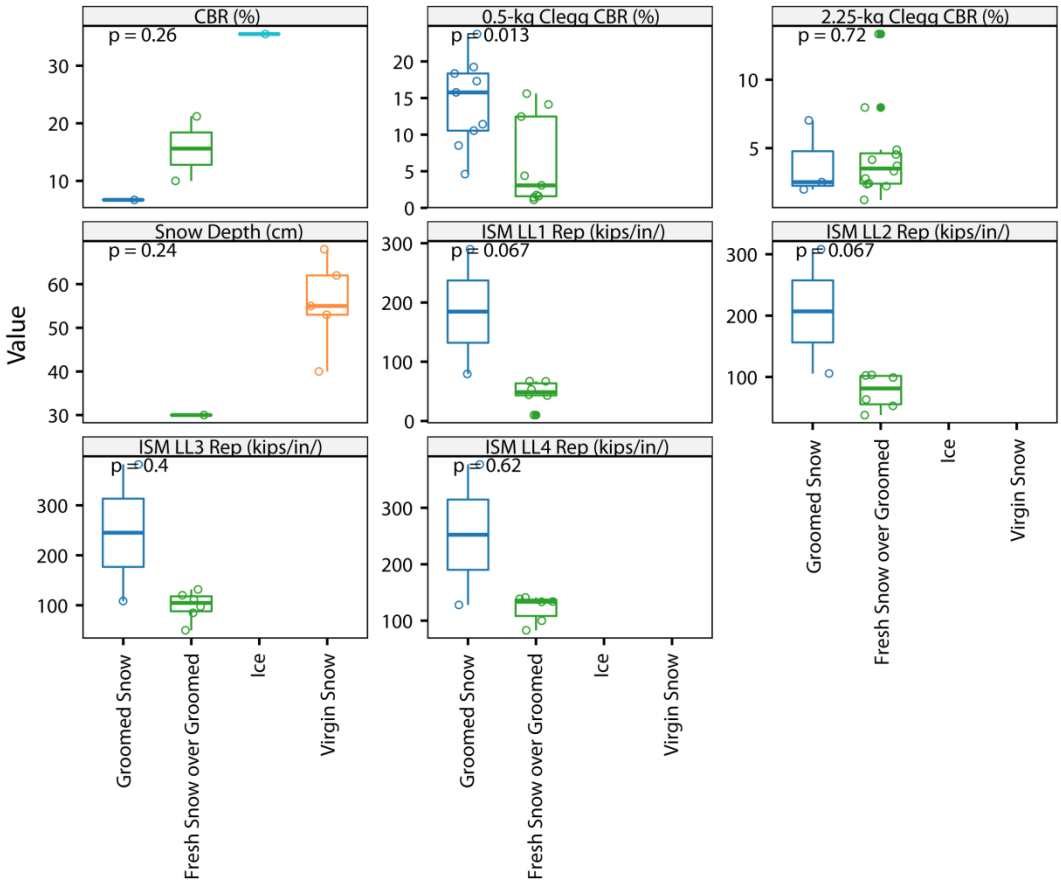


Table 6. Effectiveness matrix of field tests as rated by operators (1 = good, 5 = bad).

Instrument		Snow-Surface Condition					
		Hard Groomed Snow	Medium Groomed Snow	Fresh snow Over Groomed	Virgin Snow	Wind Crust	Ice Layers
Penetrometers	SMP	unsuitable	5	1	1	1	1
	Ram	3	2	3 or 4	3 or 4	not used	unsuitable
	RSP	1	1	not used	unsuitable	not used	not used
Bearing Capacity	Field CBR	1	2	unsuitable	unsuitable	not used	1
	LWD	4	4	1	unsuitable	not used	2
	2.25 kg Clegg	2	3	5	unsuitable	not used	unsuitable
	0.5 kg Clegg	2	2	2	1 to 5	not used	unsuitable
	Plate Sinkage 6 in.*	not used	not used	not used	2	not used	not used
	Plate Sinakge 12 in.	not used	not used	not used	5	not used	not used
MicroTools	Snow Plate Penetrometer	5	5	3	5	1	5
	Pocket Penetrometer	3	2	5	5	2	1
	Shear Vane	3	2	5	5	5	5
	Yamaha Drop Cone	5	3	2	1	3	4
	CTI	1	1	5	5	not used	not used

* Prototype unit with additional 5, 7, 9, 10, and 11 in. diameter plates.

4.2.1 Snow-strength profile data

Several of the snow measurements collect data within the snow cover as a function of depth. The most basic of these are the snow density, moisture content, and stratigraphy. We also collected snow strength with depth using the ram, the RSP, and the SMP. Each of these instruments was designed for a specific application. The ram CRREL used in this study was designed with a smaller tip for use on snow roads and airfields in Antarctica and Greenland. The RSP was designed by the Russians for groomed snow runways. The SMP was designed to operate in light alpine snowpacks and to be sensitive to structural weaknesses within the snowpack for assessing avalanche hazards (Schneebeli and Johnson 1998). Figure 27 and Figure 28 provide examples of the data from the RSP in Michigan and the SMP in Montana. Much of the profile data were averaged into layers for future analysis.

Figure 27. RSP hardness profiles from Michigan.

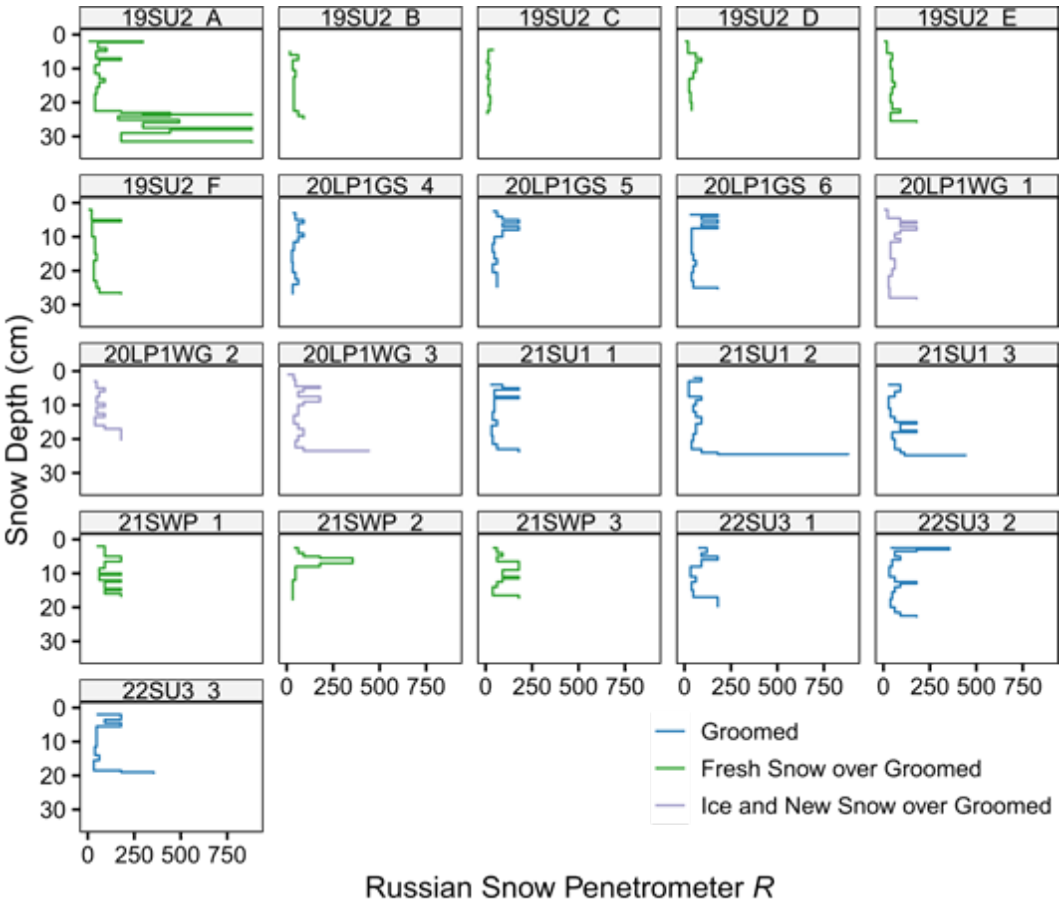
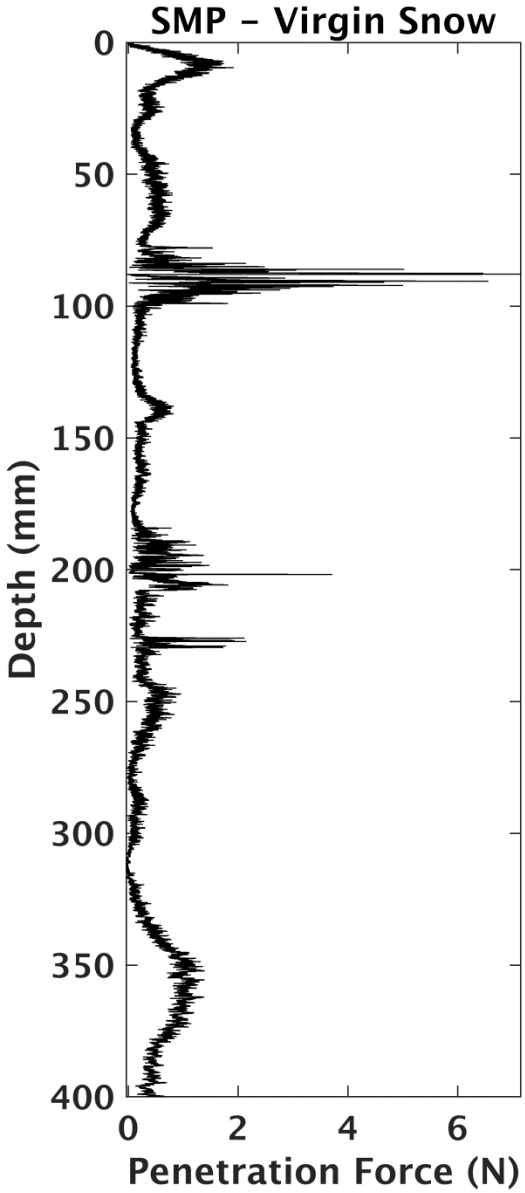


Figure 28. SMP profile from virgin snow in Montana.



4.2.2 Strength of groomed snow surfaces

Field CBR measurements are used to compare in situ strength to design parameters for roads and airfields. While this methodology is being replaced by mechanical design methods, CBR methods are still in use within the Department of Defense. Published data for true field-measured CBR for snow and ice surfaces are practically nonexistent; therefore, we performed these field CBR tests in both Michigan and Montana. Figure 29 and Figure 30 summarize the CBR measurements colored by surface type.

Figure 29. Measured CBR by site in Michigan.

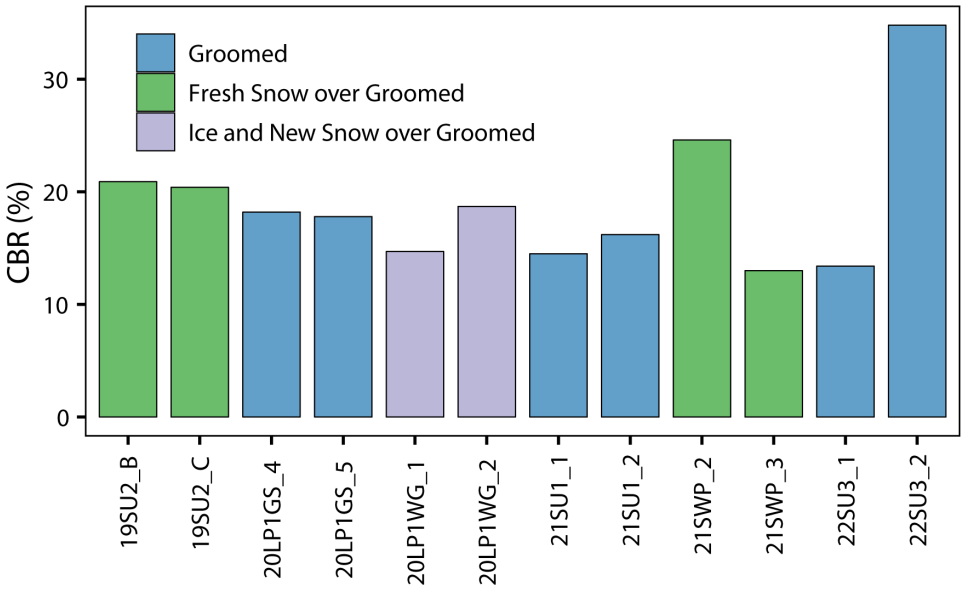
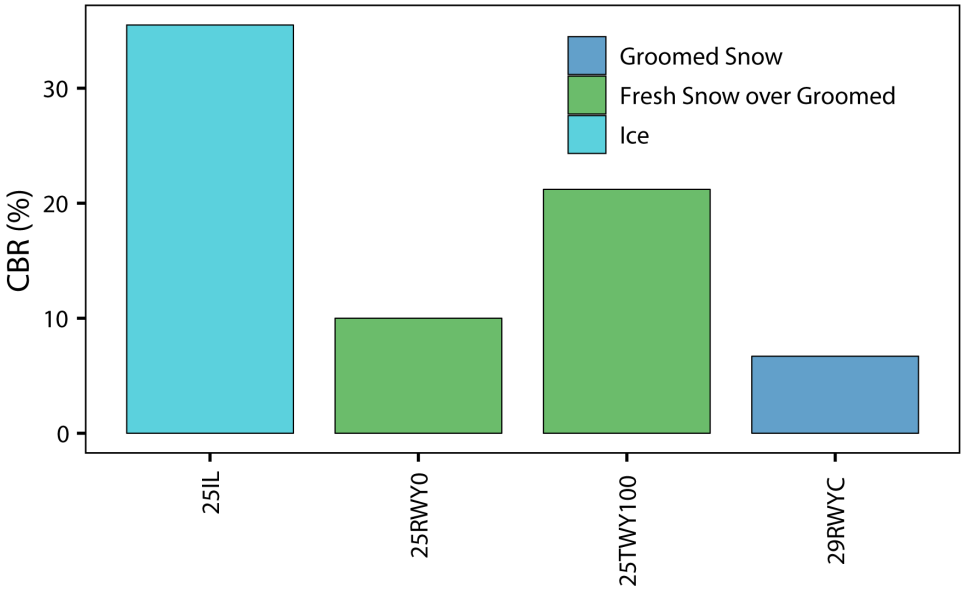


Figure 30. Measured CBR by site in Montana.



The two Cleggs proved efficient for assessing snow surfaces, being both easy to operate and quick. While the 0.5 kg (1.1 lb) Clegg was useful for many of the virgin and packed snows, the 2.25 kg (5 lb) Clegg was the most useful for a wide range of packed-snow surfaces (but not ice, which was out of the instrument range). Figure 31 and Figure 32 give the overall results for 2.25 kg Clegg measurements converted to CBR, showing the average and standard deviation by site, colored by surface type.

Figure 31. Mean site surface CBR calculated from 2.25 kg Clegg Impact Values in Michigan. Error bars are ± one standard deviation.

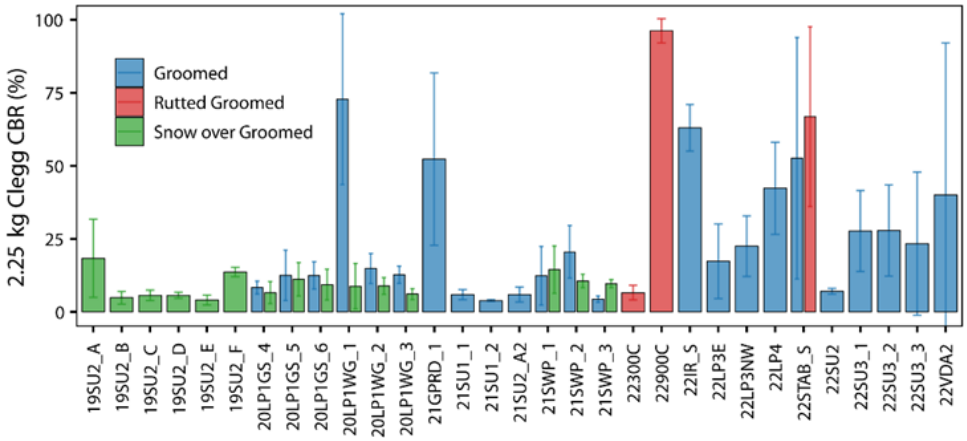
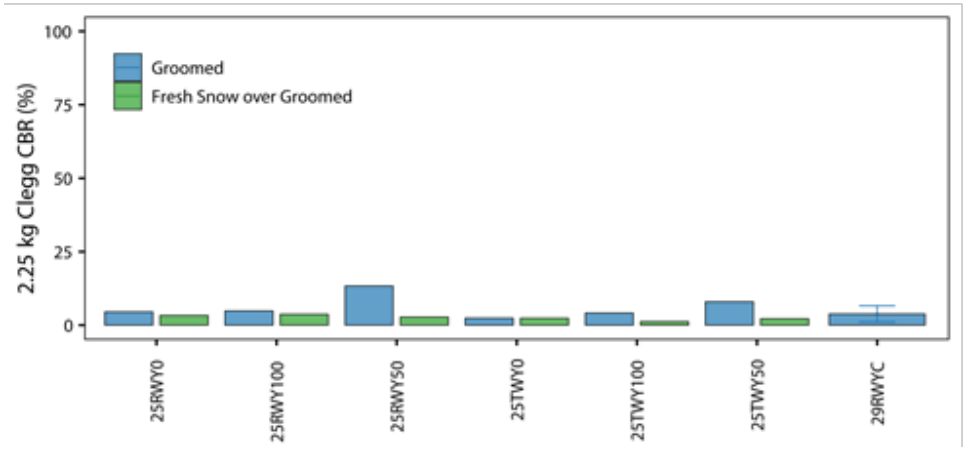


Figure 32. Mean site surface CBR calculated from 2.25 kg Clegg Impact Values in Montana. Error bars are ± one standard deviation.



The LWD was also used on groomed snow but left large indentations on many of the groomed snow surfaces, indicating that it was continuing to compact the snow under the impact of the test sequence. Wieder et al. (2019) analyzes the LWD more thoroughly.

Photos of the underlying ground conditions, shown in Appendix B, raise an important concern for groomed surfaces and may explain some of the outlier measurements for the Clegg and CBR measurements from Michigan shown in Figure 29 and Figure 31 (the groomed snow in Montana was generally over paved surfaces). If the ground surface is uneven, from either vegetation or ruts made by vehicles on an aggregate- or soil-surfaced road, then as the snow is groomed, it will most likely vary in depth and density. If test equipment with a small foot print, such as the Clegg, is placed over a high point on the underlying ground surface, we could feasibly measure a

higher value due to the influence of the nearby frozen ground, and yet the groomed snow surface is visually uniform.

Additionally, some test points in Michigan, were close to trees and other vegetation that cast shadows during parts of the day. The difference in snow strength due to difference in temperature and sun exposure could impact snow strength.

In further investigations of measures of snow strength, the corresponding depth, temperature, and density of the snow layer being tested need to be more thoroughly quantified, especially for the groomed snow surfaces. For bearing tests (i.e., CBR, Clegg, and LWD), the measurement depth, or depth of influence, varies depending on the surface contact area of the device. Knowing that the impact of the test may be deeper than the snow layer, thus penetrating into the ground surface below, would be of benefit. For the LWD, the backcalculation program requires the thickness, an initial estimate of modulus, and Poisson's ratio for each layer. Modulus and Poisson's ratio of snow both vary significantly with snow density. Wieder et al. (2019) discuss this further as it impacted the results of the LWD test the most. In Montana, the technique to measure density in the high-density groomed snow was not available, and the underlying surface was usually paved.

4.2.3 Correlation between strength measurements

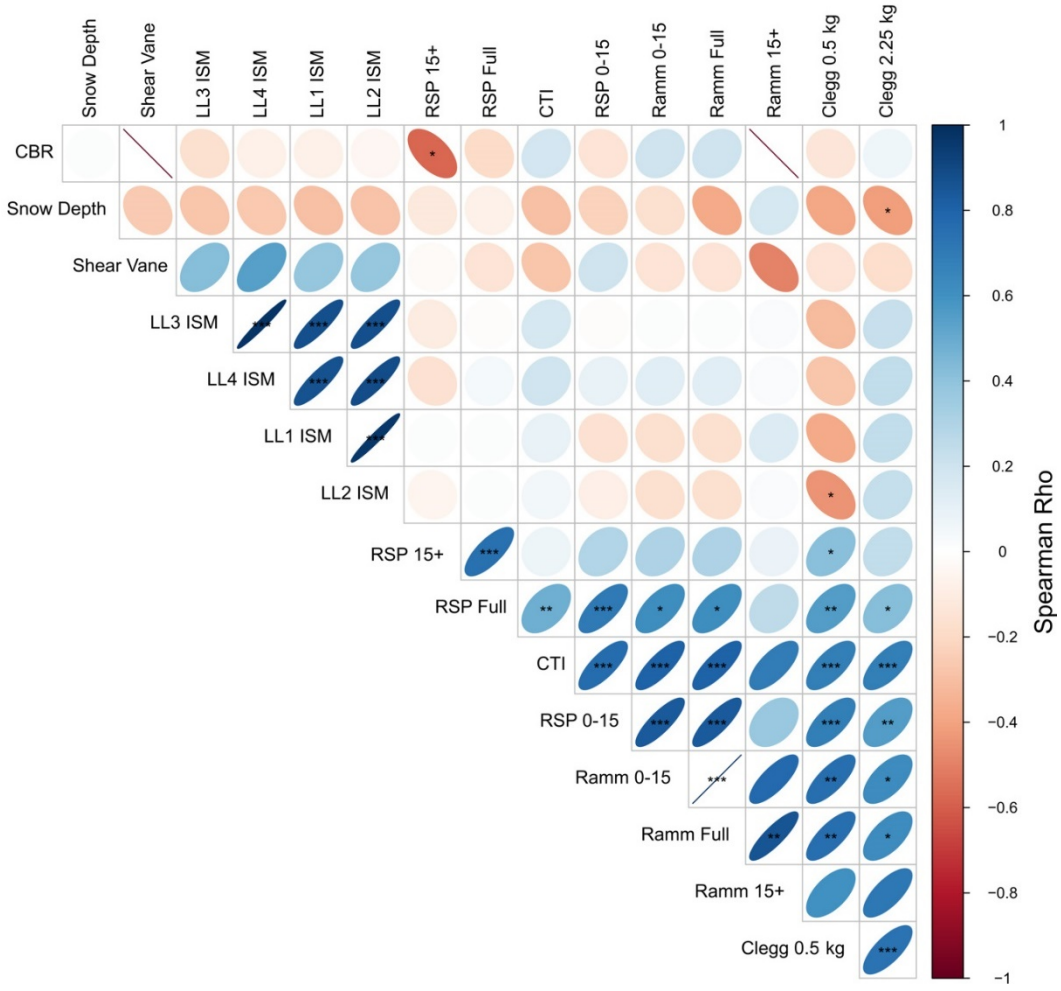
We also evaluated the strength measurements to determine which correlated with each other, as shown in the correlation matrix in Figure 33. Higher rho values are shown as darker colors and indicate a stronger correlation. The matrix indicates the following:

- Good correlations, $p < 0.01$, between the LWD ISM values at all four load levels. Further discussion of the implications of this is included in Wieder et al. (2019).

- Good correlations, $p < 0.01$, between CTI and the other surface measurements—both Cleggs and the RSP and ram averages that include the shallow readings (0–15 cm and full depth).

- Fair to good correlations, p varies from <0.1 to <0.01, between the near-surface RSP, near-surface ram, and both Cleggs.

Figure 33. Spearman correlation matrix of measured snow properties with $n > 1$ comparative observations. LWD ISM values listed are representative (averages are nearly identical). The p-values are indicated as * < 0.1, ** < 0.05, and *** < 0.01.



Bearing-strength measurements were also correlated to calibrate strength measurements to the traditional field-measured CBR. While many of these correlations are poor, a few show expected trends, such as the Clegg's CIV (Figure 34).

There were a couple other correlations of note:

- A positive trend exists between the CTI snow compaction gauge and the 0.5 kg Clegg CIV (Figure 35). Both are tools that are very light and engage only near-surface snow.
- The RSP and the 2.25 kg Clegg CIV trend similarly, both of which are tools for stronger surfaces (the RSP is used for groomed snow air-fields), Figure 36.

Figure 34. CIV versus field CBR.

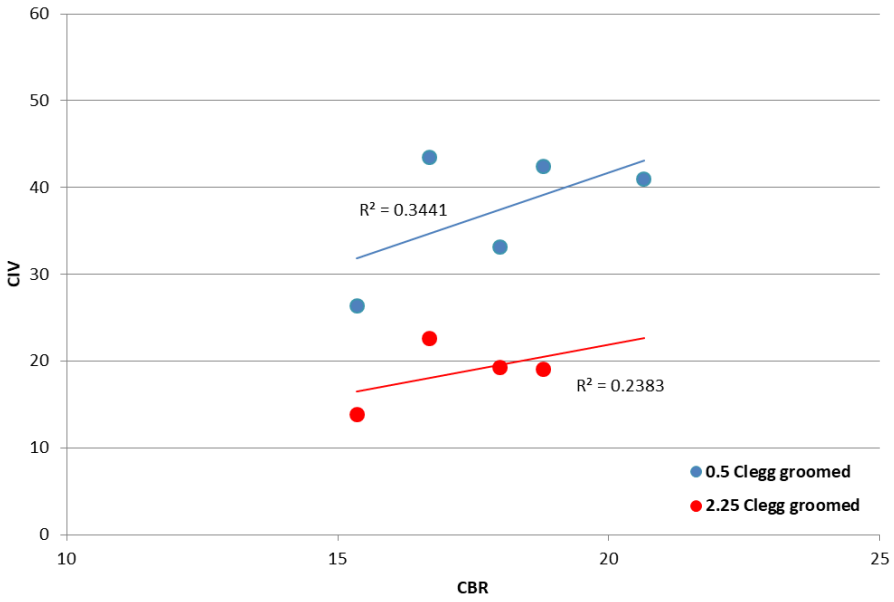


Figure 35. CTI versus 0.5 kg Clegg CIV.

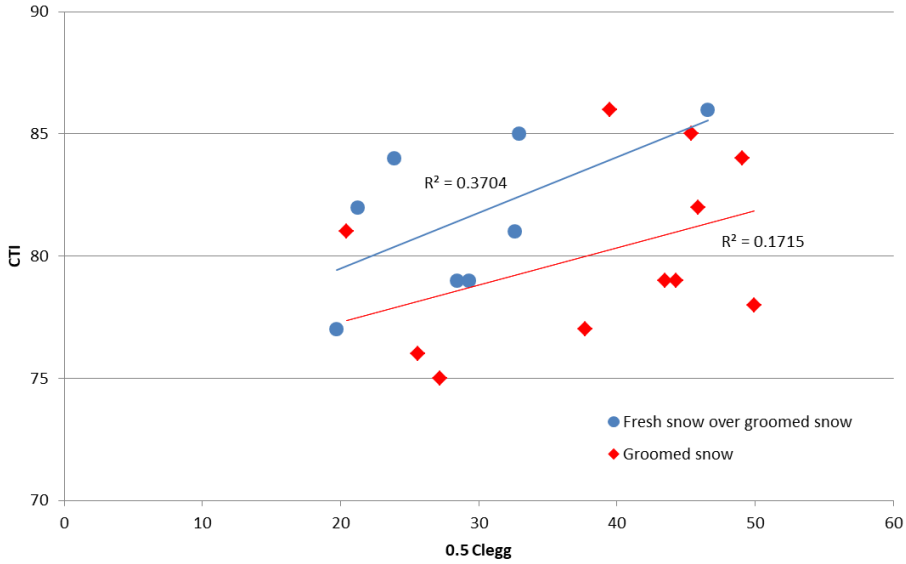
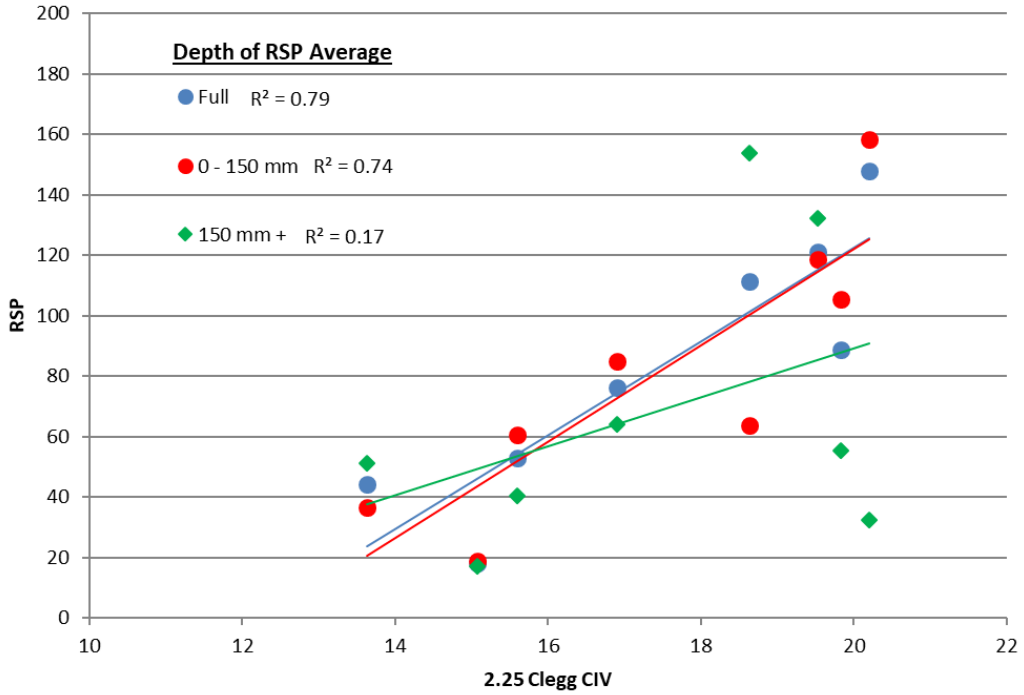


Figure 36. RSP versus 2.25 kg Clegg CIV.



4.3 Spectral measurements

4.3.1 WV2 and WV3 satellite imagery

One of the key objectives of the field campaigns was to explore the relationship between snow mechanical properties and remotely sensed data by using concurrent imagery collected by the WV2 and WV3 satellites. The WV satellite images from Montana were excessively cloudy, but the Michigan images were clear and were further analyzed based on snow-surface type and also compared to strength. The WV2 and WV3 satellites use optical sensors operating in the visible through infrared portion of the electromagnetic spectrum. The sensors measure reflected solar energy from snow or ground surfaces and not from any buried stratigraphic layers.

The spectra for the 9 pixels surrounding each measurement site (5.5 × 5.5 m [18 × 18 ft] on the ground) were collected from the image and assembled in Figure 37. The data in Figure 37 are from WV3 imagery taken on 26 February 2018. The test-point surfaces are described as they were found on the day of the ground testing at each test point, 19–22 February 2018. The colors represent the different types of surfaces:

- Clear pavement—in this case asphalt concrete
- Groomed snow—snow that, either over a road, pavement, or open area, had been groomed by plows or other equipment
- Fresh snow over groomed snow—a surface that had received new snowfall over a previously groomed snow layer
- Ice—ice surfaces specifically prepared for vehicle testing
- Ice with new snow cover over groomed snow—testing specific to a day with freezing rain and snow, which overlaid the previously groomed snow surface
- New snow—an area previously cleared with only recent snowfall accumulation
- Virgin snowpack—snow that had not been disturbed by vehicle traffic, the accumulation of season's snowfall

These spectra were further averaged by snow type and displayed to show characteristic WV3 spectra for each surface type in Figure 38. Appendix F provides additional data from the satellite imaging.

For most of the spectra, we noticed a dip in the values at 550 nm (green band) that should not be there. This is especially prominent in Figure 38 but can also be seen in Figure 37. The reason for this is not clear, and it has not been reported elsewhere. It could be either due to an error in atmospheric correction processing or to the original data from the satellite. This same dip is not observed in the on-site ASD measurements taken 22 February 2018. The WV3 imagery was reprocessed with atmospheric corrections and different algorithms to recalculate the reflectance but again resulted in the same issue with the 550 nm wavelength. Potentially, the problem could be linked to issues with the satellite sensor. These are both being further explored.

Figure 37. WV2/WV3 reflectance spectra for each Michigan study area. Each line represents a site. The colors relate to the type of surface.

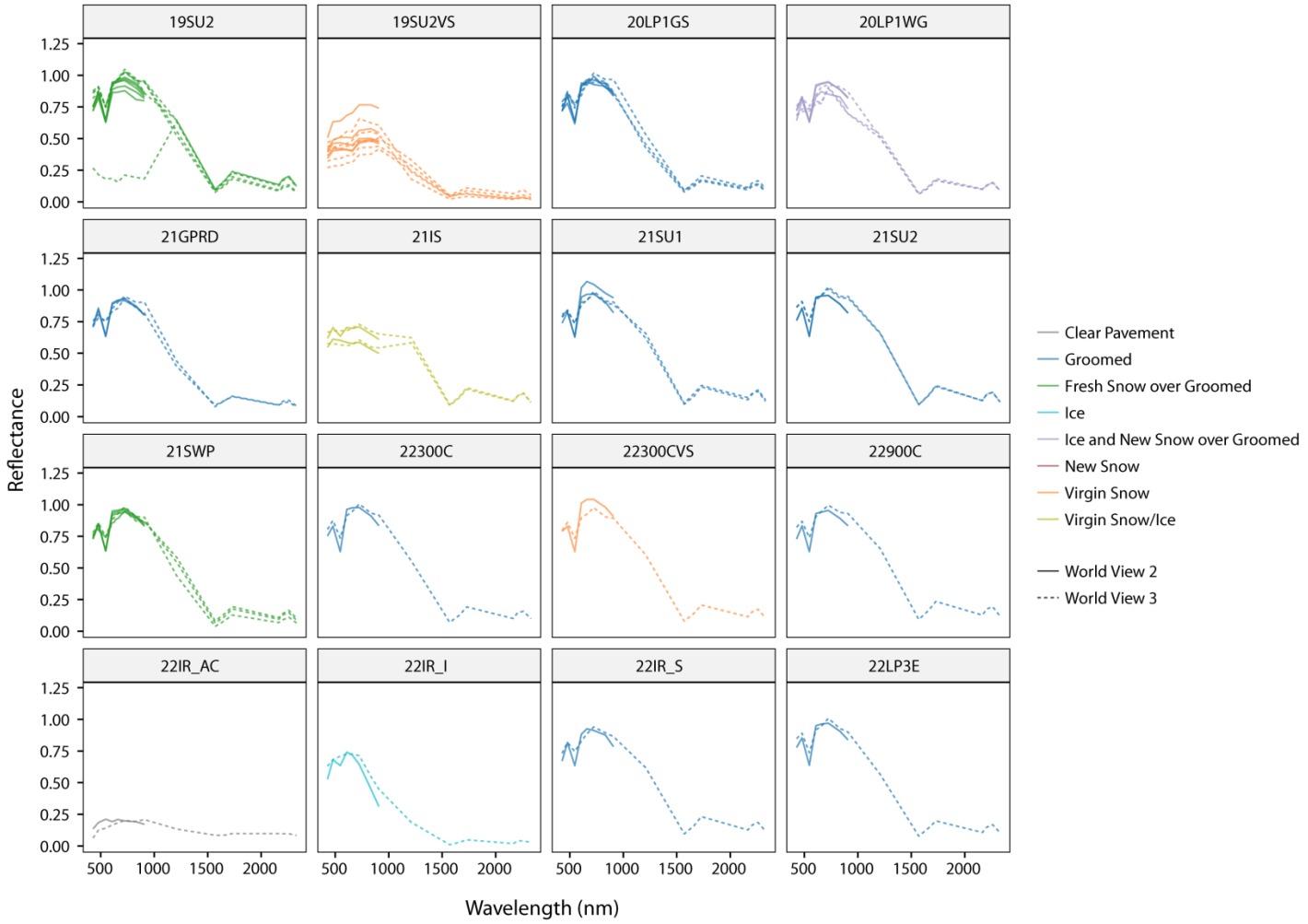


Figure 37 (cont.). WV2/WV3 reflectance spectra for each Michigan study area. Each line represents a site. The colors relate to the type of surface.

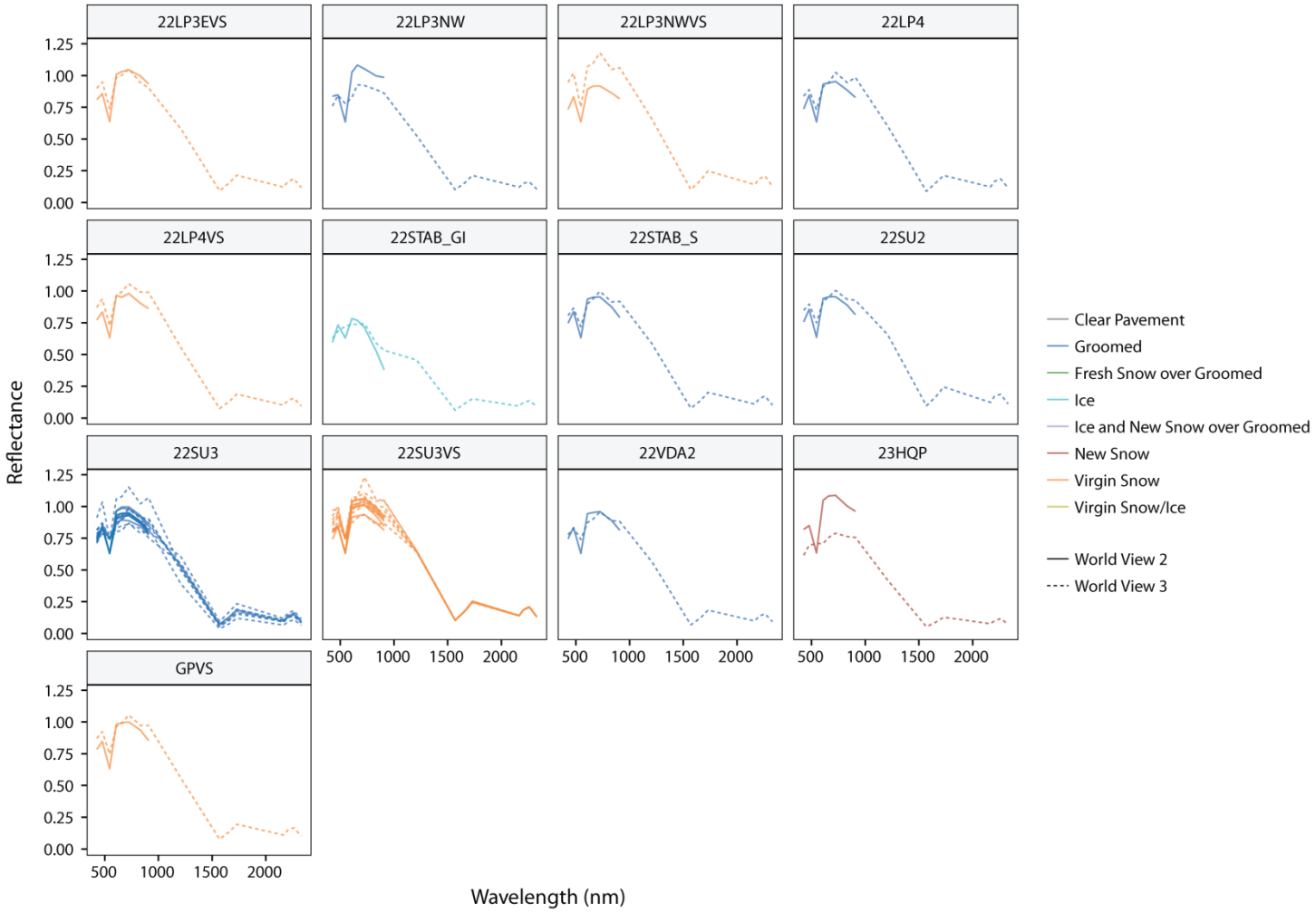
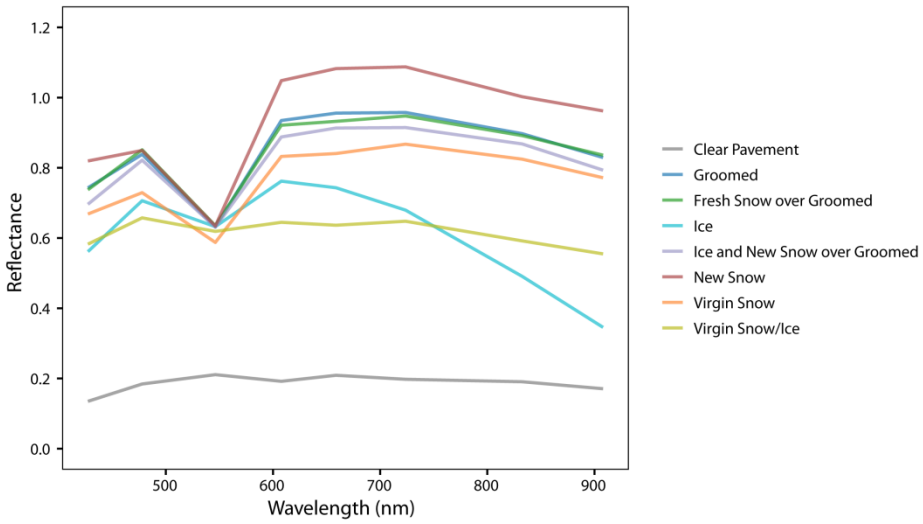


Figure 38. Michigan WorldView reflectance spectra averaged by surface type.



4.3.2 Satellite TSX imagery

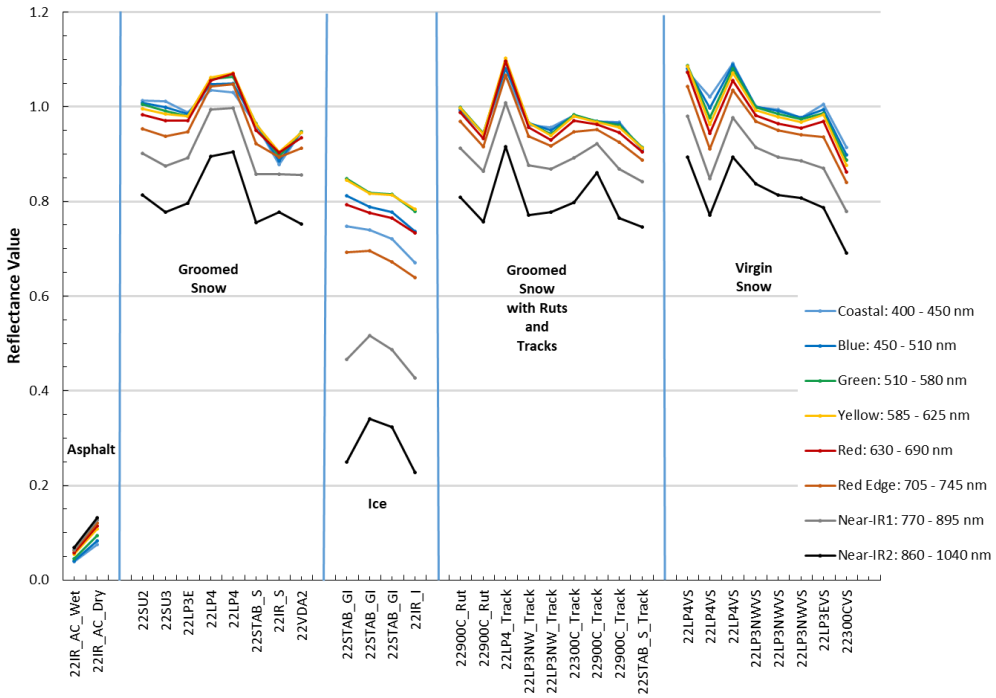
Despite the high spatial resolution of the TSX radar backscatter (X-band ~1 cm wavelength, 10 GHz frequency) allowing for general discrimination of tracked and untracked surfaces, the data appear limited by the integrated backscatter from surface roughness and volume (e.g., within snowpack) scattering. Further work will explore the benefit of multipolarization radar acquisitions (i.e., horizontal and vertical, as well as co- and cross-polarized products) toward a more quantitative relationship between radar backscatter and snow mechanical properties. The multipolarization mode of the TSX satellite has a spatial resolution limitation but may be able to separate surface versus volume scattering. Our 2019 TSX collections test this approach with larger prepared surfaces.

4.3.3 ASD field-measured reflectance

For most locations where snow properties and strength were measured, the nadir spectral reflectance of the surface was also measured using the ASD field spectrometer. Whereas the WV2 and WV3 data are discretized into bands of wavelengths, the ASD provides a more continuous waveform in 1 nm increments. The magnitude and spectral shape of the reflectance spectra are known to be related to surface snow grain size and wetness (Nolin et al. 1993; Painter et al. 1998, 2003, 2009); but how these change with surface metamorphosis and surface aging is an area of current research. We analyzed the reflectance spectra in a variety of different ways to determine if the different snow surfaces could be easily distinguished with noncontact

sensing. For simplification, we can parse these spectra into the same bands by averaging the reflectance within the wavelength intervals or bands of the WV2 and WV3 imagery. Figure 39 is a graph of the eight WV2 bands for all of the ASD measurements taken in Michigan on 22 February 2018, colored by surface type and showing general trends for the major winter surfaces of interest to vehicle mobility. Appendix G provides photo examples of the snow and ice surface conditions tested with the ASD.

Figure 39. ASD field spectrometer reflectance subsampled into the eight WV2 bands for asphalt, groomed snow, ice, and virgin snow surfaces in Michigan.



We can further look at the data in terms of the full suite of bands used in the newer WV3 satellite. Figure 40 shows the ASD spectra averaged into WV3 bands for a collection of virgin snow, groomed snow, ice, and asphalt surfaces. The asphalt, snow, and ice are clearly distinguishable, but the different types of snow surfaces are not distinguishable from one another.

Since some of the snow surfaces had been trafficked by vehicles, we also looked at the differences between the tracked and smooth snow surfaces. The tracked snow surfaces showed greater variability in reflectance due to the geometry of the tracks providing a variable nadir reflectance. The resulting variability is greater than that of groomed versus virgin snow.

Figure 40. Michigan ASD field spectrometer reflectance subsampled into the WV3 bands. *Red lines* are for asphalt, *purple* for ice, *blue* for groomed snow, and *green* for virgin snow. The panchromatic band is 450 to 800 nm.

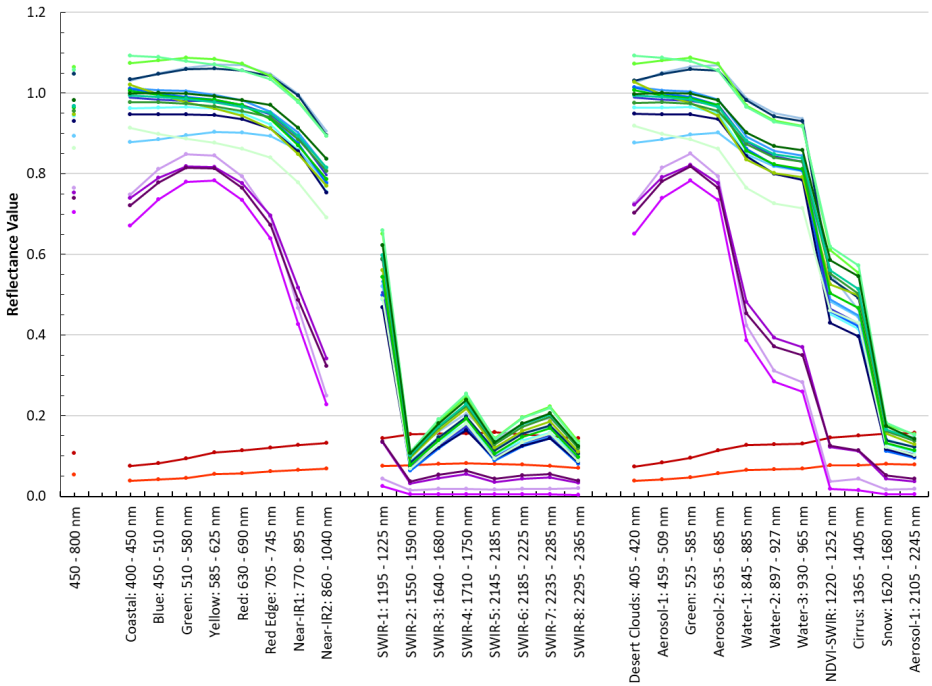
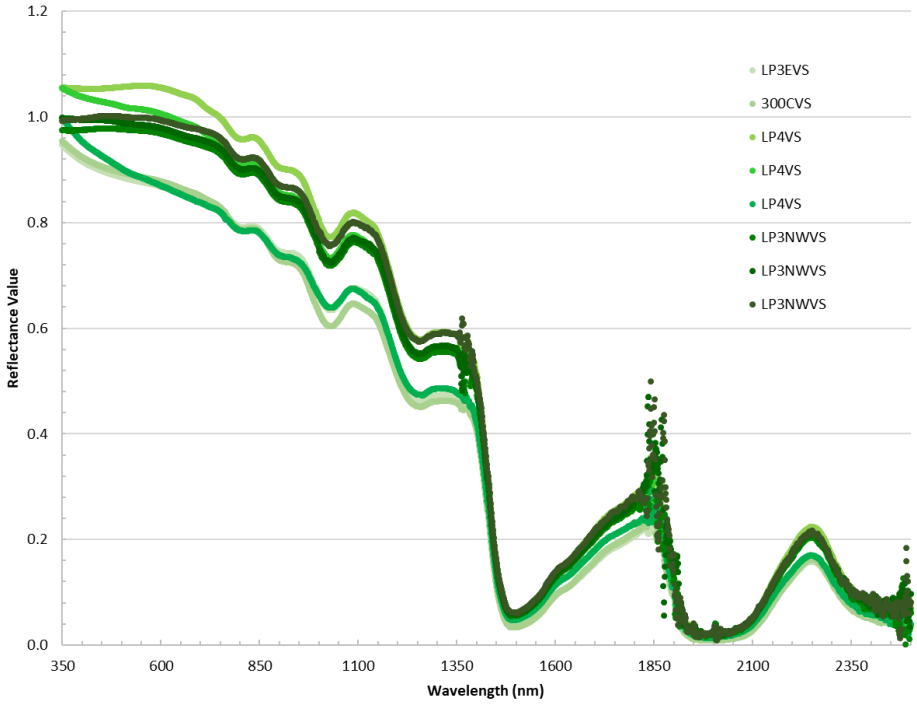


Figure 41 shows the analysis of the full spectral waveforms for all of the virgin snow spectra collected on a single day. All of these were measured within 2 hours of solar noon, and a white reference plate was used to measure incident radiation before and after each measurement and to correct the reflectance spectra. There is considerable scatter in these data from 350 nm to 1350 nm. The variability in the spectra are more than expected and are likely due to variations in cloud cover, which would impact the magnitude of the incident solar radiance. Over the course of the ASD testing, the cloud cover transitioned from cirrostratus clouds at the beginning of the measurement period to altocumulus clouds at the end of the measurements, as seen in the photos in Appendix G. Clouds can prevent some wavelengths from reaching the surface; therefore, the incident solar radiation signature changes as do the resultant reflectance values. In addition, the spectral shape at small wavelengths is inconsistent between the measurements, and some of the spectra display an upward or downward curve in the small wavelengths that is unlike a characteristic virgin-snow spectral shape (D. Perovich, CRREL, pers. comm., 2019). We will further explore these inconsistencies and fine-tune the collection and processing technique in the future. The spectra scatter at specific wavelengths of 1400, 1900, and 2500 nm is noise from small amounts of solar energy

reaching the Earth's surface at those wavelengths due to atmospheric water absorption (Wallace and Hobbs 1977).

Figure 41. Full spectra of the Michigan ASD reflectance from the virgin snow measurements.



Figures 42 and 43 show characteristic spectral shapes of the different surfaces. Figure 43 shows a more detailed view of the 800–1200 nm wavelengths to highlight that the groomed snow and virgin snow surfaces are not distinguishable even at the higher wavelengths. While the wet and dry asphalt and the smooth and grooved ice are clearly distinguishable, the groomed snow (blue lines) falls within the scatter of the virgin snow (green line) surfaces.

Figure 44 more clearly shows a representative spectra from a groomed snow surface (Spin Up Pad 2) falling directly within the range of those measured on virgin snow. This finding was unexpected. The upper wavelengths are expected to provide more insight into the type of snow surface as these higher wavelengths are more indicative of grain size (Nolin et al. 1993; Painter et al. 1998). The groomed surfaces consisted of uniform very-fine-grained snow crystals, packed and smoothed, and therefore have a higher reflectance value than the loose, newly fallen snow. The WV2 bands also did not distinguish between the groomed and virgin snow. This indicates that future analysis is needed to isolate these higher wavelengths

in the WV3 imagery for further evaluation. Ensuring consistent lighting conditions and a narrower sample size during collection may also help to distinguish these snow types and specific features remotely.

Figure 42. Michigan ASD field spectrometer reflectance values for asphalt (*red*), ice (*purple*), groomed snow (*blue*), and virgin snow (*green*) surfaces.

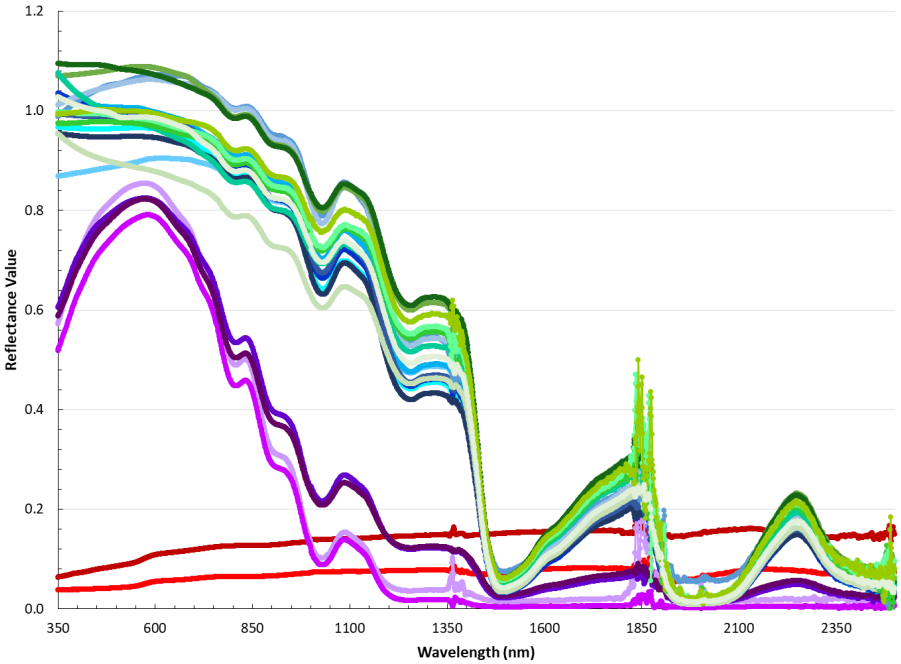


Figure 43. Michigan ASD field spectrometer reflectance values for 800–1200 nm, for asphalt (*red*), ice (*purple*), groomed snow (*blue*), and virgin snow (*green*) surfaces.

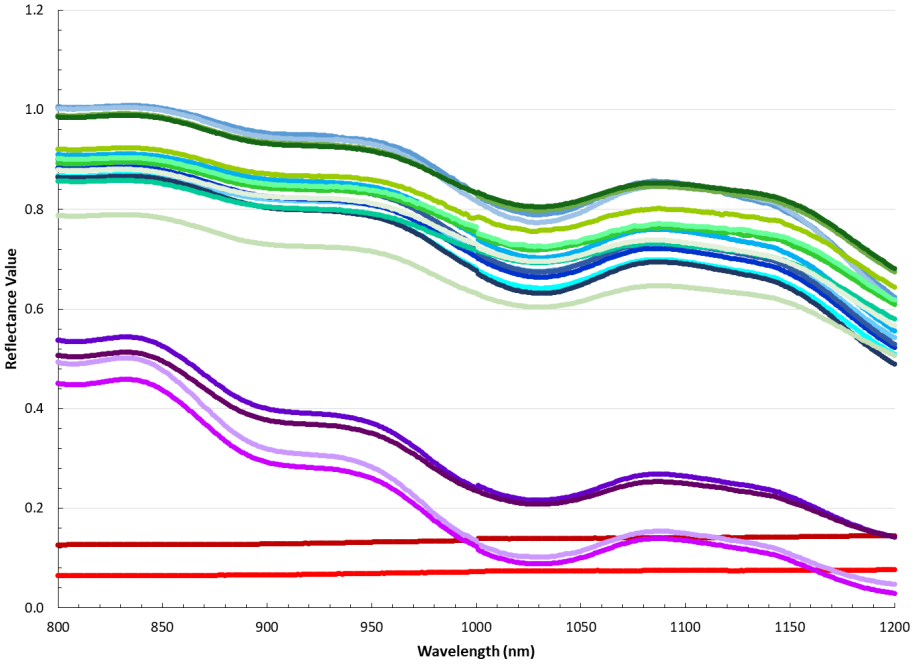
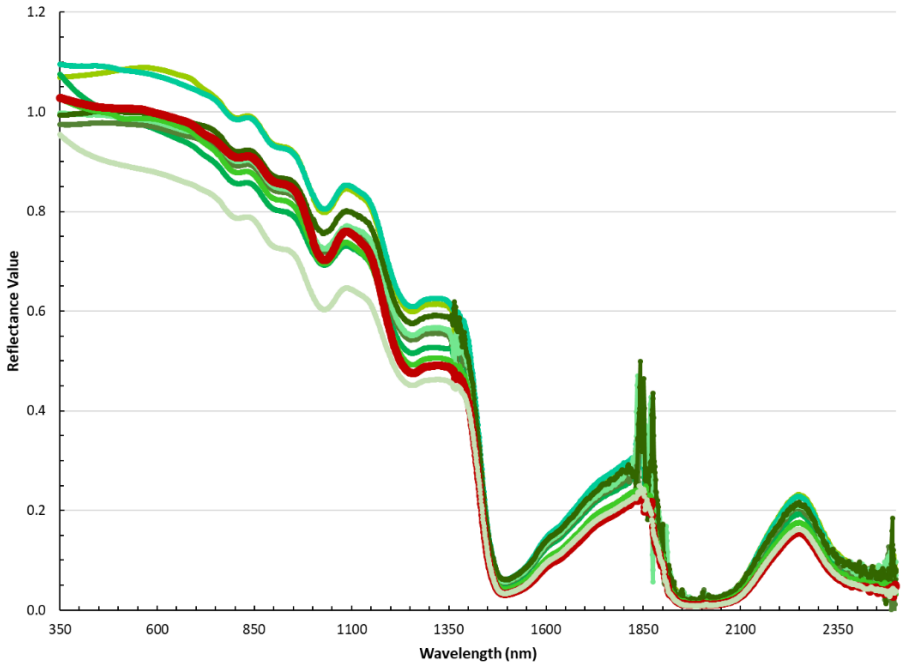


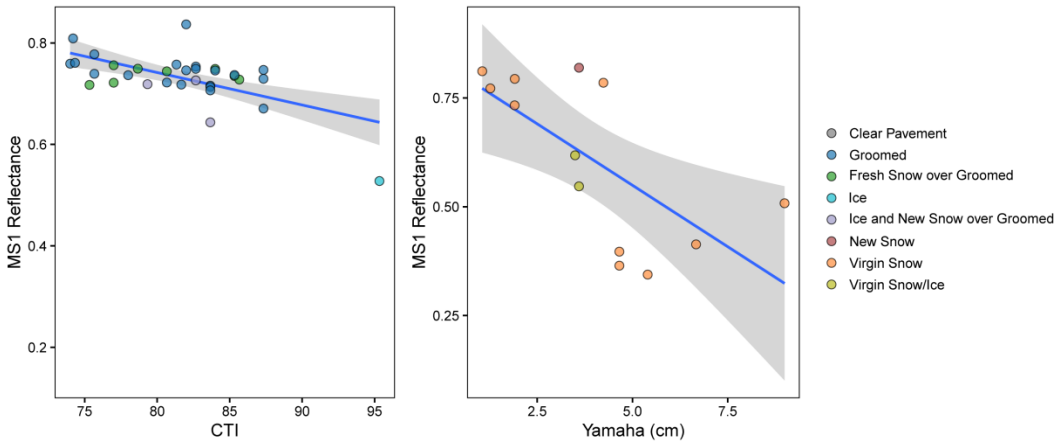
Figure 44. Michigan groomed snow (*red*) falls within the scatter of the undisturbed snow (*various greens*).



4.4 Comparison of strength measurements with spectra data

Lastly, we compared the WV2 spectra band values to strength measurements taken at each location. Because the WV2 spectra is a surface measurement, most show no correlation to underlying snow-strength characteristics; but two strength values that show promise are the CTI and the Yamaha drop cone, which are both very-near-surface measurements (see Figure 45). This relationship will be more fully explored in the future.

Figure 45. Plots of significant ($p < 0.01$) Spearman correlations between Michigan WV2 MS1 spectral band (400–450 nm) and snow strength measured with the CTI and Yamaha drop cone.



5 Conclusions and Recommendations for Future Work

As the U.S. military has been fighting predominantly in the desert for 30 years, methods to optimize operations in winter and extreme conditions in northern environments are lacking. Information on the geospatial distribution of snow physical and mechanical properties is required for mobility and other force projection and sustainment tasks. Army operations require knowledge of snow distribution and properties to support mobility and maneuver activities and therefore need methods to measure and globally predict engineering snow properties in winter and extreme environments.

This portion of the BAEM project aimed to define the existing state of the art and to develop new techniques (e.g., in situ, remotely sensed, and modeled) to adequately characterize snow mechanical properties on a variety of snow types for maneuver and sustainment purposes. Two field campaigns addressed this, one in Calumet, Michigan, in February 2018 and another in West Yellowstone, Montana, in January 2018. Not all techniques were available at both sites, some techniques did not work in certain kinds of snow cover, and additional methods have since been identified for future studies. However, this field work provides a rich data set of scientific snow characterization (stratigraphy, depth, density, moisture, etc.); mechanical properties targeting both bearing-capacity-type measurement and shear strength; on-site field spectrometry; and remotely sensed imagery through WV2, WV3, and TSX satellite data collections.

From these data sets and analysis, the mechanical measurements could be summarized as those that work well on groomed snow (CBR, 2.25 kg Clegg, CTI, and RSP), those that work well on virgin snow (Yamaha drop cone, shear vane, and plate sinkage), those that are best for profiling strength (SMP, Rammsonde, and RSP), and those that would specifically benefit from modifications for use in varied snow conditions (plate sinkage, SMP, and shear vanes). Based on these results, we plan to explore additional techniques to measure shear and friction properties (e.g., spectral analysis of surface waves and surface-friction measurement equipment).

Furthermore, our analysis of the X-band satellite radar (TSX) is preliminary. Previous radar work using multiple frequencies and dual polarizations has shown a sensitivity to bulk snow properties. In the future, we

intend to leverage satellite radar acquisitions (e.g., TSX and Sentinel) with different frequencies and polarization modes to continue our investigation toward a sensitivity to snow micromechanical properties.

Satellite-based optical remote sensing in snow-covered terrain provides multi-spectral characterization of the snow surface, and previous work has shown a relationship to snow microstructure (grain size), impurities (dust and carbon), and qualitative classifications such as snow age. In the future, we intend use these same satellites in a stereo mode where overlapping images may be processed into a digital surface model, providing a fine-scale (on the order of meters) characterization of the surface roughness and its impacts on mobility and maneuver.

Snow is extremely variable in its physical and mechanical properties and can change drastically temporally and spatially and perhaps most significantly with loading and changes in temperature. Our data collection included a wide range of snow types to assess which techniques worked best in specific conditions and which techniques worked across a wide range of conditions. We also aimed to collect data at very different geographic locations (western snow adjacent to mountainous terrain and eastern snow adjacent to a major waterbody).

Preliminary analysis of the results indicate

1. some correlation between strength measures, especially when grouped based on the snow-surface type;
2. some strength measures did not seem useful for characterizing snow for vehicle mobility purposes; and
3. trends between visible and near-infrared snow spectra and some surface strength measurements.

There are many questions regarding the use of some of the more sophisticated measurements that have not previously been used in the cold or in snow. Some of the instruments seemed to drift with temperature, even after a period of approximately 1 hour for temperature equilibration; and others contained components that were not well suited for use in cold (e.g., differential contraction of materials leading to poor fit of components). These were evaluated more thoroughly in controlled cold room testing to develop operational techniques and equipment modifications as needed (Menke et al. 2019). Shear vanes and their associated equations

also need to be modified for vane sizes better suited to a variety of snow surfaces. The depth of influence of several tests needs to be investigated to determine what material, the snow or the underlying surface, is actually being evaluated.

The 2018 field data collection provides a rich data set for further analysis, particularly for relating strength and remotely sensed measurements, in addition to helping refine future data collection objectives. These data will be further analyzed in FY19 to

1. assess in situ micromechanical properties of snow (e.g., SMP and GPR data sets) from the January 2018 campaign and the correlation of these data with coordinated satellite-based radar acquisitions (at X-band and C-band);
2. provide a basis for detailed exploration of temperature effects on some of the equipment components to fully understand operating techniques for cold environments;
3. further explore the statistical and theoretical relationship of snow physical and mechanical properties to remotely sensed data; and
4. develop a new SMP prototype for applications in "hard" snow conditions (e.g., for mobility), including incorporating a higher capacity force sensor, an embedded Linux platform for instrument control, display and data logging capabilities, and the associated hardware and software required for accurate measurements.

Experiments planned for FY19 focus on assessing and refining new field in situ and remote techniques:

1. Developing operation guidance for low-temperature evaluation of new techniques for bearing capability, shear modulus, and friction measurement through cold room experiments
2. Assessing the most promising suite of instruments on a controlled, groomed snow airfield test section in the Frost Effects Research Facility
3. Conducting snow mobility experiments to expand the mechanistic observations and performance database of modern vehicle operations in a variety of snow surfaces
4. Leveraging the NASA (National Air and Space Administration) SnowEx experiments by adding mechanical property and stand-off measurements

at select field sites being monitored by NASA ground and satellite collections and supplemented with the CRREL Helipod instrumentation package that leverages lidar, thermal, and optical remote-sensing opportunities
5. Exploring a mechanistic approach to snow mobility modeling and methodology to incorporate simple terramechanics into a geospatial framework, especially needed for deep snow mobility (Shoop et al. 2019a)
6. Creating remote-sensing algorithms to estimate spatial variability of snow density, to be used as a proxy for snow mechanical properties

Future work will integrate enhancements to snow physics algorithms and satellite-based remote-sensing techniques specifically focused on snow mechanical properties, such as compactive behavior, modulus, bearing, and shear strength, and will develop algorithms to capture this behavior within the framework of cross-country mobility models. We will also be looking at methods to geospatially distribute these types of snow properties for use in maneuver and sustainment analysis (Deeb et al. 2019). These efforts will provide critical scientific and engineering data and models to enable maneuver support and sustainment planning for all-season capabilities in northern environments.

References

Abele, G. 1963. *A Correlation of Unconfined Compressive Strength and Ram Hardness of Processed Snow*. Technical Report 85. Hanover, NH: U.S. Army Cold Regions Research and Engineering Laboratory.

———. 1968. *An Experimental Snow Runway Pavement in Antarctica*. Technical Report 211. Hanover, NH: U.S. Army Cold Regions Research and Engineering Laboratory.

———. 1990. *Snow Roads and Runways*. Monograph 90-3. Hanover, NH: U.S. Army Cold Regions Research and Engineering Laboratory.

AMS. 2018. Part #59035 GeoTester Penetrometer Technical Data Sheet. American Falls, ID: AMS, Inc. http://www.ams-samplers.com/.

ASTM. 2010. *Standard Test Method for CBR (California Bearing Ratio) of Soils in Place*. ASTM D4429-09a. West Conshohocken, PA: ASTM International. https://www.astm.org/Standards/D4429.htm.

———. 2016a. *Standard Test Methods for Determination of the Impact Value (IV) of a Soil*. ASTM D5874-16. West Conshohocken, PA: ASTM International. https://www.astm.org/Standards/D5874.htm.

———. 2016b. *Standard Test Methods for Single Wheel Driving Traction in a Straight Line on Snow- and Ice-Covered Surfaces*. ASTM F1805-16. West Conshohocken, PA: ASTM International. https://www.astm.org/Standards/F1805.htm.

———. 2018. *Standard Test Method for Field Vane Shear Test in Saturated Fine-Grained Soils*. ASTM D2573-18. West Conshohocken, PA: ASTM International. https://www.astm.org/Standards/D2573.htm.

Blaisdell, G. L., V. Klokov, and D. Diemand. 1995. "Compacted Snow Runway Technology on the Ross Ice Shelf Near McMurdo, Antarctica." *Contributions to Antarctic Research IV* 67:153–173.

Carroll, T. 1977. "A Comparison of the CRREL 500 cm^3 Tube and the ILTS 200 and 100 cm^3 Box Cutters Used for Determining Snow Densities." *Journal of Glaciology* 18 (79): 334–337.

Clegg, B. 1980. "An Impact Soil Test as Alternative to California Bearing Ratio." In *Proceedings, 3rd Australian-New Zealand (ANZ) Geomechanics Conference*, Wellington, New Zealand, 1:225–230.

Conger, S. M., and D. M. McClung. 2009. "Comparison of Density Cutters for Snow Profile Observations." *Journal of Glaciology* 55 (189): 163–169.

Conover, W. J., and R. L. Iman. 1979. *On Multiple-Comparisons Procedures*. LA-7677-MS. Los Alamos, NM: Los Alamos Scientific Laboratory.

Deeb, E., C. Polashenski, Z. Courville, C. Hiemstra, A. Wagner, J. Eylander, and R. Davis. 2019. "Geospatial Snow Estimation for Engineering Applications and Operations." In *Proceedings of the International Conference on Cold Regions Engineering*, 18–22 August, Quebec City, Quebec, Canada. Reston, VA: American Society of Civil Engineers.

Denoth, A. 1989. "Snow Dielectric Measurements." *Advances in Space Research* 9 (1): 233–243.

DigitalGlobe. 2012. *WorldView-2*. Data Sheet DS-WV2 Rev 6/12. Westminster, CO: DigitalGlobe.

———. 2014. *DigitalGlobe Constellation >> WorldView-3*. Data Sheet DS-WV3 05/14. Westminster, CO: DigitalGlobe.

Elder, B., S. Shoop, M. Feyrer, and S. Beal. 2019. "Methods for Measuring Snow Moisture and Density." In *Proceedings of the International Conference on Cold Regions Engineering*, 18–22 August, Quebec City, Quebec, Canada. Reston, VA: American Society of Civil Engineers.

Feyrer, M., J. Balch, B. Elder, and S. Shoop. 2018. "Methods for Measuring Snow Moisture and Density." Poster presented at the CRREL Student Poster Session, August 2018, Hanover, NH, U.S. Army Engineer Research and Development Center.

Kruse, F. A. 2015. *Final Report: Soil Characterization Using Spectral Measurements*. NPS/CRREL FY15 Collaboration. Monterey, CA: Naval Postgraduate School, Remote Sensing Center.

Longbotham, N., F. Pacifici, B. Baugh, and G. Camps-Valls. 2014. "Prelaunch Assessment of WorldView-3 Information Content." In *IEEE GRSS Workshop on Hyperspectral Image and Signal Processing (WHISPERS)*, 479–486.

Marshall, H.-P., and J. B. Johnson. 2009. "Accurate Inversion of High-Resolution Snow Penetrometer Signals for Microstructural and Micromechanical Properties." *Journal of Geophysical Research* 114 (F4): F04016. https://doi.org/10.1029/2009JF001269.

Matzl, M., and M. Schneebeli. 2006. "Measuring Specific Surface Area of Snow by Near-Infrared Photography." *Journal of Glaciology* 52 (179): 558–564. https://doi.org/10.3189/172756506781828412.

Meehan, T., H. P. Marshall, E. Deeb, S. Shoop. 2019a. *SnowMicroPenetrometer Applications for Winter Vehicle Mobility*. ERDC/CRREL TR-19-14. Hanover, NH: U.S. Army Engineer Research and Development Center.

———. 2019b. "SnowMicroPenetrometer Applications for Winter Vehicle Mobility." In *Proceedings of the International Conference on Cold Regions Engineering*, 18–22 August, Quebec City, Quebec, Canada. Reston, VA: American Society of Civil Engineers.

Menke, A., W. Wieder, and S. Shoop. 2019. "Using the Light Weight Deflectometer in Winter Climates." In *Proceedings of the International Conference on Cold Regions Engineering*, 18–22 August, Quebec City, Quebec, Canada. Reston, VA: American Society of Civil Engineers.

Millar, L. R. 1977. "Application of the Soil Impact Tester to Road Pavement Construction." Honors Thesis, Department of Civil Engineering, University of Western Australia, Crawley, Western Australia.

Nolin, A. W., J. Dozier, and L. A. K. Mertes. 1993. "Mapping Alpine Snow Using a Spectral Mixture Modeling Technique." *Annals of Glaciology* 17:121–124.

Painter, T. H., D. A. Roberts, R. O. Green, and J. Dozier. 1998. "The Effect of Grain Size on Spectral Mixture Analysis of Snow-Covered Area from AVIRIS Data." *Remote Sensing of Environment* 65 (3): 320–332. https://doi.org/10.1016/S0034-4257(98)00041-8.

Painter, T. H., J. Dozier, D. A. Roberts, R. E. Davis, and R. O. Green. 2003. "Retrieval of Subpixel Snow-Covered Area and Grain Size from Imaging Spectrometer Data." *Remote Sensing of Environment* 85 (1): 64–77. https://doi.org/10.1016/S0034-4257(02)00187-6.

Painter, T. H., K. Rittger, C. McKenzie, P. Slaughter, R. E. Davis, and J. Dozier. 2009. "Retrieval of Subpixel Snow Covered Area, Grainsize, and Albedo from MODIS." *Remote Sensing of Environment* 113 (4): 868–879. https://doi.org/10.1016/j.rse.2009.01.001.

Pielmeier, C., and M. Schneebeli. 2003. "Stratigraphy and Changes in Hardness of Snow Measured by Hand, Ramsonde and Snow Micro Penetrometer: A Comparison with Planar Sections." *Cold Regions Science and Technology* 37 (3): 393–405. https://doi.org/10.1016/S0165-232X(03)00079-X.

R Core Team. 2017. *R: A Language and Environment for Statistical Computing*. Vienna, Austria: R Foundation for Statistical Computing. https://www.R-project.org/.

Schneebeli, M., and J. B. Johnson. 1998. "A Constant-Speed Penetrometer for High-Resolution Snow Stratigraphy." *Annals of Glaciology* 26:107–111. https://doi.org/10.3189/1998AoG26-1-107-111.

Senseney, C. T., and M. A. Mooney. 2010. "Characterization of Two-Layer Soil System Using a Lightweight Deflectometer with Radial Sensors." *Transportation Research Record: Journal of the Transportation Research Board* 2186:21–28. https://doi.org/10.3141/2186-03.

Shaw, G. A., and H. K. Burke. 2003. "Spectral Imaging for Remote Sensing." *Lincoln Laboratory Journal* 14 (1): 3–28.

Shoop, S. A., J. Crandell, and M. Knuth. 2012. "Using a Clegg Impact Hammer to Measure Snow Strength." In *Proceeding of the 15th International Conference on Cold Regions Engineering*, Quebec, Canada, 19–22 August, 811–822.

Shoop, S., W. Wieder, and B. Elder. 2019a. "Mechanical Property Measurements on Various Snow Surfaces." In *Proceedings of the International Conference on Cold Regions Engineering*, 18–22 August, Quebec City, Quebec, Canada. Reston, VA: American Society of Civil Engineers.

Shoop, S., M. Bodie, S. Frankenstein, M. Parker, and M. Bigl. 2019b. "Recent Improvements to Snow Mobility Algorithms." In *Proceedings of the 15th ISTVS European-African Regional Conference*, 9–11 September 2019, Prague, Czech Republic.

Sturm, M., and J. Holmgren. 1999. Self-Record Snow Depth Probe. U.S. Patent US5864059A, filed 9 June 1997.

Tiuri, M., and A. Sihvola. 1986. "Snow Fork for Field Determination of the Density and Wetness Profiles of a Snow Pack." In *Hydrologic Applications of Space Technology* (Proceedings of the Cocoa Beach Workshop, Florida, August 1985), IAHS Publ. no. 160.

U.S. Army and Air Force. 1994. *Planning and Design of Roads, Airfield, and Heliports in the Theater of Operations—Road Design*. FM 5-430-00-1. AFJPAM 32-8013, Vol. 1. Washington, DC: Department of the Army and Department of the Air Force.

U.S. Army, Air Force, and Navy. 1987. *Materials Testing*. FM 5-530, AFM 89-3, and NAVFAC MO-330. Washington, DC: Department of the Army, Department of the Air Force, and Department of the Navy.

Wallace, J. M., and P. V. Hobbs. 1977. *Atmospheric Science: An Introductory Survey*. New York: Academic Press.

Wieder, W. L., S. A. Shoop, and L. Barna. 2019. *Using the Light Weight Deflectometer to Assess Groomed Snow and Ice Surfaces*. ERDC/CRREL TR-19-5. Hanover, NH: U.S. Army Engineer Research and Development Center.

Appendix A: Additional Site Imagery

Figure A-1. West Yellowstone Airport central runway, taxiway, and ice lane test points as they relate to the airport pavement surfaces.



Figure A-2. Michigan Spin Up Pads 1 and 2 test points.



Figure A-3. Michigan Spin Up Pads 1 and 2 test points winter imagery.

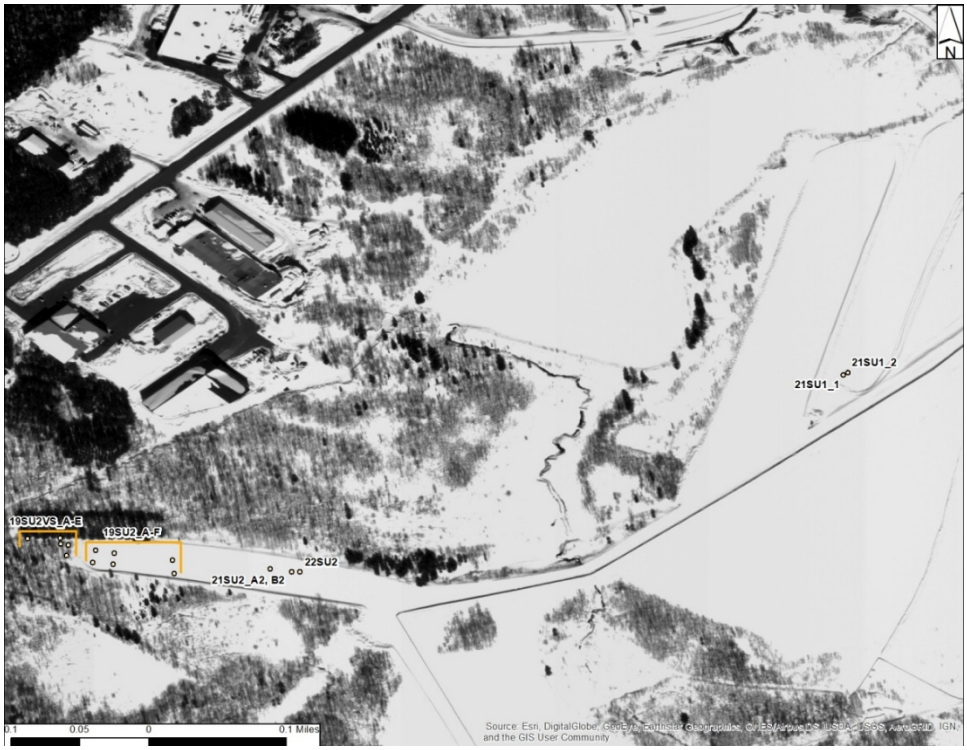


Figure A-4. Michigan Spin Up Pad 3, Loop 1, Vehicle Dynamics Area 2, and the 900 and 300 ft circles test points.

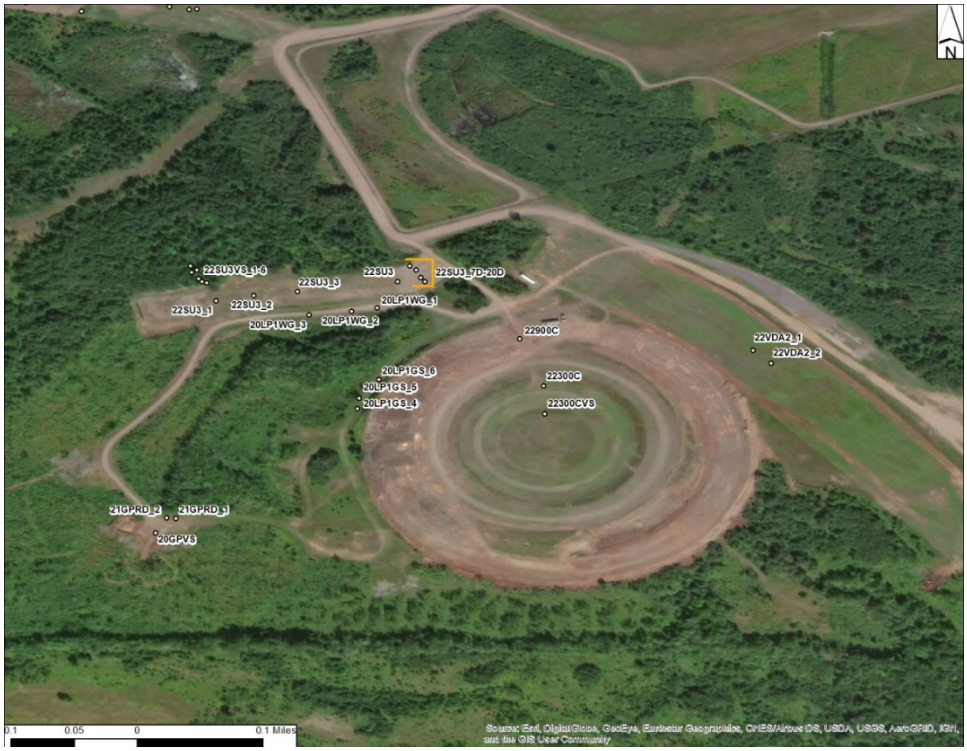


Figure A-5. Michigan Spin Up Pad 3, Loop 1, Vehicle Dynamics Area 2, and the 900 and 300 ft circles test points winter imagery.

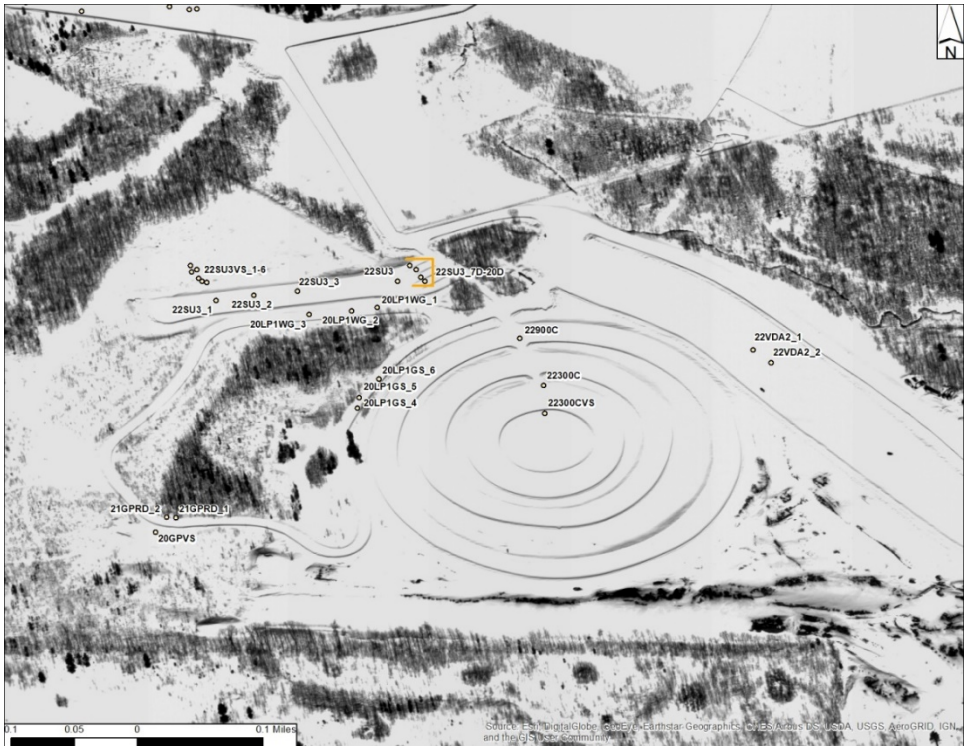


Figure A-6. Michigan Ice Rink and Sweeper parking pad test points.



Figure A-7. Michigan Ice Rink and Sweeper parking pad test points winter imagery.



Figure A-8. Michigan Loop 3, Stability Area, and Loop 4 test points.



Figure A-9. Michigan Loop 3, Stability Area, and Loop 4 test points winter imagery.



Appendix B: Michigan Ground-Surface Photos

Figure B-1. Spin Up Pad 2 (points 19SU2_A through F, 21SU2, 22SU2). Note that the *bottom* photo looks out into the wooded area of points 19SU2VS_A through E.



Figure B-2. Loop 1 washed gravel road (points 20LP1WG_1 through 3).



Figure B-3. Loop 1 grass-surfaced road (points 20LP1GS_4 through 6).





Figure B-4. Gravel pad (points 20GPVS and 21GPVS).

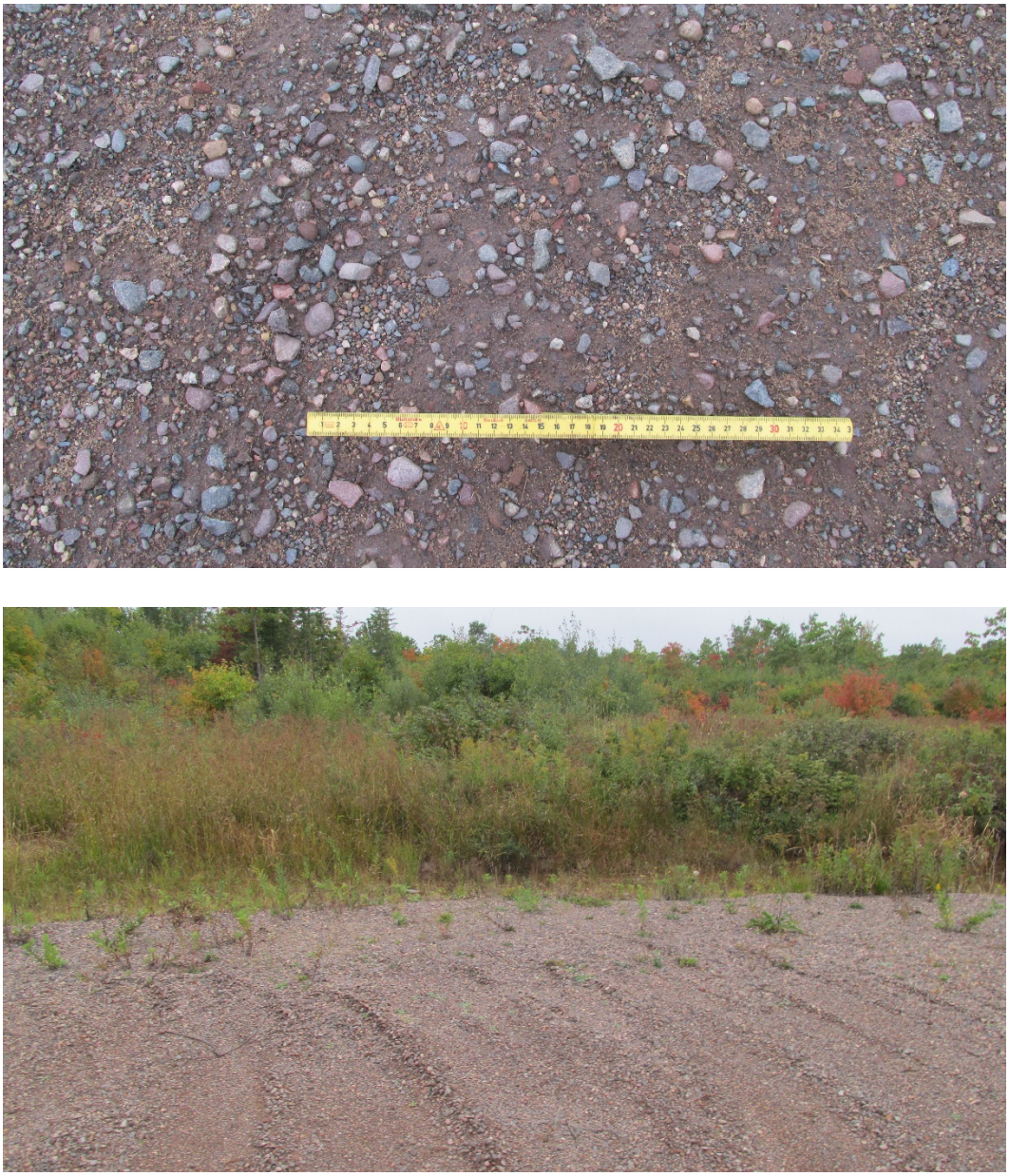


Figure B-5. Sweeper parking pad (points 21SPW_1 through 3).



Figure B-6. Ice slope: entire slope (*top*), steep slope area (*middle*) (point 21IS_S), and lower slope area (*bottom*) (point 21IS_L).



Figure B-7. Spin Up Pad 1 (points 21SU1_1 and 2).



Figure B-8. Gravel road adjacent to the gravel pad, part of Loop 1 (point 22GPRD_1 and 2).



Figure B-9. Spin Up Pad 3 (points SU3_1 through 3).



Figure B-10. Terrain north of Spin Up Pad 3 (points 22SU3VS_1 through 6).



Figure B-11. Ice Rink area (points 22IR_S and 22IR_I).



Figure B-12. Stability Test Area (points 22STAB_S and 22SATB_GI).



Figure B-13. Vehicle Dynamics Area 2 (points 22VDA2_1 and 2).



Figure B-14. Loop 4 (point 22LP4).



Figure B-15. Terrain off Loop 4 (point 22LP4VS).



Appendix C: Snow Pit and Weather Data

Figures C-1 through C-15 show plots of snow densities, snow and air temperatures, and snow moisture. The data are from the snow pits prepared at both the Montana and Michigan sites. Section 3 details the procedures for these measurements. Snow density measurements for these figures were made by both direct volume sampling (in green and labeled "Pit") and with the Finnish fork (in blue and labeled "Fork"). The black dotted line in the plots represents the calculated average between these measurements, with a shaded area in between. Temperature measurements were made with a handheld type-T thermocouple. Dashed lines and the shaded area (pink) represent a ±1.0 degree standard error (typical for a type-T thermocouple). Black diamonds shows air temperature as measured 15 cm (6 in.) above the ground using the thermocouple. Snow moisture measurements were made using one or two Denoth meters. In cases where two Denoth meters were used, the results were averaged and are shown as a black dotted line with a shaded area in between. In cases where only one meter was used, those data are plotted with a standard ±0.3%$_{VOL}$ error (shaded area). For any depths where a measurement was missing, data were linearly interpolated.

Figures C-16 through C-29 provide the meteorological data (temperature, humidity, and wind) for each day as recorded during the Montana and Michigan field campaigns by the local Automated Weather Stations (AWS). The Montana AWS is located at the West Yellowstone Airport itself, where NATC operates. The Michigan AWS is located at the Houghton County Airpark, 9.5 km (6 miles) south of Calumet, Michigan, which is adjacent to KRC. All data are shown with a second-order locally weighted smoothing (black line with bin-width of 15 minutes).

Figure C-1. Snow-pit density, temperature, and snow moisture profiles for the two snow pits at Montana test point 27RWYS, 27 January 2018.

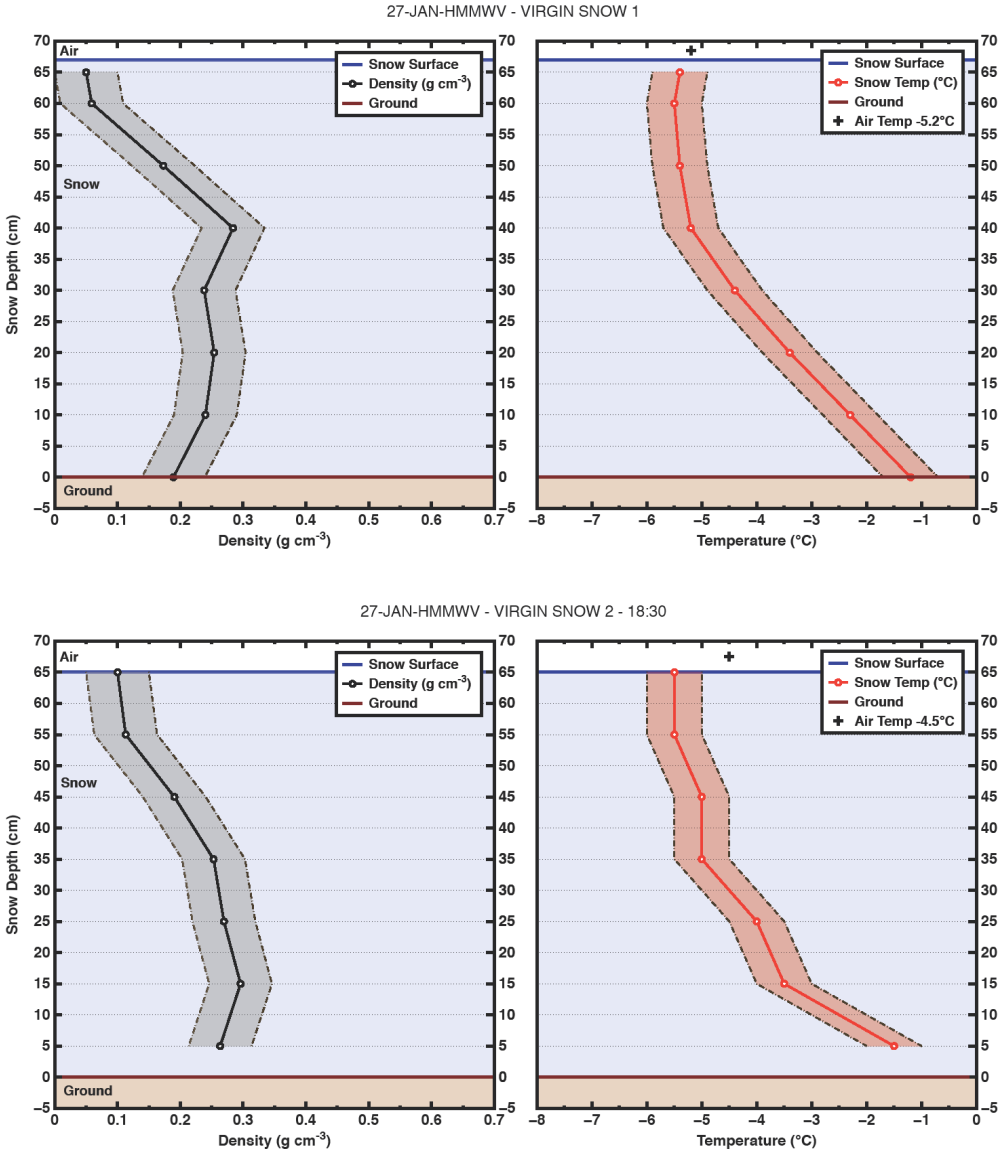


Figure C-2. Snow-pit density, temperature, and snow moisture profiles for the snow pit at Montana test point 27TWYS, 27 January 2018.

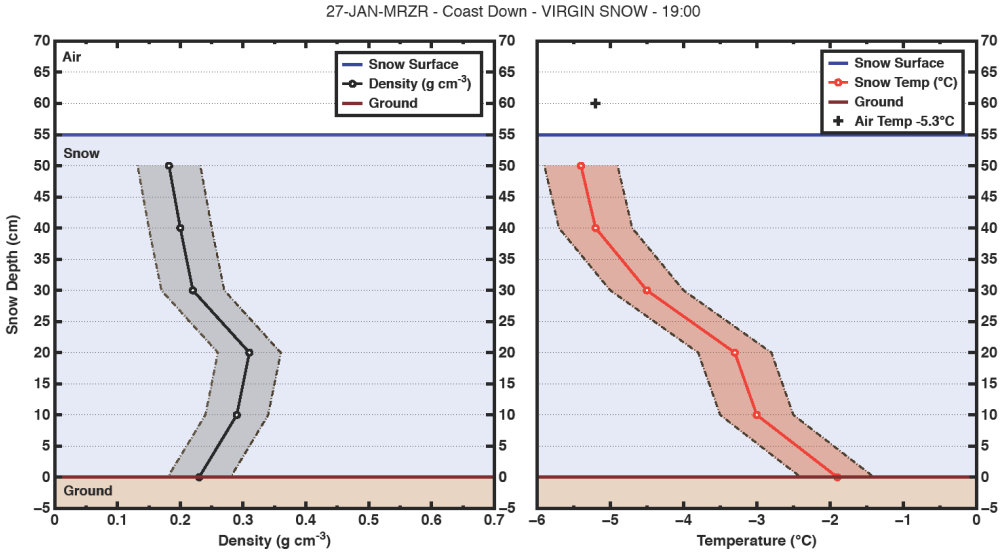


Figure C-3. Snow-pit density, temperature, and snow moisture profiles for the snow pit at Montana test point 28MLPW, 28 January 2018.

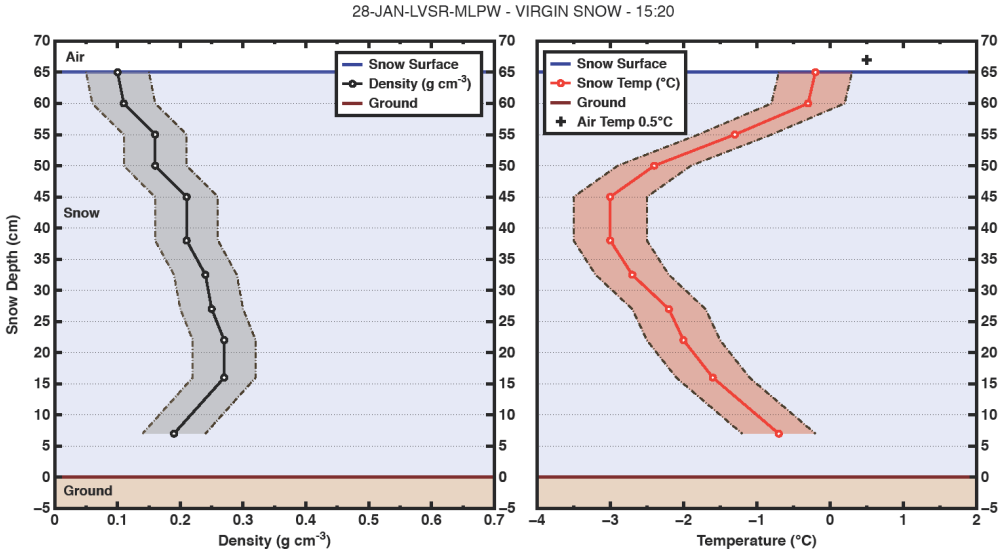


Figure C-4. Snow-pit density, temperature, and snow moisture profiles for the snow pit at Montana test point 27TWYS, 29 January 2018.

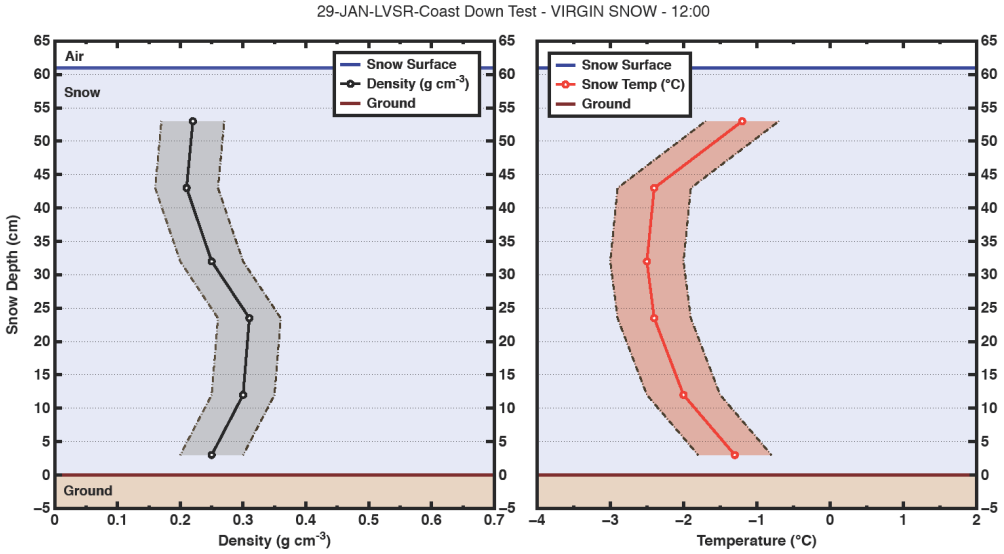


Figure C-5. Snow-pit density, temperature, and snow moisture profiles for the snow pit at Montana test point 27RWYS, 29 January 2018.

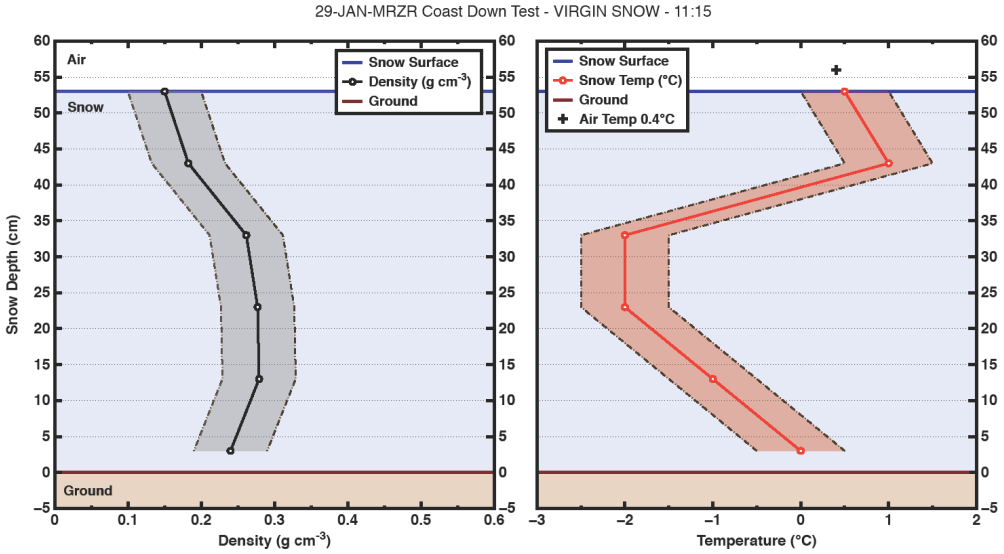


Figure C-6. Snow-pit density, temperature, and snow moisture profiles for the snow pit at Montana test point 27RWYS, 30 January 2018.

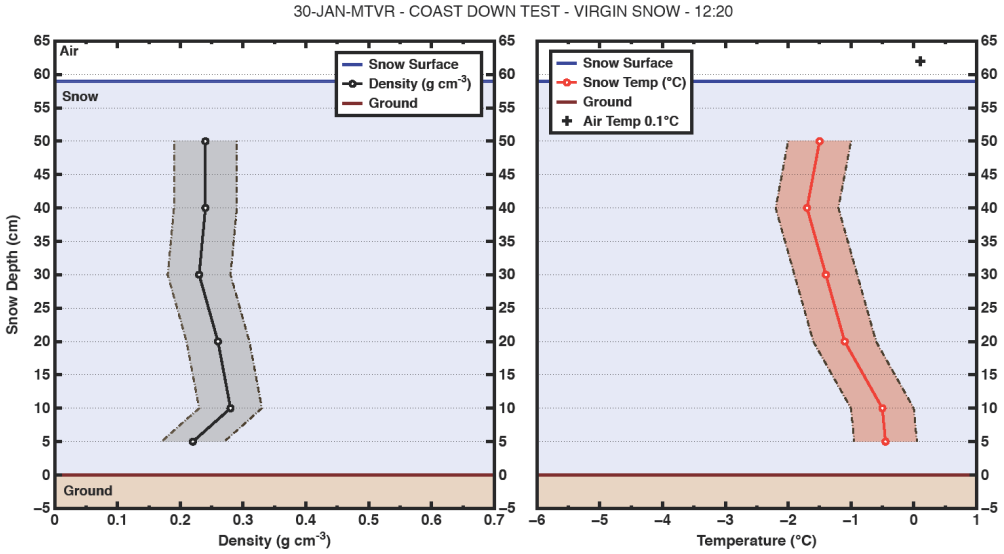


Figure C-7. Snow-pit density, temperature, and snow moisture profiles for the snow pit at Montana test point 30MLPN, 30 January 2018.

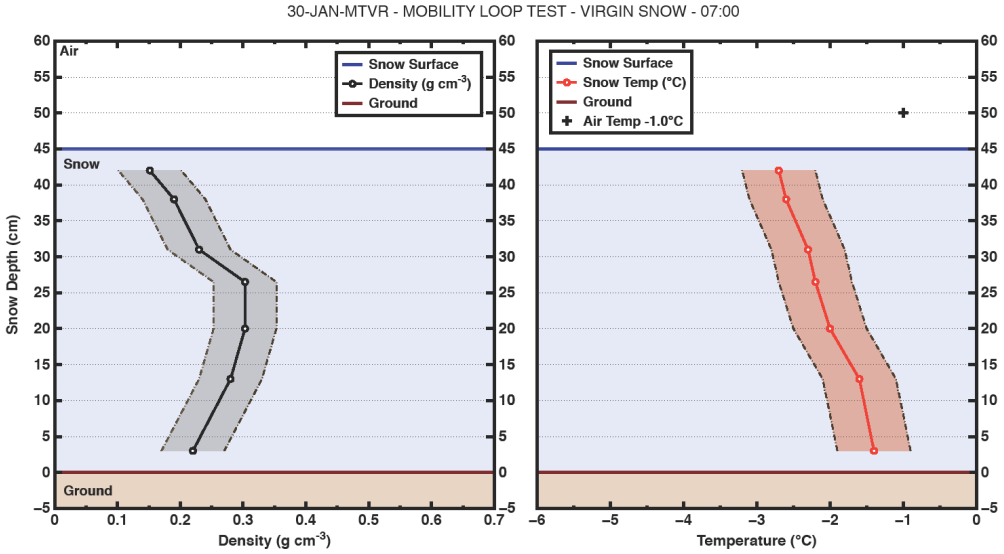


Figure C-8. Snow-pit density, temperature, and snow moisture profiles for the snow pit at Montana test point 27RWYS, 31 January 2018.

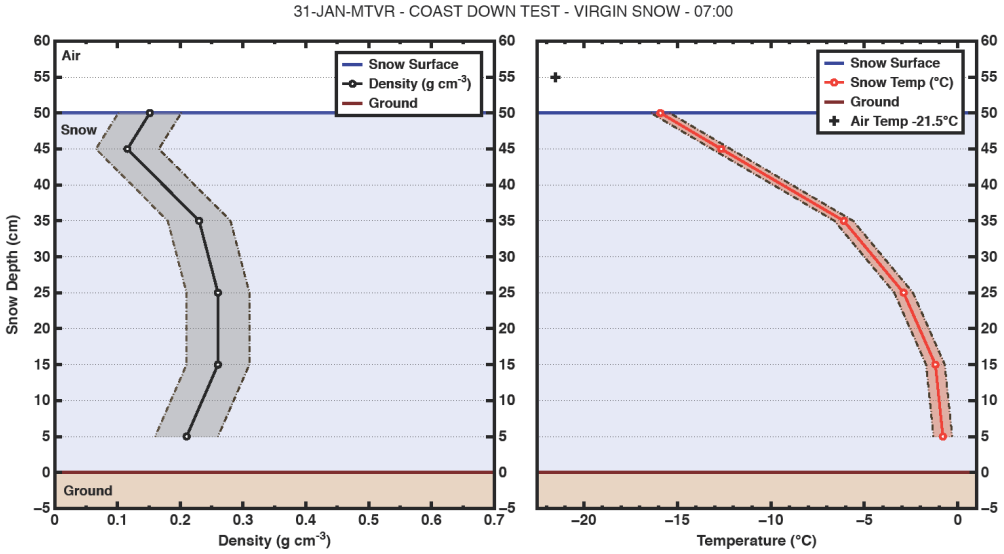


Figure C-9. Snow-pit density, temperature, and snow moisture profiles for the snow pit at Michigan test point 19SU2VS_A, 19 February 2018.

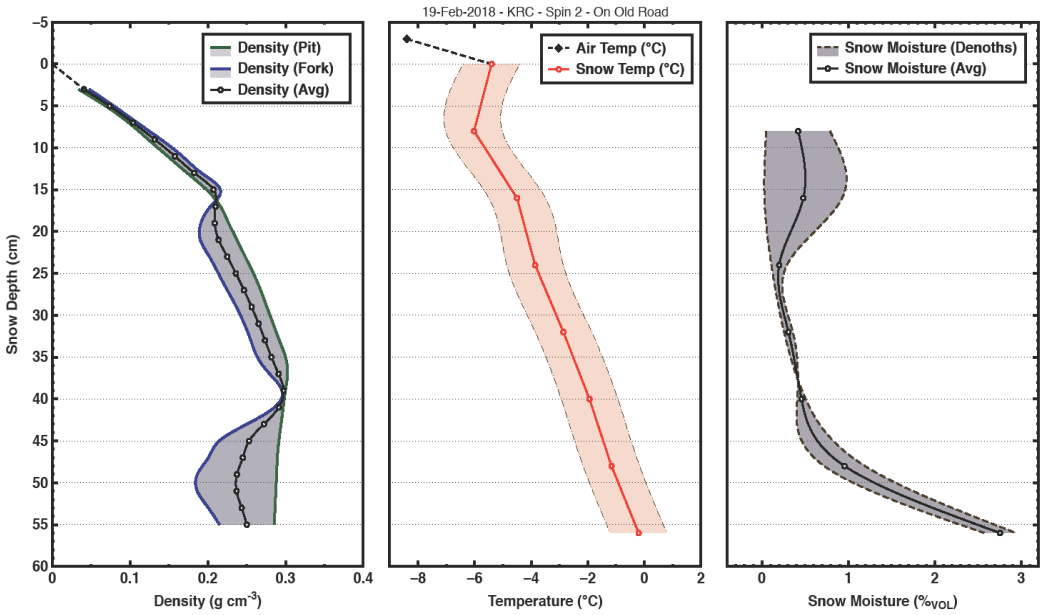


Figure C-10. Snow-pit density, temperature, and snow moisture profiles for the snow pit at Michigan test point 19SU2VS_E, 19 February 2018.

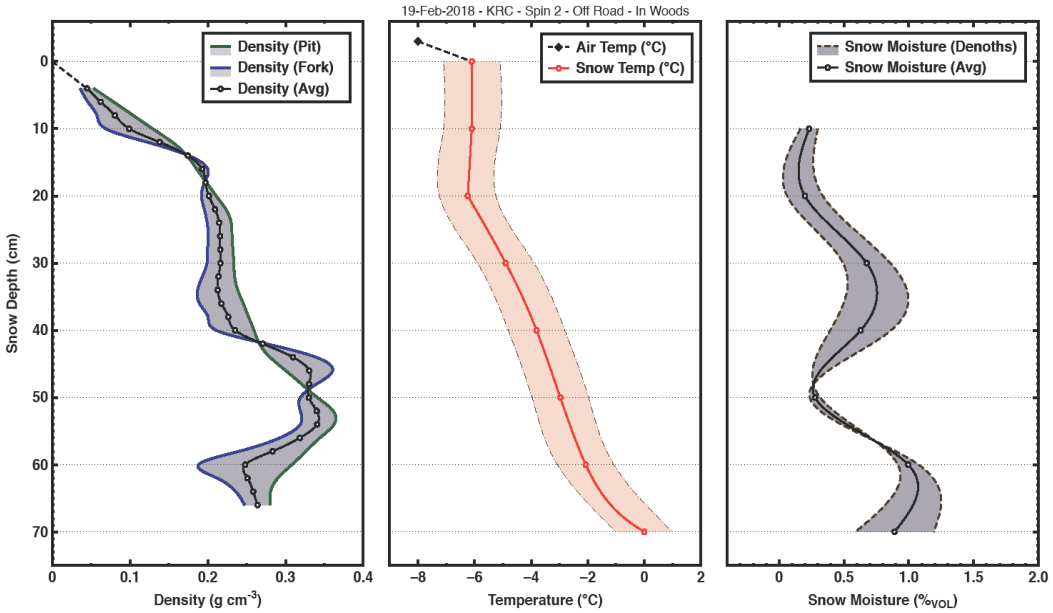


Figure C-11. Snow-pit density, temperature, and snow moisture profiles for the snow pit at Michigan test point 20GPVS, 20 February 2018.

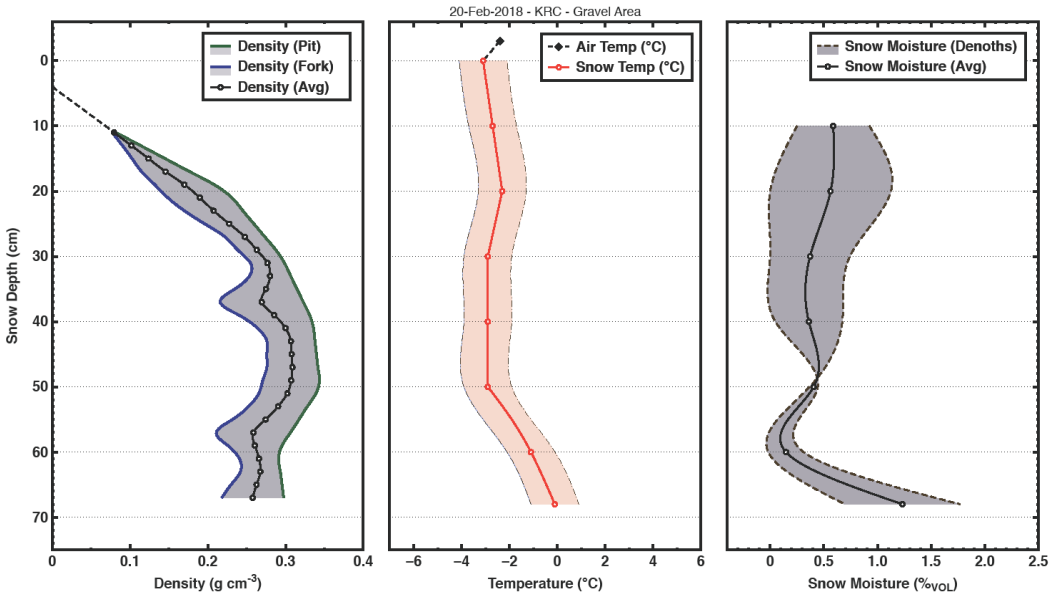


Figure C-12. Snow-pit density, temperature, and snow moisture profiles for the snow pit at Michigan test point 21IS_S, 21 February 2018.

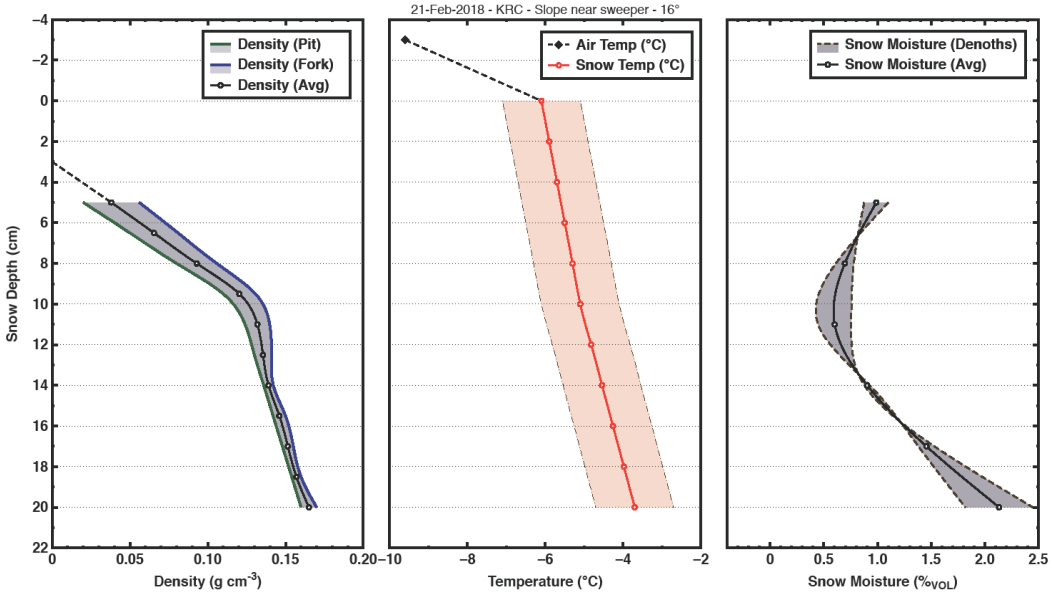


Figure C-13. Snow-pit density, temperature, and snow moisture profiles for the snow pit at Michigan test point 21IS_L, 21 February 2018.

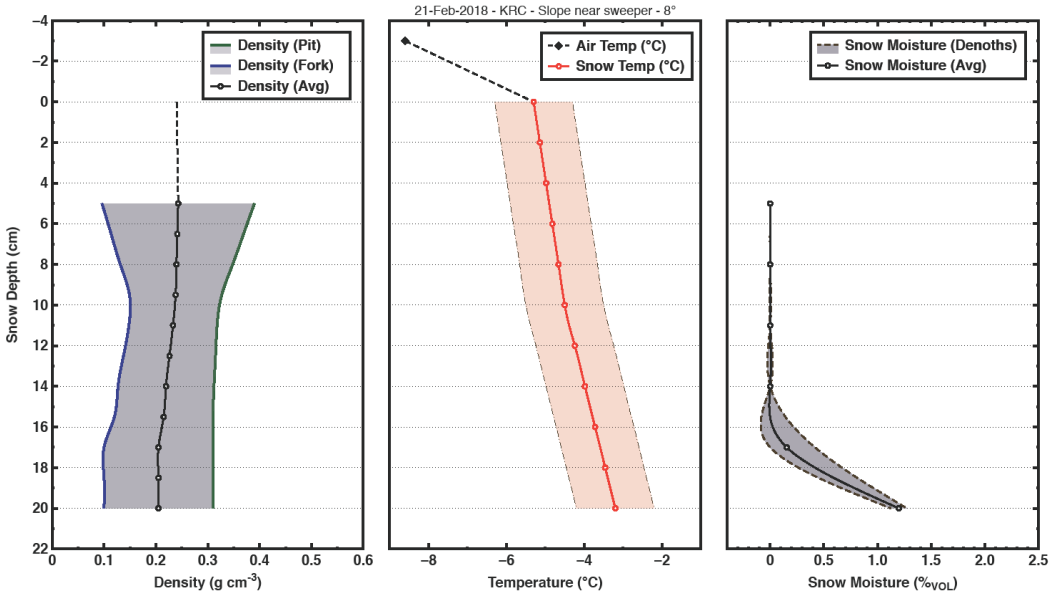


Figure C-14. Snow-pit density, temperature, and snow moisture profiles for the snow pit at Michigan test point 22SU3VS, 21 February 2018.

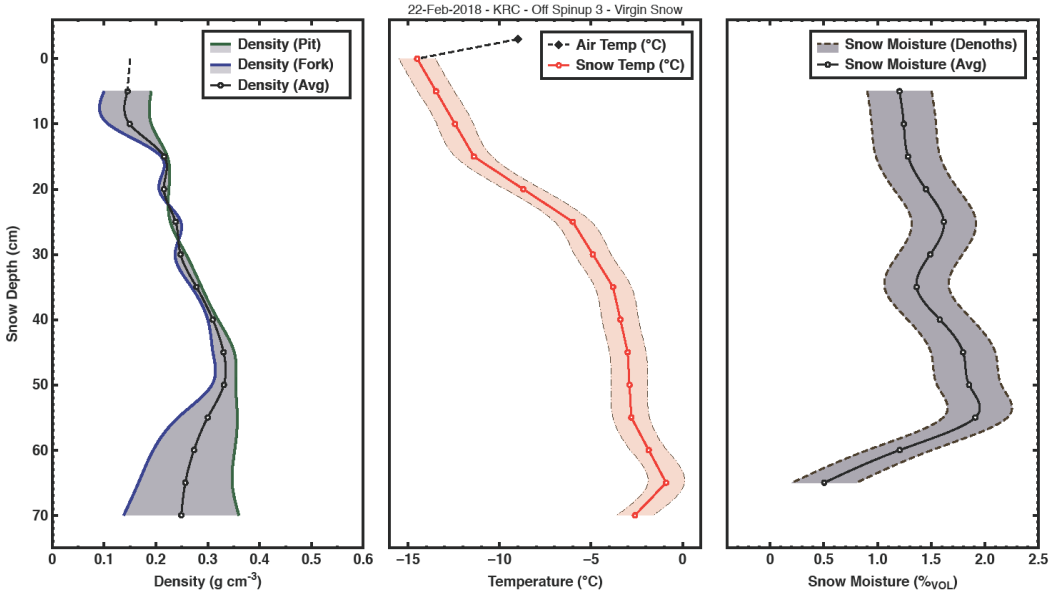


Figure C-15. Snow-pit density, temperature, and snow moisture profiles for the snow pit at Michigan test point 23HQP, 23 February 2018.

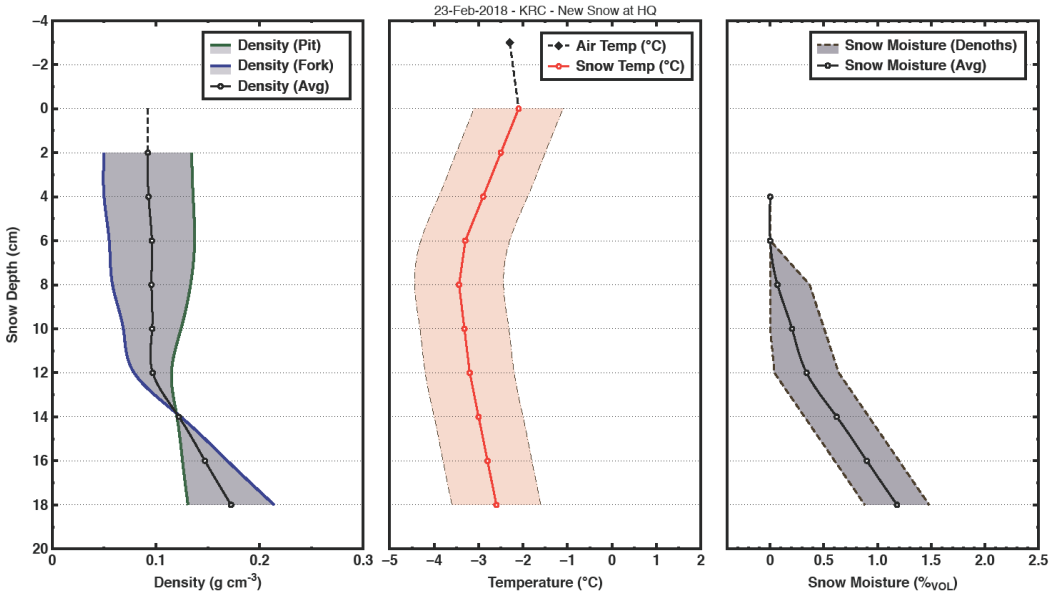


Figure C-16. Montana meteorological data for 24 January 2018.

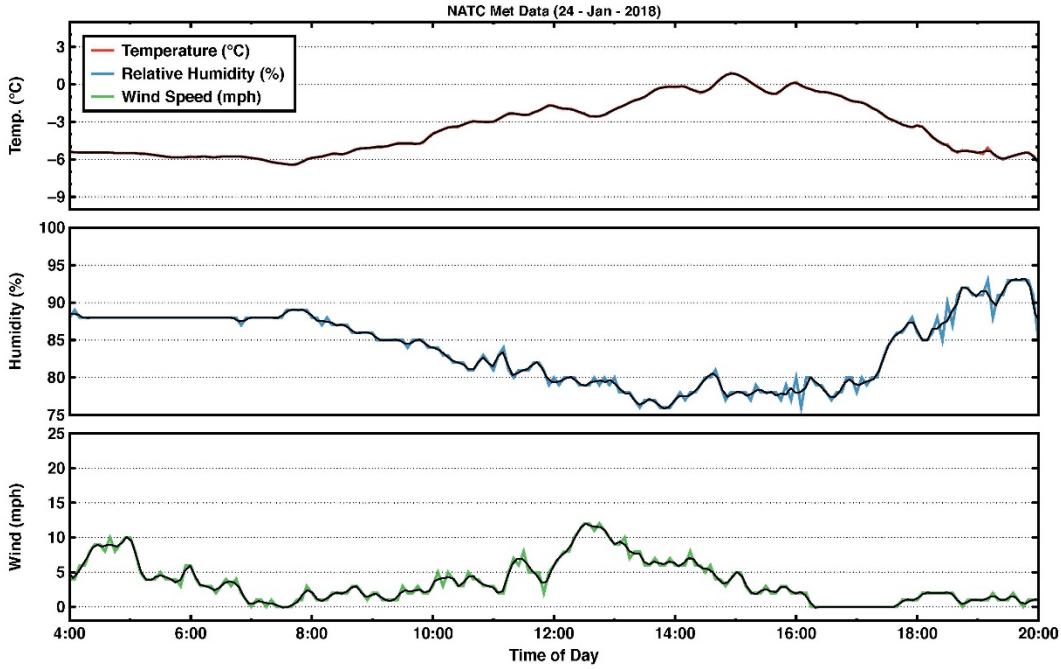


Figure C-17. Montana meteorological data for 25 January 2018.

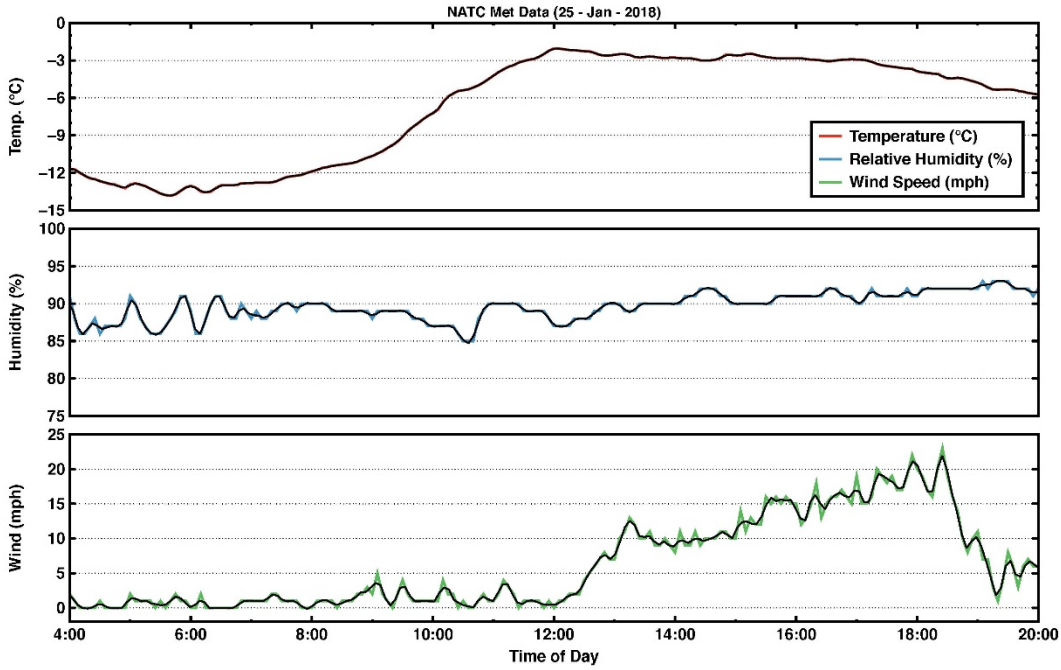


Figure C-18. Montana meteorological data for 26 January 2018.

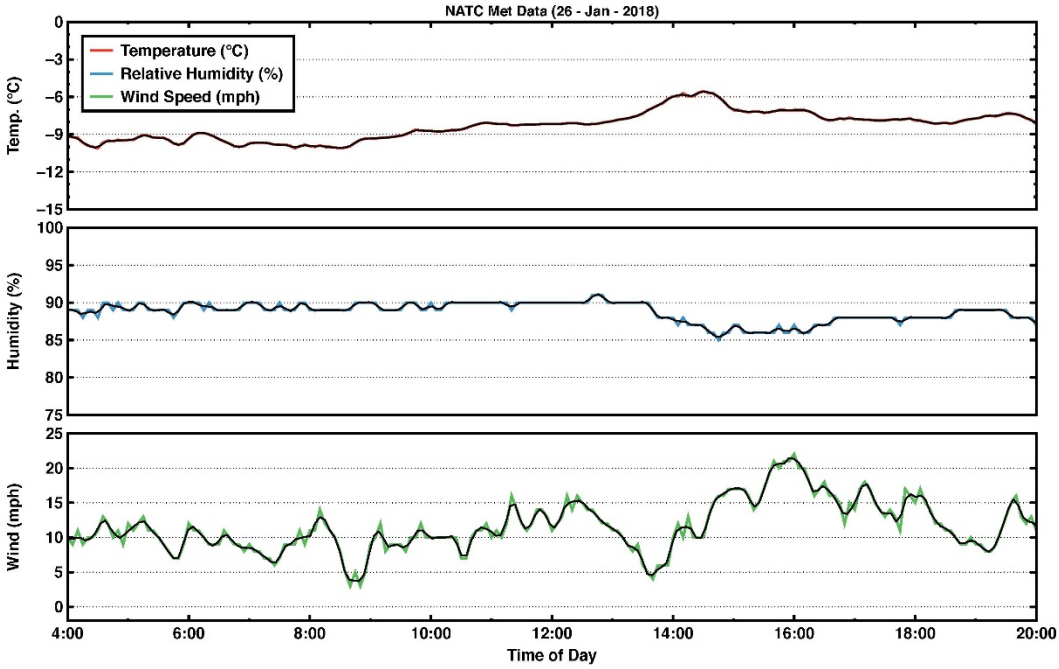


Figure C-19. Montana meteorological data for 27 January 2018.

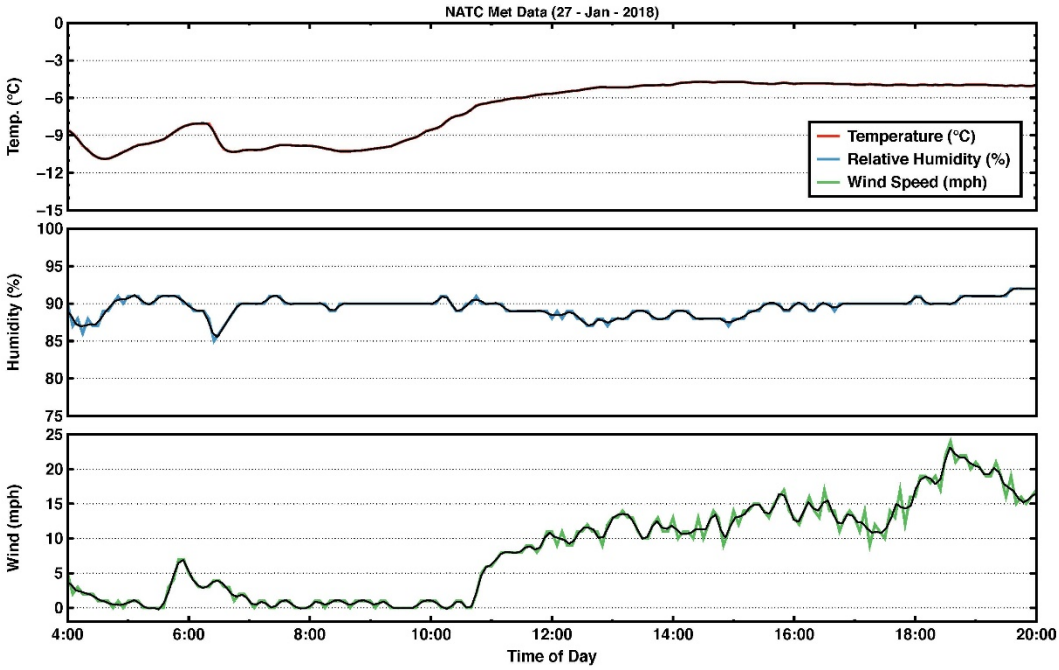


Figure C-20. Montana meteorological data for 28 January 2018.

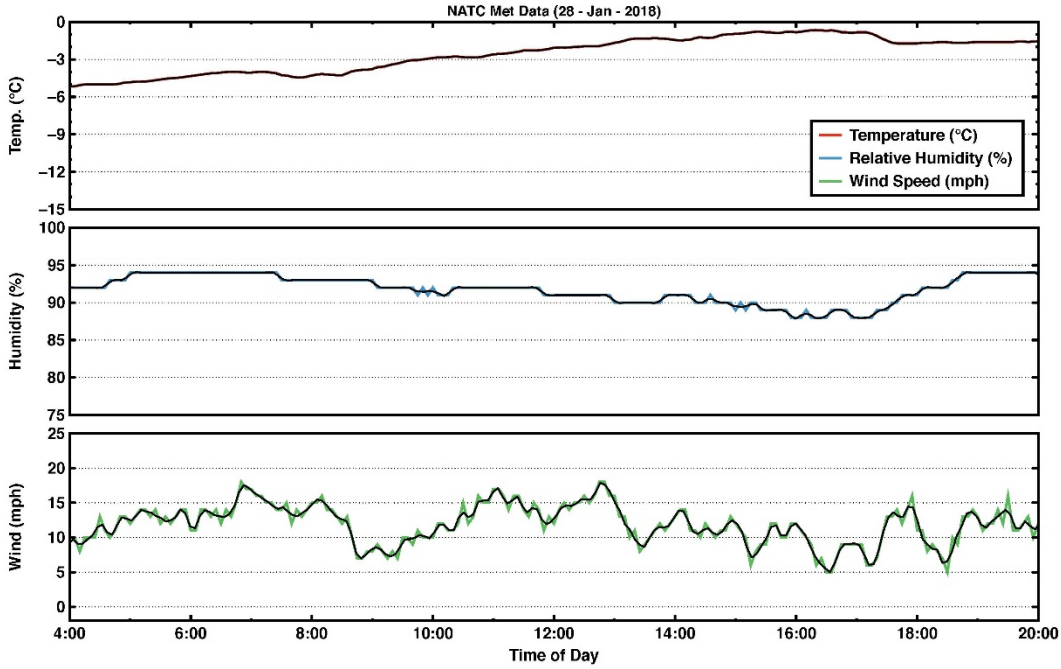


Figure C-21. Montana meteorological data for 29 January 2018.

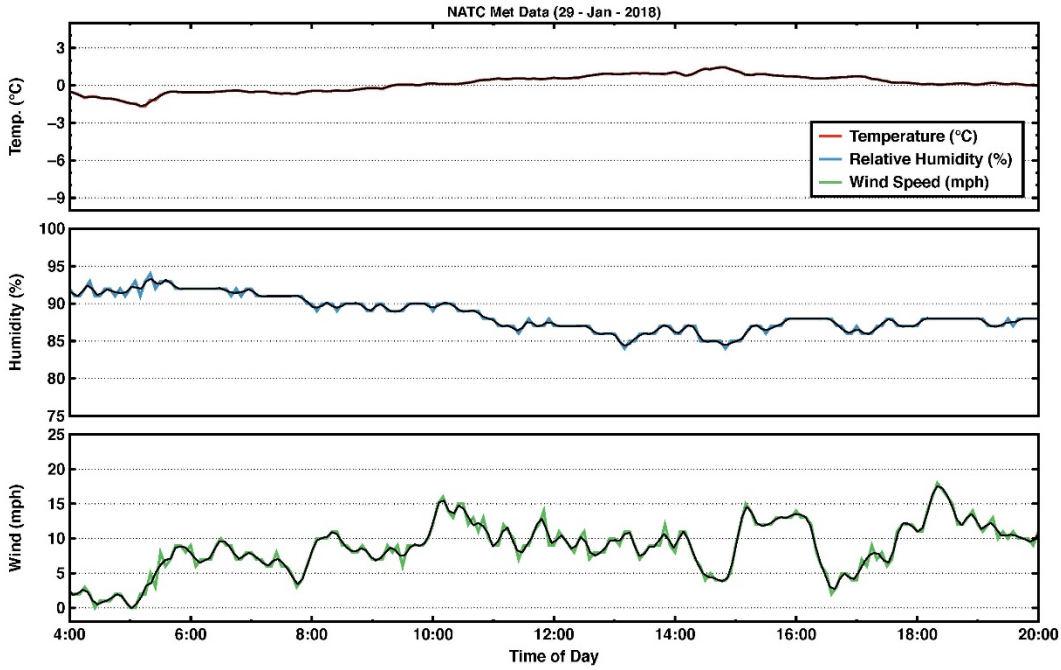


Figure C-22. Montana meteorological data for 30 January 2018.

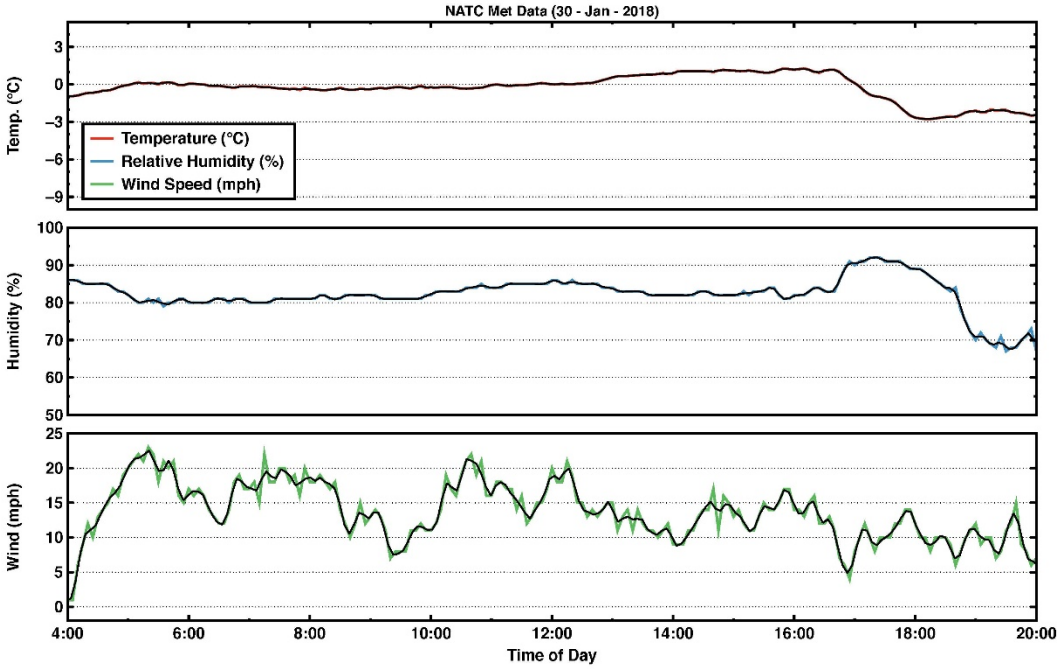


Figure C-23. Montana meteorological data for 31 January 2018.

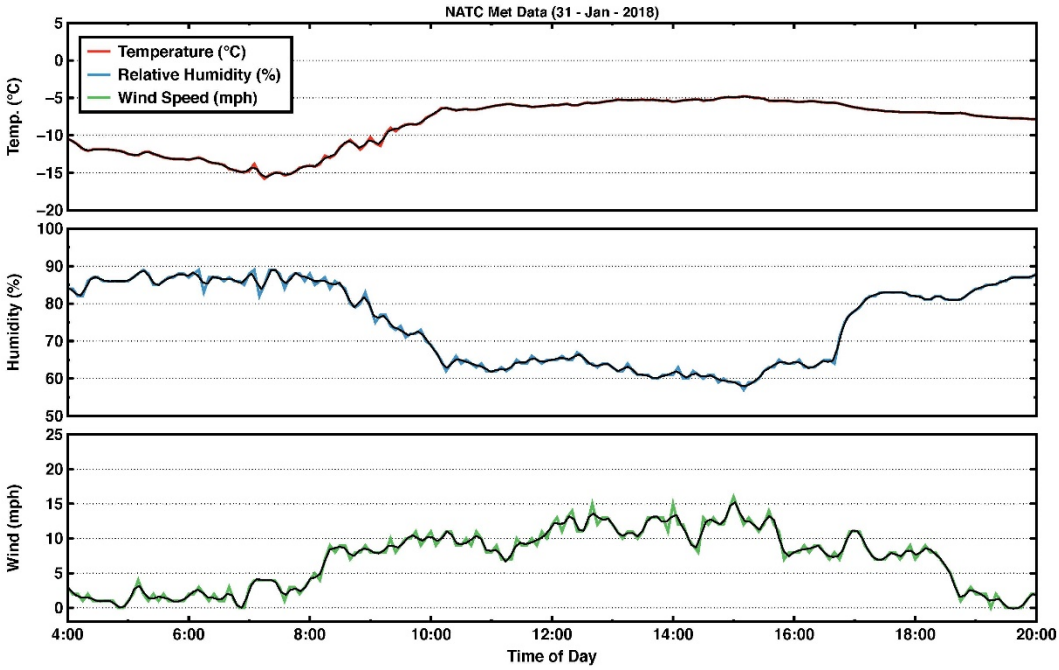


Figure C-24. Michigan meteorological data for 18 February 2018.

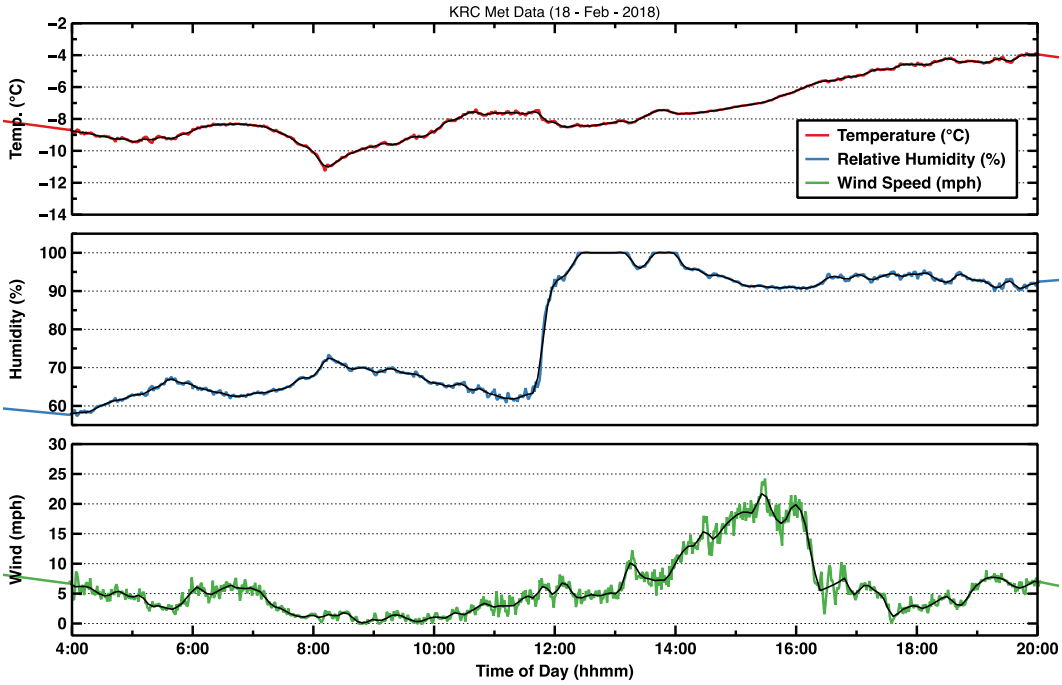


Figure C-25. Michigan meteorological data for 19 February 2018.

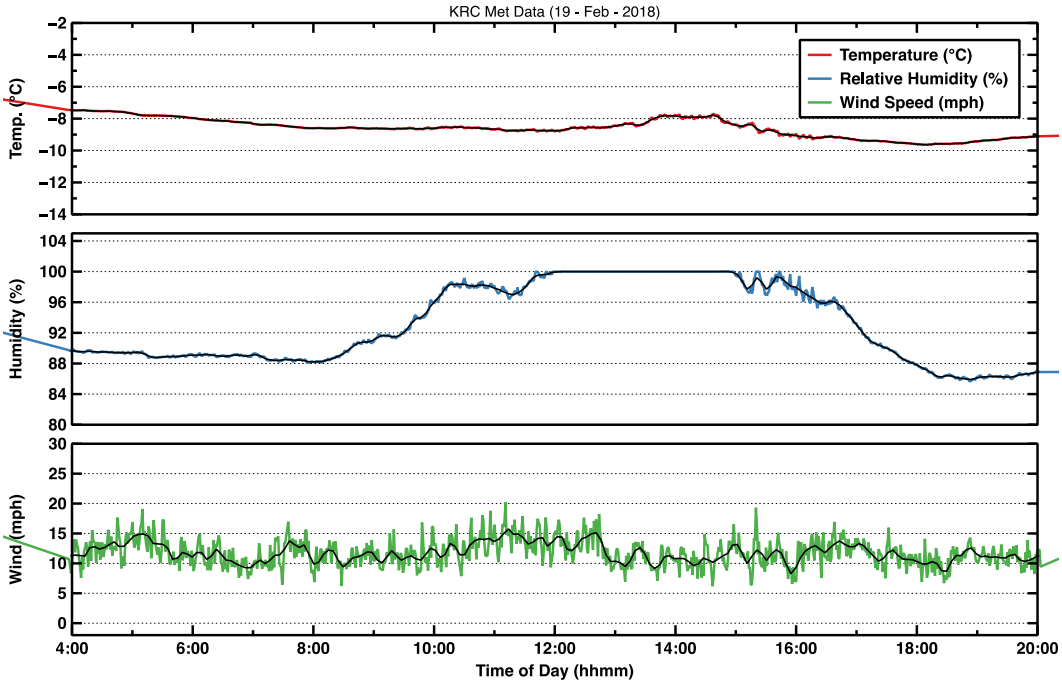


Figure C-26. Michigan meteorological data for 20 February 2018.

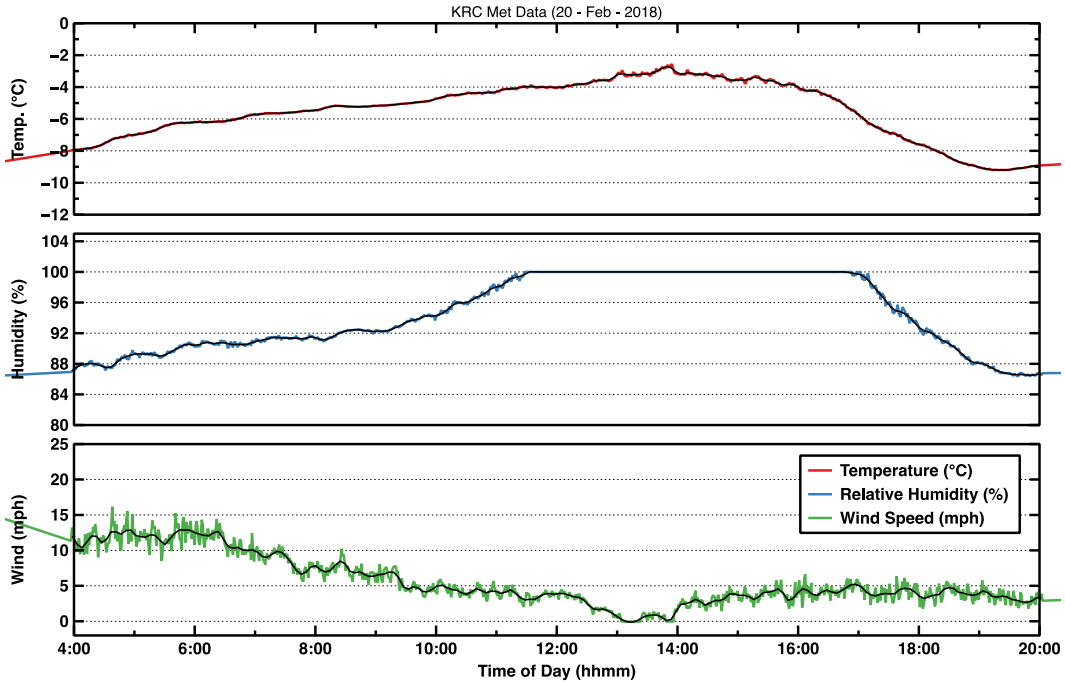


Figure C-27. Michigan meteorological data for 21 February 2018.

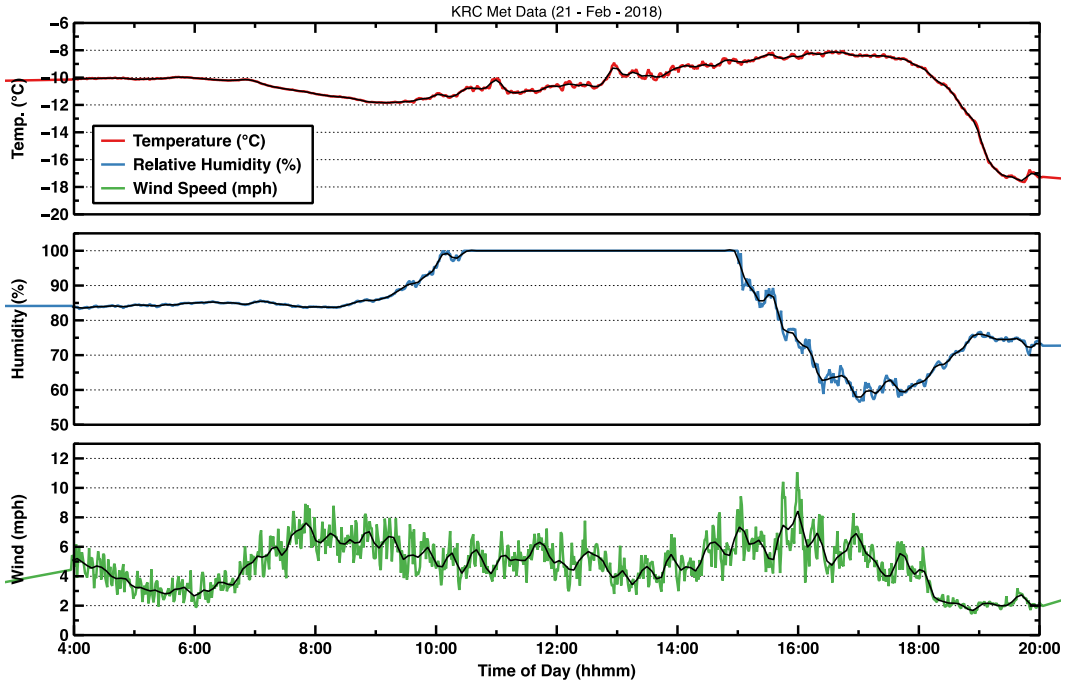


Figure C-28. Michigan meteorological data for 22 February 2018.

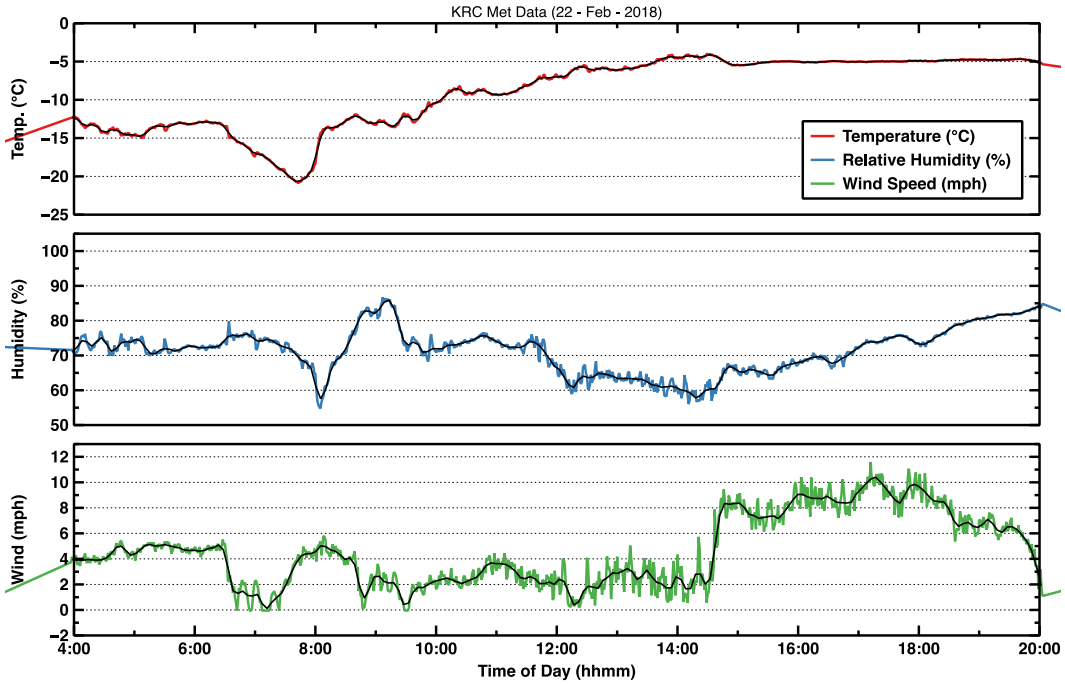
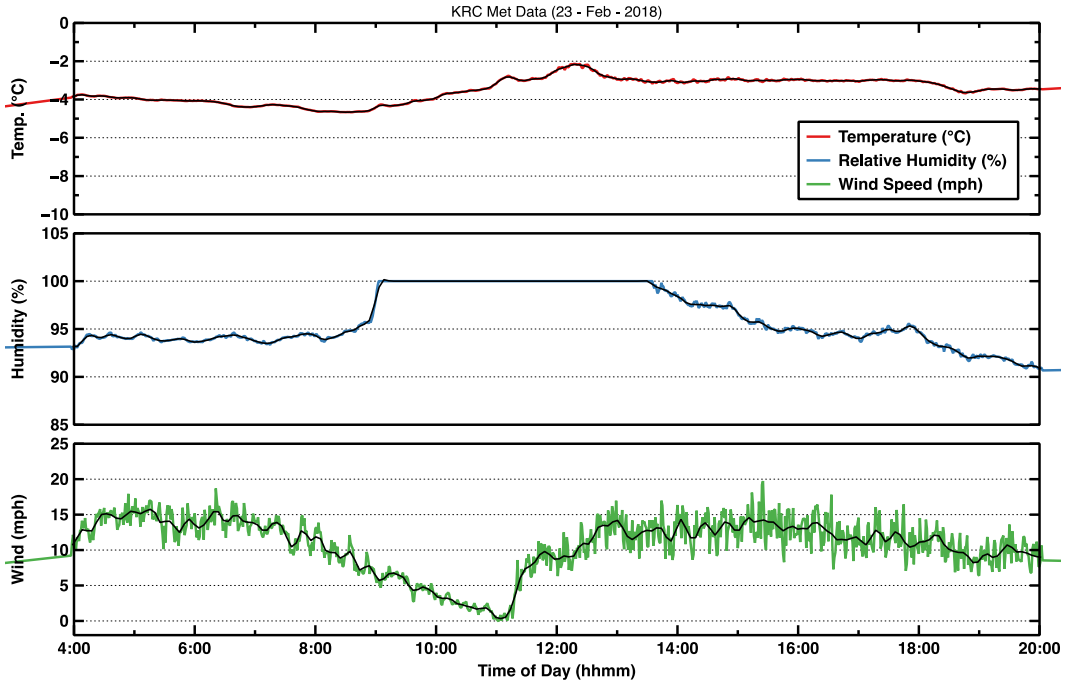


Figure C-29. Michigan meteorological data for 23 February 2018.



Appendix D: Summary of Snow Measurements by Site

Table D-1. Montana snow data summary.

Program Title	Air Temp (°C)	Snow Temp (°C)	Snow Depth (cm)	Snow Density		Yamaha Drop Cone (cm)	CTI	Shear Vane (kPa)	LWD ISM	0.5 Clegg[1]	0.5 Clegg[2]	2.25 Clegg[1]	2.25 Clegg[2]	CBR	Ram Index			RSP Index		
				Top 5 cm (g/cm³)	Average (g/cm³)										0–150 mm	150+ mm	Full Depth	0–150 mm	150+ mm	Full Depth
25RWY0	−7.7	−8.7						82		4.7	30.2	11	13.5	9.4						410
25RWY50								64		3.8	24.5	9.6	22.1							330
25RWY100								91		7.4	27.5	11.9	14.1							156
25TWY0								42		4.4		8.3	8.5							
25TWY50										9.8		7.8	18							
25TWY100	−9.7	−11.8	30					55		5		3	12.8	19						
26MLPN	−14	−17	40	0.18	0.22															
27TWYSVS	−5.3	−5.4	53	0.18	0.24												2			
27RWYSVS	−5.2	−5.4	68	0.05	0.19															
28MLPW	0.5	−0.2	62	0.11	0.21												19			
28MLPN																				
28TWYS	1.5	0.5	55	0.15	0.19															
29RWYC	0.3	−1.1									28.0		10.9	6.7						
30MLPN																	15			
31RWYC																				

[1] Measurement taken on fresh snow over a groomed snow surface.

[2] Measurement taken on groomed snow (fresh snow brushed off).

Table D-2. Michigan snow data summary.

Program Title	Air Temp (°C)	Snow Temp (°C)	Snow Depth (cm)	Snow Density		Yamaha Cone (cm)	CTI	Shear Vane (kPa)	LWD ISM	0.5 Clegg[1]	0.5 Clegg[2]	2.25 Clegg[1]	2.25 Clegg[2]	CBR	Ram Index			RSP Index		
				Top 5 cm (g/cm³)	Average (g/cm³)										0–150 mm	150+ mm	Full Depth	0–150 mm	150+ mm	Full Depth
19SU2_A	−7.8	−7.6	35				84.0	73		36.7	49.3	22.7			720	338	593	93	361	258
19SU2_B			25				78.7	55		28.4	44.3	13.6		20.9	453	194	393	36	54	44
19SU2_C			27.5	0.59			77.0	max		19.7	37.7	15.1		20.4	372	228	345	19	17	18
19SU2_D			26.5				77.0	103		22.9	37.6	15.3			344	147	330	49	32	44
19SU2_E			23				75.3	80		17.9	35.3	12.3			216	136	201	34	72	54
19SU2_F			31.5				77.0	63		21.9	42.3	22.3			417	223	360	50	67	59
19SU2VS_A	−8.4	−5.4	56	0.06	0.21	4.7														
19SU2VS_B						4.7														
19SU2VS_C						9.0														
19SU2VS_D						6.7														
19SU2VS_E	−8	−6.1	70	0.04	0.23	5.4														
20LP1WG_1			21				83.7	max		23.9	55.1	16.9	37.9	14.7				85	64	76
20LP1WG_2			24.5				79.3	max		29.3	43.5	18.6	22.6	18.7				64	154	111
20LP1WG_3							82.7	max		27.3	55.5	15.7	21.6					98	116	105
20LP1GS_4			31				81.7			21.2	45.9	15.6	18.2	18.2			762	61	40	53
20LP1GS_5	−0.4	−2.4	29	0.55			80.7			32.6	49.7	19.8	20.4	17.8				106	55	89
20LP1GS_6			29.5				83.7			19.0	43.9	18.1	21.2					104	70	91
20GPVS	−2.4	−3.1	68	0.07	0.26	4.2														
21SWP_1			19				80.7	max		24.0	51.1	21.8	19.8				1032	118	150	123
21SWP_2			22	0.34	0.28		85.3	100		32.9	45.4	20.2	25.0	24.6			878	158	33	148
21SWP_3			21.5				85.7	100		46.6	39.5	19.5	13.1	13.0			760	119	132	121
21IS_S	−9.6	−6.1	17			3.6		max												
21IS_L	−8.6	−5.3	17			3.5														
21SU1_1			28				74.2				27.2		15.4	14.5				82	92	86
21SU1_2			29				75.7				25.6		12.3	16.2				64	182	64
21GPRD_1							75.7						31.9							
21GPRD_2			67				75.7													
21GPVS						4.7														
21SU2_A2							74.0	77					15.2							
21SU2_B2							74.3	DNP												
22SU3_1			24				78.0				49.9		27.1					86	160	121

Table D-2 (cont.). Michigan snow data summary.

Program Title	Air Temp (°C)	Snow Temp (°C)	Snow Depth (cm)	Snow Density		Yamaha Cone (cm)	CTI	Shear Vane (kPa)	LWD ISM	0.5 Clegg[1]	0.5 Clegg[2]	2.25 Clegg[1]	2.25 Clegg[2]	CBR	Ram Index			RSP Index		
				Top 5 cm (g/cm³)	Average (g/cm³)										0–150 mm	150+ mm	Full Depth	0–150 mm	150+ mm	Full Depth
22SU3_2	−13.6	−15	22				84.0				49.1		27.2	13.4				114	80	101
22SU3_3			23.5				82.7				57.3		23.2	34.8				110	157	123
22SU3VS	−9	−14.5	65–91	0.19	0.28															
22SU3VS_1			76			1.9														
22SU3VS_6			74																	
22SU3VS_5			79																	
22SU3VS_3			83																	
22SU3VS_4			76																	
22SU2	−7	−9.2						DNP					17.0							
22SU3	−6	−11.1																		
22SU3_20D	−4.8	−10.1																		
22SU3_15D																				
22SU3_10D	−11.4	−5																		
22SU3_7D																				
22LP3E	−6	−11.2					75.7	DNP					22.3							
22LP3EVS	−5.3	−7.4				1.1	x													
22IR_I	−8.6	−5.3		0.19	0.21		95.3	DNP												
22IR_S	−9.6	−6.1		0.02	0.10		87.3	DNP					34.4							
22IR_AC								DNP												
22STAB_S	−6.5	−8.7					87.3						34.2							
22STAB_GI								DNP												
22VDA2_1	−6.9	−8.2					82.0	DNP					26.3							
22900C	−5.3	−8.1					87.3	DNP					37.8							
22300C	−6	−8					82.7	DNP					16.1							
22300CVS	−6	−4.6																		
22LP4	−5	−7					85.3	DNP					30.8							
22LP4VS	−4.8	−1.8				0.6														
22LP3NW	−4	−7					82.0	DNP					25.6							
22LP3NWVS	−2.6	−2.3				1.9														
22STAB_GI2								DNP												
23HQP	−2.3	−2.1	16	0.13	0.13	3.6														

[1] Measurement taken on fresh snow over a groomed snow surface.

[2] Measurement taken on groomed snow (fresh snow brushed off).

Table D-3. Montana Clegg data.

Site	Snow surface	Test	0.5 kg Clegg				2.25 kg Clegg			
			Drop 1	Drop 2	Drop 3	Drop 4	Drop 1	Drop 2	Drop 3	Drop 4
25RWY0	Fresh snow over groomed	1	1	2.5	3.5	4.7	0	6	11	17.1
25RWY50	Fresh snow over groomed	1	0.8	1.8	2.7	3.8	3.9	9.1	9.6	14.4
25RWY100	Fresh snow over groomed	1	1.4	3.6	6	7.4	5.5	9.9	11.9	14
25RWY0	Groomed	1	13.4	16.3	23.5	30.2	6.6	10.5	13.5	13.5
25RWY50	Groomed	1	6.4	12	17.4	24.5	10.7	17.6	22.1	22.6
25RWY100	Groomed	1	10.1	17.5	24.6	27.5	6.6	11.4	14.1	13.9
25TWY0	Fresh snow over Groomed	1	0.7	2	3.4	4.4	2.4	5.7	8.3	11.2
25TWY50	Fresh snow over Groomed	1	1.7	2.2	6.7	9.8	2.4	6.2	7.8	10.3
25TWY100	Fresh snow over Groomed	1	0	2.2	3.2	5	0	0	3	8.9
25TWY0	Groomed	1					5.5	7.4	8.5	11.2
25TWY50	Groomed	1					19.1	19.9	18	21
25TWY100	Groomed	1					7.4	10.3	12.8	15.7
29CRWY	Groomed	1	6.2	7.3	6.8	10.2	5.1	7.1	8.8	14.1
29CRWY	Groomed	2	8.5	14.4	16.6	21	8.8	13.7	17	19.2
29CRWY	Groomed	3	6.6	12.2	17.6	17.3	4	5.7	6.9	9.3
30CRWY_1	Groomed	1	6.8	16.6	20.9	35.2				
30CRWY_1	Groomed	2	3.4	6.5	17.5	22.6				
30CRWY_1	Groomed	3	4.7	11.6	19.6	30.5				
30CRWY_2	Groomed	1	34.8	36.9	33.8	45				
30CRWY_2	Groomed	2	14.3	23.4	28.5	33.3				
30CRWY_2	Groomed	3	14.9	24	30.8	36.8				

Table D-4. Michigan Clegg data.

Site	Snow surface	Test	0.5 kg Clegg				2.25 kg Clegg			
			Drop 1	Drop 2	Drop 3	Drop 4	Drop 1	Drop 2	Drop 3	Drop 4
19SU2_A	Fresh snow over Groomed	1	13	23.7	29	35.3	13	23.7	29	35.3
19SU2_A	Fresh snow over Groomed	2	18.9	22.1	24.6	29	18.9	22.1	24.6	29
19SU2_A	Fresh snow over Groomed	3	8.3	11.2	14.4	19.6	8.3	11.2	14.4	19.6
19SU2_B	Fresh snow over Groomed	1	11.2	14.4	11.4	13.5	11.2	14.4	11.4	13.5
19SU2_B	Fresh snow over Groomed	2	8.2	11.4	12.1	15.1	8.2	11.4	12.1	15.1
19SU2_B	Fresh snow over Groomed	3	6.6	11.6	17.4	15.7	6.6	11.6	17.4	15.7
19SU2_C	Fresh snow over Groomed	1	9.9	13.2	15.8	18.3	9.9	13.2	15.8	18.3
19SU2_C	Fresh snow over Groomed	2	6.2	14.8	17.3	21.2	6.2	14.8	17.3	21.2
19SU2_C	Fresh snow over Groomed	3	5.5	12.6	12.1	12.3	5.5	12.6	12.1	12.3
19SU2_D	Fresh snow over Groomed	1	13.9	16	16.9	17.1	13.9	16	16.9	17.1
19SU2_D	Fresh snow over Groomed	2	8.5	13.2	14.4	14.1	8.5	13.2	14.4	14.1
19SU2_D	Fresh snow over Groomed	3	9.8	13.5	14.6	15.3	9.8	13.5	14.6	15.3
19SU2_E	Fresh snow over Groomed	1	6.6	11.2	11.2	13.5	6.6	11.2	11.2	13.5
19SU2_E	Fresh snow over Groomed	2	4.1	8.2	9.9	13.7	4.1	8.2	9.9	13.7
19SU2_E	Fresh snow over Groomed	3	5.8	11.4	15.8	17.4	5.8	11.4	15.8	17.4
19SU2_F	Fresh snow over Groomed	1	11.7	18.7	21.2	22.4	11.7	18.7	21.2	22.4
19SU2_F	Fresh snow over Groomed	2	14.4	18.9	23	24.9	14.4	18.9	23	24.9
19SU2_F	Fresh snow over Groomed	3	15.1	19.4	22.6	24.4	15.1	19.4	22.6	24.4
20LP1WG_1	Fresh snow over Groomed	1	29	18.5	24.4	29.6	29	18.5	24.4	29.6
20LP1WG_1	Fresh snow over Groomed	2	8.3	10.1	13.3	18.2	8.3	10.1	13.3	18.2
20LP1WG_1	Fresh snow over Groomed	3	9.4	13.9	13	18.9	9.4	13.9	13	18.9
20LP1WG_1	Groomed	1	19.2	24.2	31.2	35.7	19.2	24.2	31.2	35.7
20LP1WG_1	Groomed	2	30.1	40.8	46.5	38.2	30.1	40.8	46.5	38.2
20LP1WG_1	Groomed	3	32.4	54.1	36	57.6	32.4	54.1	36	57.6
20LP1WG_2	Fresh snow over Groomed	1	2.6	12.4	17.1	24.2	2.6	12.4	17.1	24.2
20LP1WG_2	Fresh snow over Groomed	2	8.2	18.3	17.4	29.6	8.2	18.3	17.4	29.6
20LP1WG_2	Fresh snow over Groomed	3	11.2	17.1	21.4	26.5	11.2	17.1	21.4	26.5
20LP1WG_2	Groomed	1	15.1	18.9	20.1	22.3	15.1	18.9	20.1	22.3
20LP1WG_2	Groomed	2	21.2	21.7	22.3	21.2	21.2	21.7	22.3	21.2
20LP1WG_2	Groomed	3	17.4	20.3	25.5	29.4	17.4	20.3	25.5	29.4
20LP1WG_3	Fresh snow over Groomed	1	8.3	16.2	13.5	16.4	8.3	16.2	13.5	16.4
20LP1WG_3	Fresh snow over Groomed	2	0	13.2	15.3	19.6	0	13.2	15.3	19.6
20LP1WG_3	Fresh snow over Groomed	3	6	11.2	18.2	23	6	11.2	18.2	23
20LP1WG_3	Groomed	1	12.8	15.5	21.4	21.6	12.8	15.5	21.4	21.6
20LP1WG_3	Groomed	2	18.7	18.9	23.5	23.9	18.7	18.9	23.5	23.9
20LP1WG_3	Groomed	3	14.4	13.9	19.9	26.7	14.4	13.9	19.9	26.7
20LP1GS_4	Fresh snow over Groomed	1	3.3	7.8	10.8	14.4	3.3	7.8	10.8	14.4
20LP1GS_4	Fresh snow over Groomed	2	7.8	16	20.3	21.6	7.8	16	20.3	21.6
20LP1GS_4	Fresh snow over Groomed	3	9.1	14.2	15.7	19.4	9.1	14.2	15.7	19.4
20LP1GS_4	Groomed	1	10.5	13.7	15.8	16	10.5	13.7	15.8	16
20LP1GS_4	Groomed	2	5.5	11.4	18.7	20.7	5.5	11.4	18.7	20.7

Table D-4 (cont.). Michigan Clegg data.

Site	Snow surface	Test	0.5 kg Clegg				2.25 kg Clegg			
			Drop 1	Drop 2	Drop 3	Drop 4	Drop 1	Drop 2	Drop 3	Drop 4
20LP1GS_4	Groomed	3	15.5	18.3	20.1	25.8	15.5	18.3	20.1	25.8
20LP1GS_5	Fresh snow over Groomed	1	8.7	14.2	14.4	18.7	8.7	14.2	14.4	18.7
20LP1GS_5	Fresh snow over Groomed	2	11.4	18.3	23.7	28.3	11.4	18.3	23.7	28.3
20LP1GS_5	Fresh snow over Groomed	3	8.5	16.4	21.4	22.1	8.5	16.4	21.4	22.1
20LP1GS_5	Groomed	1	13.3	17.8	16.2	18.5	13.3	17.8	16.2	18.5
20LP1GS_5	Groomed	2	11.9	13.7	18.9	21.4	11.9	13.7	18.9	21.4
20LP1GS_5	Groomed	3	16.7	21.4	26.2	26.4	16.7	21.4	26.2	26.4
20LP1GS_6	Fresh snow over Groomed	1	9.1	14.9	20.3	22.8	9.1	14.9	20.3	22.8
20LP1GS_6	Fresh snow over Groomed	2	4.6	10.5	11.6	17.8	4.6	10.5	11.6	17.8
20LP1GS_6	Fresh snow over Groomed	3	7.6	18.3	22.4	21.9	7.6	18.3	22.4	21.9
20LP1GS_6	Groomed	1	22.6	20.3	24.4	27.3	22.6	20.3	24.4	27.3
20LP1GS_6	Groomed	2	11.2	16.4	20.1	24.1	11.2	16.4	20.1	24.1
20LP1GS_6	Groomed	3	14.8	14.2	19.2	23	14.8	14.2	19.2	23
21SWP_1	Fresh snow over Groomed	1	10.3	19.8	26.4	30.3	10.3	19.8	26.4	30.3
21SWP_1	Fresh snow over Groomed	2	16.7	18.5	22.4	25.3	16.7	18.5	22.4	25.3
21SWP_1	Fresh snow over Groomed	3	5.3	14.1	16.6	21	5.3	14.1	16.6	21
21SWP_1	Groomed	1	20.1	22.6	26.7	29.6	20.1	22.6	26.7	29.6
21SWP_1	Groomed	2	3.5	9.1	14.6	18.7	3.5	9.1	14.6	18.7
21SWP_1	Groomed	3	9.9	16.2	18.2	20.7	9.9	16.2	18.2	20.7
21SWP_2	Fresh snow over Groomed	1	9.1	15.3	19.4	19.6	9.1	15.3	19.4	19.6
21SWP_2	Fresh snow over Groomed	2	9.2	14.6	19.1	21.6	9.2	14.6	19.1	21.6
21SWP_2	Fresh snow over Groomed	3	17.4	23.5	22.1	14.8	17.4	23.5	22.1	14.8
21SWP_2	Groomed	1	20.7	25.8	28.5	33	20.7	25.8	28.5	33
21SWP_2	Groomed	2	20.1	19.4	25.3	24.4	20.1	19.4	25.3	24.4
21SWP_2	Groomed	3	13.3	20.8	21.2	26	13.3	20.8	21.2	26
21SWP_3	Fresh snow over Groomed	1	11.2	18.9	19.4	22.3	11.2	18.9	19.4	22.3
21SWP_3	Fresh snow over Groomed	2	9.1	18.5	20.7	21.6	9.1	18.5	20.7	21.6
21SWP_3	Fresh snow over Groomed	3	7.4	14.4	18.5	18.5	7.4	14.4	18.5	18.5
21SWP_3	Groomed	1	12.1	12.6	15.3	20.7	12.1	12.6	15.3	20.7
21SWP_3	Groomed	2	7.8	7.6	12.3	16.9	7.8	7.6	12.3	16.9
21SWP_3	Groomed	3	6	9.4	11.6	16.4	6	9.4	11.6	16.4
21SU1_1	Groomed	1	8.9	14.2	15.5	19.4	8.9	14.2	15.5	19.4
21SU1_1	Groomed	2	6.9	13.7	17.8	19.8	6.9	13.7	17.8	19.8
21SU1_1	Groomed	3	8.3	10.1	13	18.2	8.3	10.1	13	18.2
21SU1_2	Groomed	1	7.6	11.7	13.2	18	7.6	11.7	13.2	18
21SU1_2	Groomed	2	7.6	9.8	12.1	15.1	7.6	9.8	12.1	15.1
21SU1_2	Groomed	3	7.6	8.3	11.7	14.4	7.6	8.3	11.7	14.4
21GPRD_1	Groomed	1	31.4	29.6	26	27.3	31.4	29.6	26	27.3
21GPRD_1	Groomed	2	28.2	37.4	36.4	22.4	28.2	37.4	36.4	22.4
21GPRD_1	Groomed	3	20.7	31	33.3	31.7	20.7	31	33.3	31.7
21SU2_A2	Groomed	1	10.5	17.6	11.9	16.1	10.5	17.6	11.9	16.1

Table D-4 (cont.). Michigan Clegg data.

Site	Snow surface	Test	0.5 kg Clegg				2.25 kg Clegg			
			Drop 1	Drop 2	Drop 3	Drop 4	Drop 1	Drop 2	Drop 3	Drop 4
21SU2_A2	Groomed	2	13	15.8	18.7	21.6	13	15.8	18.7	21.6
21SU2_A2	Groomed	3	8.5	13	15.1	17.8	8.5	13	15.1	17.8
22SU3_1	Groomed	1	19.8	23.9	30.8	32.6	19.8	23.9	30.8	32.6
22SU3_1	Groomed	2	12.8	22.3	28.7	33	12.8	22.3	28.7	33
22SU3_1	Groomed	3	11.7	13.3	21.7	28	11.7	13.3	21.7	28
22SU3_2	Groomed	1	22.8	26	31.9	38.5	22.8	26	31.9	38.5
22SU3_2	Groomed	2	16.9	22.6	25.5	29.2	16.9	22.6	25.5	29.2
22SU3_2	Groomed	3	14.9	18.3	24.2	32.3	14.9	18.3	24.2	32.3
22SU3_3	Groomed	1	19.6	19.4	22.4	24.4	19.6	19.4	22.4	24.4
22SU3_3	Groomed	2	21.6	25.8	32.8	39.2	21.6	25.8	32.8	39.2
22SU3_3	Groomed	3	17.8	21.4	14.4	27.4	17.8	21.4	14.4	27.4
22SU2	Groomed	1	14.2	16.2	18.2	22.6	14.2	16.2	18.2	22.6
22SU2	Groomed	2	10.3	11.2	16	19.8	10.3	11.2	16	19.8
22SU2	Groomed	3	14.1	13	16.8	21	14.1	13	16.8	21
22LP3E	Groomed	1	16.2	26.7	28.7	36.4	16.2	26.7	28.7	36.4
22LP3E	Groomed	2	7.3	16.6	23.7	29.2	7.3	16.6	23.7	29.2
22LP3E	Groomed	3	11.6	13.3	14.6	20.3	11.6	13.3	14.6	20.3
22IR_S	Groomed	1	34.8	32.3	35.1	36.4	34.8	32.3	35.1	36.4
22IR_S	Groomed	2	29.9	32.1	33.2		29.9	32.1	33.2	
22IR_S	Groomed	3	30.5	30.1	34.9	34	30.5	30.1	34.9	34
22STAB_S	Groomed	1	26	30.1	26.9	28.7	26	30.1	26.9	28.7
22STAB_S	Groomed	2	34.8	44.8	46.2	46.7	34.8	44.8	46.2	46.7
22STAB_S	Groomed	3	33.2	30.8	29.4	27.1	33.2	30.8	29.4	27.1
22STAB_S	Rutted groomed	1	27.3	31.5	30.7	23.9	27.3	31.5	30.7	23.9
22STAB_S	Rutted groomed	2	30.1	37.3	34.2	35.8	30.1	37.3	34.2	35.8
22STAB_S	Rutted groomed	3	36	43.2	48.7	51.9	36	43.2	48.7	51.9
22VDA2	Groomed	1	13.7	15.8	17.6	16.2	13.7	15.8	17.6	16.2
22VDA2	Groomed	2	17.1	21.7	21.7	25.1	17.1	21.7	21.7	25.1
22VDA2	Groomed	3	22.1	28	39.6	37.3	22.1	28	39.6	37.3
22900C	Rutted groomed	1	32.3	32.4	37.4	43.2	32.3	32.4	37.4	43.2
22900C	Rutted groomed	2	28.2	35.7	38	43.2	28.2	35.7	38	43.2
22900C	Rutted groomed	3	35.8	34.4	38	43	35.8	34.4	38	43
22300C	Rutted groomed	1	14.2	23.3	19.2	20.5	14.2	23.3	19.2	20.5
22300C	Rutted groomed	2	11.6	16.7	13.2	18.9	11.6	16.7	13.2	18.9
22300C	Rutted groomed	3	13.7	15.7	16	18	13.7	15.7	16	18
22LP4	Groomed	1	25.8	24.2	26.9	34.2	25.8	24.2	26.9	34.2
22LP4	Groomed	2	21	26.4	32.4	36.2	21	26.4	32.4	36.2
22LP4	Groomed	3	20.3	25.5	33.2	37.4	20.3	25.5	33.2	37.4
22LP3NW	Groomed	1	19.1	21.6	26.9	34.4	19.1	21.6	26.9	34.4
22LP3NW	Groomed	2	10.7	21.7	29	31.4	10.7	21.7	29	31.4
22LP3NW	Groomed	3	0	16.7	20.8	17.8	0	16.7	20.8	17.8

Table D-5. Montana Rammsonde data.

27TWYSVS		27TWYSVS		28MLPW		28MLPW		30MLPN	
Depth (cm)	Index	Depth (cm)	Index	Depth (cm)	Index	Depth (cm)	Index	Depth (cm)	Index
19		17		47.5	3	55		23	
57	2	55	2	48	5	56	5	23	
57				49	6	57	10	24	10
				51	4	58	18	25	10
				53	4	59	18	25	
				53.5	10	60	34	27	10
				54	18	60.5	49	27.5	34
				54.5	18	61	65	28	49
				55	34	61.5	23	29	18
				55				31	11
								35	8
								40	6
								42	6
								43	7
								44	12
								46	12
								47	12
								48	12

Table D-6. Michigan Rammsonde data.

19SU2_A		19SU2_B		19SU2_C		19SU2_D		19SU2_E	
Depth (cm)	Index	Depth (cm)	Index	Depth (cm)	Index	Depth (cm)	Index	Depth (cm)	Index
−2	119	19	119	0	119	0	119	1	119
0	119	34	213	1	213	0.5	400	2	213
0				2	400	3	325	2	NA
1	400	34	213	2	NA	4	775	3	213
1.5	1150	124	775	4	400	5.5	410	4	400
2	1525	244	1525	5	775	7	310	6	160
4	1431	184	460	6	310	9	235	7	310
7	510	184	460	7	460	10	460	8.5	210
10	510	124	194	8	460	11	287	10	210
16	162	244	381	8	NA	12	287	11	194
18	241	124	194	10	310	13	287	12	194
19	475	124	194	11	381	14	287	13	194
20	475	124	194	12	381	15	287	14	194
		124	194	13	381	17	147	15	194
				15	241			16	194
				16	45			17	21
				17	475			18	194

Table D-7. Additional Michigan Rammsonde data.

19SU2_F		22SU3VS		21SWP_1		21SWP_2		21SWP_3		20LP1GS_4	
Depth (cm)	Index	Depth (cm)	Index	Depth (cm)	Index	Depth (cm)	Index	Depth (cm)	Index	Depth (cm)	Index
2	119	29.5	7	34	213	−1.5	213	2	119	−1.5	150
3	213	30	6	34	213	−1	400	3	400	0	275
3	NA	30	NA	64	400	0	400	4	400	1	400
4	775	30	NA	124	775	1	400	4.5	775	2	400
5	775	30	NA	184	1150	1.25	1525	4.75	2275	2	NA
6	310	30	NA	184	1150	2	1525	6	370	2.5	1900
6.5	610	31	26	244	1525	3	1150	7	460	4	1275
7	910	31	NA	124	775	4	775	8	910	5	2837
8.5	310	31.5	34	244	1525	5	1525	9	760	6	760
10	310	32	34	304	1900	6	610	10	1135	7	760
11	287	32.5	34	304	1900	7	1135			8	760
13	194	33	42	304	760					9	760
15	194	33.5	50	455	1135					10	760
16	381	34	50							11.5	319
19	131	49	4							13	319
22	28	50	3							14	45
24	194	52	14							15	475
25	381	54.5	21								
		56	23								
		57.5	13								
		59	13								
		60	18								
		61	18								
		62	18								
		63	18								
		64	18								
		65.5	13								
		67.5	10								
		69	13								
		70	18								
		71	18								
		72	26								
		74	14								
		75	26								
		77	14								
		78.5	18								
		86	6								

Table D-8. Montana Russian Snow Penetrometer data.

25RWY0		25RWY50		25RWY100	
Depth (mm)	Index	Depth (mm)	Index	Depth (mm)	Index
20	2	30	59	15	2
70	19	50	44	25	87
90	44	70	87	40	59
100	87	75	514	60	44
105	1708	90	229	75	59
115	599	100	428	90	59
		110	428	100	87
		115	855	105	855

Table D-9. Michigan Russian Snow Penetrometer data.

19SU2_A		19SU2_B		19SU2_C		19SU2_D		19SU2_E		19SU2_F		20LP1WG_1	
Depth (mm)	Index	Depth (mm)	Index	Depth (mm)	Index	Depth (mm)	Index	Depth (mm)	Index	Depth (mm)	Index	Depth (mm)	Index
20	3	50	21	45	45	20	3	20	3	20	3	20	3
23	297	60	18	60	60	55	19	55	19	50	21	45	23
40	55	75	62	75	75	70	62	75	47	55	179	55	91
49	101	105	33	85	85	80	91	100	38	100	23	60	179
70	45	125	47	105	105	95	62	120	47	125	38	70	91
75	179	150	38	120	120	110	62	140	47	150	38	80	179
90	62	175	38	130	130	130	47	155	62	170	47	90	91
115	38	200	38	150	150	170	25	175	47	200	33	105	62
130	62	225	38	165	165	200	33	200	38	230	33	115	91
140	91	240	62	180	180	225	38	220	47	250	47	140	38
155	62	250	91	205	205			230	91	265	62	165	38
175	47			225	225			255	38	270	179	180	62
200	38			235	235			260	179			195	62
225	38											215	47
230	179											250	28
232	443											280	33
235	297											285	179
236	883												
240	443												
251	163												
260	492												
275	297												
280	883												
290	443												
315	179												
320	883												

Table D-10. Additional Michigan Russian Snow Penetrometer data.

20LP1WG_2		20LP1WG_3		20LP1GS_4		20LP1GS_5		20LP1GS_6		21SWP_1		21SWP_2		21SWP_3		21SU1_1		21SU1_2	
Depth (mm)	Index	Depth (mm)	index	Depth (mm)	Index	Depth (mm)	Index	Depth (mm)	Index	Depth (mm)	Index	Depth (mm)	Index	Depth (mm)	Index	Depth (mm)	Index	Depth (mm)	Index
30	33	10	3	20	3	25	38	35	28	20	47	25	38	25	38	40	25	20	47
50	47	25	38	50	21	40	62	40	179	30	91	40	62	40	62	50	91	30	91
60	91	45	47	55	179	50	91	50	91	40	91	50	91	50	91	55	179	75	23
75	62	50	179	100	23	55	179	55	179	50	91	55	179	65	62	75	47	85	91
95	47	60	91	125	38	60	179	60	179	55	179	60	355	70	179	80	179	100	62
105	91	75	62	150	38	70	91	70	91	60	179	65	355	75	179	100	47	120	47
125	47	80	179	170	47	75	179	75	179	65	179	70	355	80	179	120	47	135	62
135	91	85	179	200	33	80	179	100	38	75	91	80	179	85	179	145	38	145	91
160	38	90	179	230	33	90	91	125	38	85	91	100	47	90	179	160	62	155	91
170	91	100	91	250	47	100	91	150	38	100	62	120	47	100	91	190	33	170	62
175	179	115	62	265	62	120	47	170	47	105	179	150	33	110	91	215	38	185	62
180	179	130	62	270	179	145	38	185	62	120	62	180	33	115	179	230	62	205	47
185	179	155	38			165	47	205	47	125	179			125	91	235	179	230	38
190	179	170	62			180	62	230	38	135	91			140	62	240	179	240	91
195	179	180	91			205	38	250	47	145	91			165	38			245	179
200	179	190	91			220	62	255	179	150	179			170	179			246	883
205	179	205	62			235	62			160	91			175	179				
		225	47			250	62			165	179								
		235	91							170	179								
		237	443																

Table D-11. Further Michigan Russian Snow Penetrometer data.

21SU1_3		22SU3_1		22SU3_2		22SU3_3	
Depth (mm)	Index	Depth (mm)	Index	Depth (mm)	Index	Depth (mm)	Index
40	25	25	74	25	38	20	47
50	91	40	121	30	355	25	179
60	91	50	91	35	179	30	179
75	62	60	179	50	62	35	179
110	28	80	91	60	91	45	91
135	38	110	33	80	47	50	179
150	62	125	62	110	33	55	179
155	179	150	38	125	62	75	47
165	91	170	47	130	179	95	47
175	91	175	179	140	91	115	47
180	179	180	179	155	62	140	38
200	47	185	179	175	47	155	62
215	62	190	179	200	38	185	33
230	62	195	179	215	62	190	179
240	91	200	179	225	91	195	355
248	113			230	179		
250	443						

Appendix E: Comparison of Snow Moisture and Density Measurement Techniques (Student Intern Poster)

Methods for Measuring Snow Moisture and Density

Mary Feyrer, Jackie Balch, Bruce Elder, and Sally Shoop
Point of contact information: Sally Shoop / Sally.A.Shoop@usace.army.mil
Author contact information: Mary Feyrer / mcf85@cornell.edu

US Army Corps of Engineers® BUILDING STRONG®

ERDC Engineer Research and Development Center

Objective

- Determine the accuracy and reliability of the Finnish Snowfork by comparing the density and moisture data it collects to moisture data from Denoth meters and sample densities.
- Compare different Denoth meters used by CRREL to each other in order to ensure that they are producing similar results

Conclusion

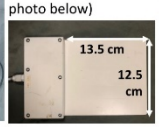
- The Finnish fork is a reliable tool for measuring the moisture content of snow
- Denoths can sometimes produce negative moistures, in particular in dry snow
- The Finnish fork consistently reports densities that are lower than the recorded sample density
- Finnish fork densities are generally reliable in dry snow but become inaccurate in wet snow
- The five Denoths we tested report similar moisture values

Comparison of Moisture and Density Measurement Methods from the Field

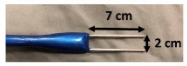
Moisture and density profiles were measured in snowpits using a Finnish Fork and Denoth meters to measure moisture and the Finnish Fork and LaChappelle cutters to measure density



The Denoth meters measure moisture 1.5 cm above and below the flat plate that is inserted into the snow (see photo below)



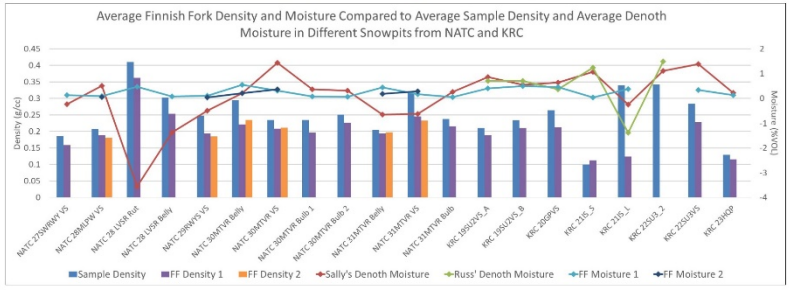
The snowfork only measures the snow between its tines.





Statistics

- Sample density and snowfork density are not statistically equivalent (T-Test, p = 0.00043)
- Sample density is on average 0.0368 g/cc greater than the snowfork density
- Moisture measured by the snowfork and by the denoth are not statistically equivalent (Wilcoxon rank test, p = 0.001)
- Denoth moisture values are on average 0.0539 %Vol higher than the Finnish fork moisture, and 0.236 %Vol higher when negative moisture values are rounded to 0
- Russ's and Sally's denoth are statistically equivalent (Wilcoxon rank test, p = 0.73)



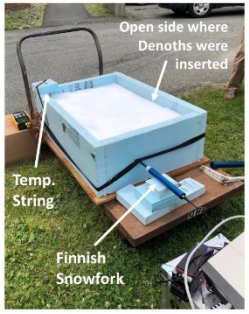
Acknowledgements: Samuel Beal, Lauren Farnsworth, John Fegyveresi, and Zoe Courville
Funding was provided by ERDC Military Engineering Program on Remote Assessment of Infrastructure for Ensured Maneuver (RAFTER) Boreal Aspects of Ensured Maneuver (BAEM)

Denoth and Snowfork Comparison Test in Melting Snow

Objective: Test the calibration of CRREL's five Denoths by comparing them to each other and to the Finnish Snowfork at varying moisture levels

Setup: Denoth and snowfork sensors were tested in a snowbox of sieved snow which was placed outside and left to melt for five hours.

Data Collected: Temperature, Moisture from 5 Denoth meters, Moisture and Density from the Finnish Snowfork, Sample Density, Data from 3 De Roo Snow Sensors, 3 Mirco-CT Scans



The snow box setup

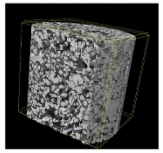


A Denoth meter being inserted into the open side of the snow box

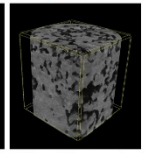


Uncovered snowfork at the end of the experiment

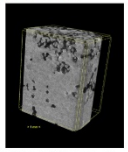
Change in snow throughout the experiment



Micro-CT scan at 9:55 – start of experiment

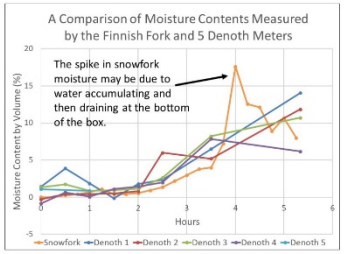


Micro-CT scan at 12:05

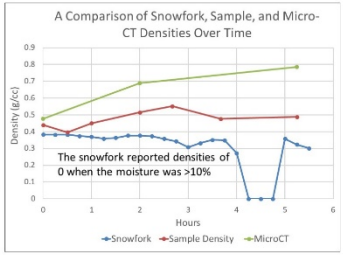


Micro-CT scan at 15:00 – end of experiment

Results of Comparison Test



- The measurements from the five Denoths follow each other relatively closely
- The snowfork moisture measurement is consistently lower than the Denoths', most likely due to the snowfork being position in the middle of the box and the Denoth measurements being taken at the edge
- The last measurement with Denoth 4 was taken in a different location in the box than the other Denoths



- Densities measured by the Micro-CT are significantly greater then the sample densities
- Densities measured by the Snowfork are significantly less than the sample densities
- The accuracy of the Snowfork density measurements went down considerably in wet snow conditions.

INNOVATIVE SOLUTIONS for a safer, better world

Research supported by the US Army Corps of Engineers, Engineer Research and Development Center. The views expressed are those of the authors and do not reflect the official policy or position of the Department of the Army, Department of Defense, or the U.S. Government.

www.erdc.usace.army.mil

Appendix F: WV2 and WV3 Data Concurrent with Michigan Field Campaign

Figure F-1. WorldView-2 reflectance spectra averaged by study area.

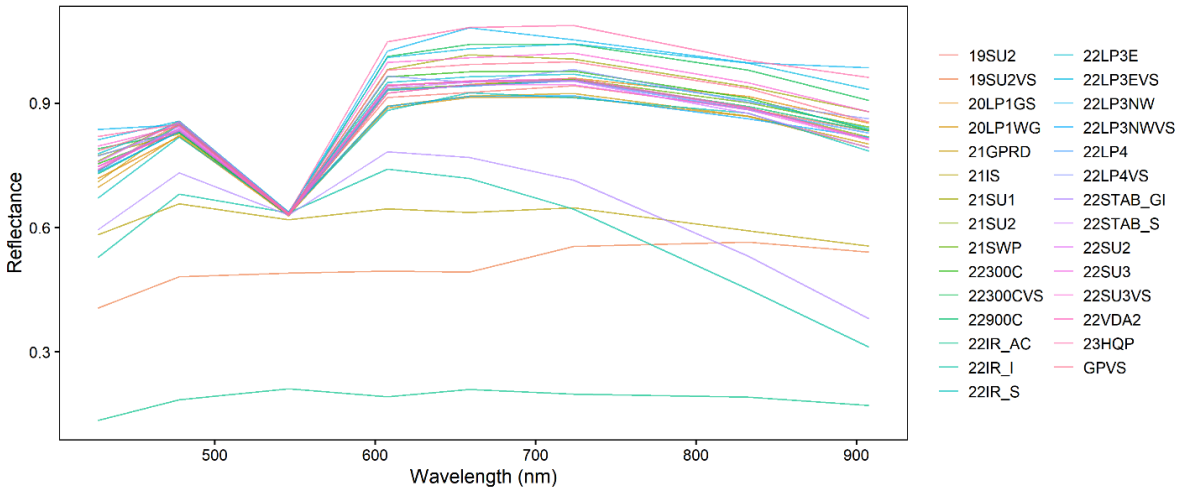


Figure F-2. WorldView-2 reflectance spectra averaged by subgrade.

Figure F-3. WorldView-3 reflectance spectra averaged by study area.

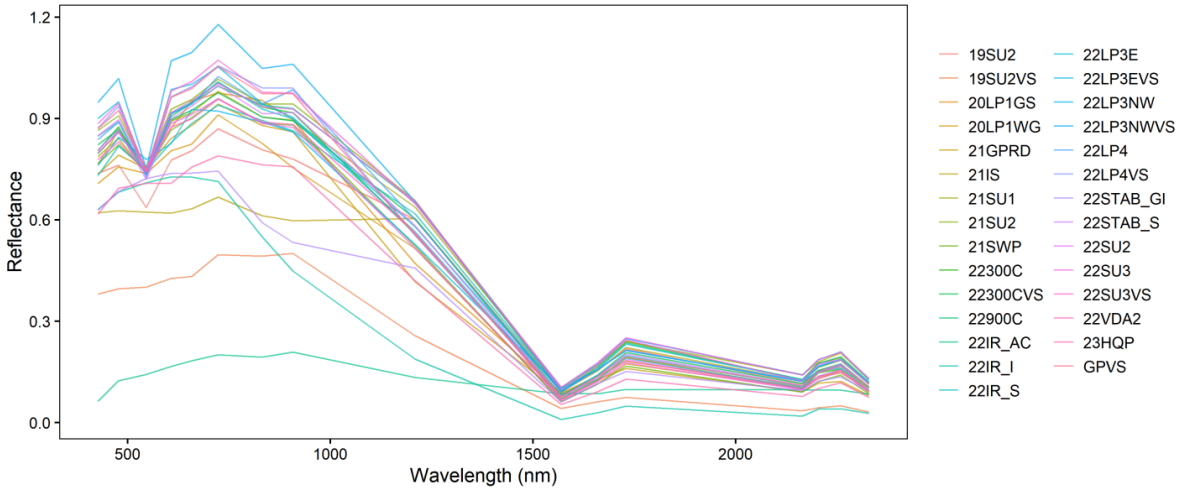


Figure F-4. WorldView-3 reflectance spectra averaged by snow surface type.

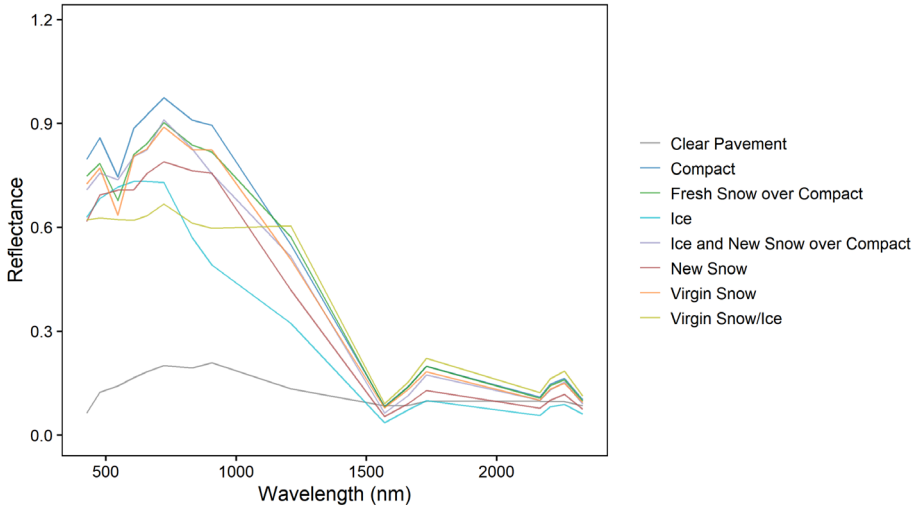
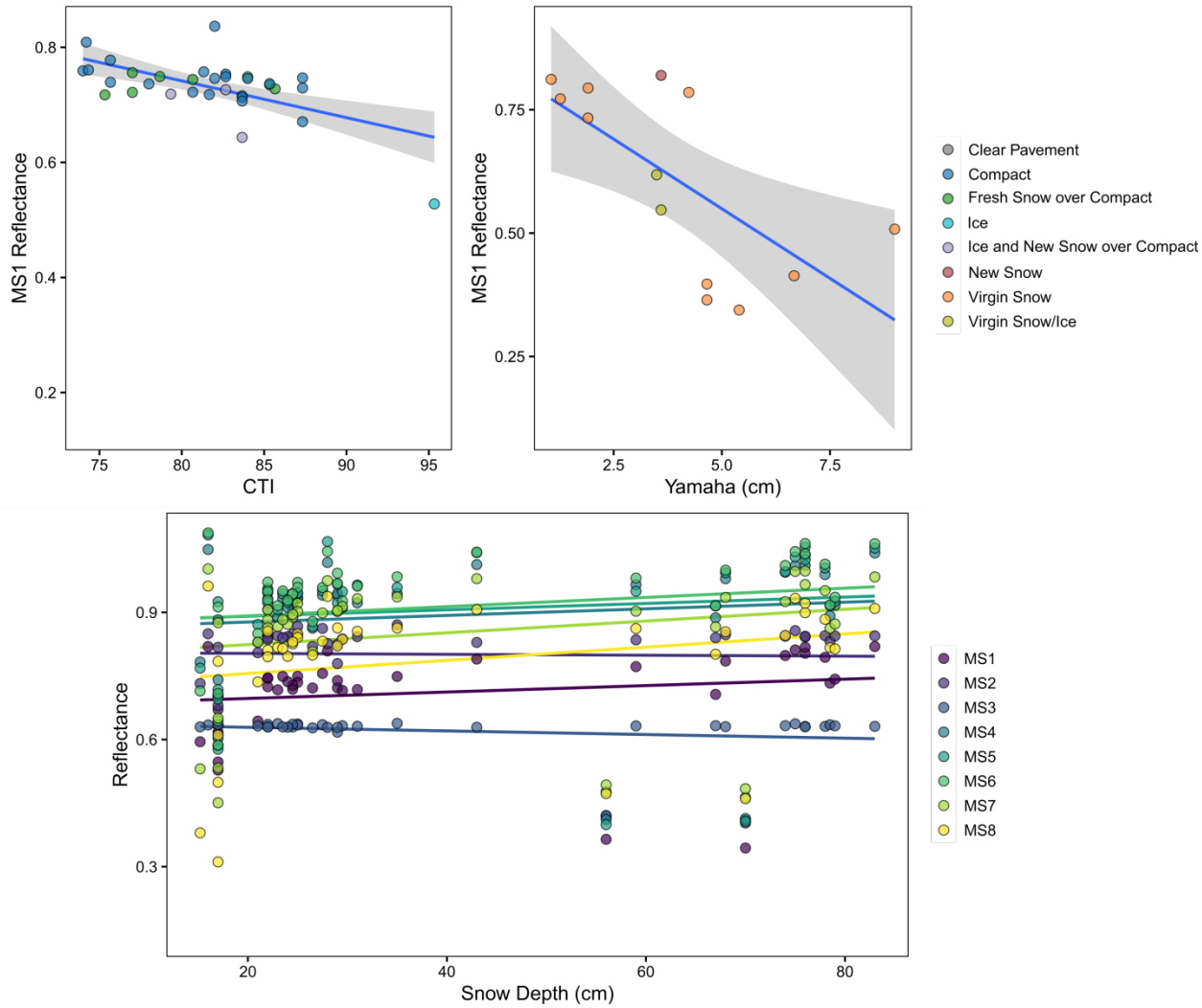


Figure F-5. WorldView-3 reflectance spectra averaged by subgrade.

Table F-1. Spearman correlations between WorldView-2 multispectral bands and snow mechanical measurements (Michigan). The *p*-values are indicated as * <0.05, ** <0.01, and *** <0.001.

Mechanical Measurement	Spearman's Rho							
	WorldView-2 Band							
	MS1	MS2	MS3	MS4	MS5	MS6	MS7	MS8
CTI	−0.453**	−0.211	0.136	−0.382*	−0.311	−0.342	−0.237	−0.251
Ram 0–15 cm	0.133	0.133	−0.183	0.517	0.617	0.600	0.533	0.650
Ram 15+ cm	−0.029	0.714	0.486	0.086	0.086	0.029	0.029	0.029
Ram Full	−0.176	0.248	0.115	0.103	0.176	0.164	0.115	0.200
RSP 0–15 cm	0.014	0.020	0.028	0.141	0.058	0.084	0.061	0.086
RSP 15+ cm	0.204	0.045	−0.044	0.220	0.195	0.130	0.068	−0.081
RSP Full	0.179	0.157	0.056	0.316	0.247	0.235	0.170	0.077
0.5 kg Clegg	0.193	0.142	0.039	0.027	−0.142	0.011	−0.161	−0.204
2.25 kg Clegg	−0.213	−0.101	0.011	−0.194	−0.218	−0.223	−0.317	−0.329
Yamaha	−0.711**	−0.683*	−0.449	−0.667*	−0.623*	−0.631*	−0.601*	−0.634*
Shear Vane	−0.036	−0.649	−0.714*	−0.429	−0.429	−0.571	−0.571	−0.714
CBR	0.189	0.291	0.273	0.154	0.238	0.210	0.112	0.112
LWD LL1 Average	0.293	0.015	−0.017	0.321*	0.307*	0.120	−0.006	−0.127
LWD LL2 Average	0.253	0.034	0.020	0.267	0.245	0.055	−0.078	−0.186
LWD LL3 Average	0.317	0.088	0.026	0.255	0.245	0.040	−0.044	−0.138
LWD LL4 Average	0.408*	0.156	0.093	0.364*	0.338	0.145	0.055	−0.034
LWD LL1 Representative	0.275	0.021	−0.022	0.291	0.265	0.102	−0.036	−0.103
LWD LL2 Representative	0.263	0.010	−0.056	0.267	0.244	0.075	−0.058	−0.127
LWD LL3 Representative	0.358	0.114	0.050	0.307	0.295	0.099	0.026	−0.036
LWD LL4 Representative	0.353	0.069	−0.030	0.299	0.281	0.114	0.024	−0.026
Density 0–5 cm	0.430	0.467	0.236	0.430	0.321	0.430	0.345	0.406
Density Average	0.167	0.119	−0.500	0.190	0.190	0.167	0.238	0.238
Snow Depth	0.444**	0.245	−0.080	0.426**	0.402*	0.428**	0.424**	0.461**
Air Temp	0.462*	0.356*	0.058	0.527**	0.418*	0.578**	0.515**	0.608***
Snow Temp	−0.119	−0.417*	−0.086	−0.032	−0.188	0.014	−0.046	0.075

Figure F-6. Plots of significant ($p < 0.01$) Spearman correlations between WorldView-2 multispectral bands (MS1–MS8) and snow strength measurements, with linear regression models (Michigan data set).



Appendix G: Surface-Condition Photos and Michigan Cloud-Cover Photos for Field Spectrometer (ASD) Data Collection

Photos G-1 through G-6 depict examples of the surfaces at the ASD measurement points. The five general surfaces sampled were asphalt concrete, groomed snow, ice, groomed snow with ruts and tracks, and virgin snow, as plotted in Figure 39 for the Michigan sites. ASD testing in Montana was limited due to weather and other factors.

Figure G-1. Montana ice lane (Montana point 28IL).



Figure G-2. Asphalt concrete pavement at Ice Rink (Michigan point 22IR_AC) both wet and dry conditions.



Figure G-3. Michigan groomed snow points 22SU3 (*top*) and 22SU2 (*bottom*).



Figure G-4. Michigan smooth ice surface point 22IR_I (*top*) and grooved ice surface point 22STAB_GI (*bottom*).



Figure G-5. Michigan rutted snow surface point 22900C (*top*) and tracked snow surface point 22LP3NW (*bottom*).



Figure G-6. Michigan virgin snow points 22SU3VS (*top*) and 22300CVS (*bottom*).



Photos G-7 through G-9 depict the changing cloud cover during the ASD testing on 22 February 2018 in Michigan.

Figure G-7. Cirrostratus cloud cover at the beginning of ASD testing (9:43 local time).



Figure G-8. Cirrostratus and altostratus cloud cover at noon during ASD testing.



Figure G-9. Altocumulus cloud cover at the end ASD testing (~16:30 local time).



REPORT DOCUMENTATION PAGE

Form Approved
OMB No. 0704-0188

Public reporting burden for this collection of information is estimated to average 1 hour per response, including the time for reviewing instructions, searching existing data sources, gathering and maintaining the data needed, and completing and reviewing this collection of information. Send comments regarding this burden estimate or any other aspect of this collection of information, including suggestions for reducing this burden to Department of Defense, Washington Headquarters Services, Directorate for Information Operations and Reports (0704-0188), 1215 Jefferson Davis Highway, Suite 1204, Arlington, VA 22202-4302. Respondents should be aware that notwithstanding any other provision of law, no person shall be subject to any penalty for failing to comply with a collection of information if it does not display a currently valid OMB control number. **PLEASE DO NOT RETURN YOUR FORM TO THE ABOVE ADDRESS.**

1. REPORT DATE *(DD-MM-YYYY)*	**2. REPORT TYPE**	**3. DATES COVERED** *(From - To)*
August 2019	Technical Report/Final	

4. TITLE AND SUBTITLE

Assessment of Field Methods for Measuring Mechanical Properties of Snow

5a. CONTRACT NUMBER

5b. GRANT NUMBER

5c. PROGRAM ELEMENT NUMBER

6. AUTHOR(S)

Sally A. Shoop, Wendy L. Wieder, Bruce C. Elder, Samuel A. Beal, and Elias J. Deeb

5d. PROJECT NUMBER
465395 & 471941

5e. TASK NUMBER

5f. WORK UNIT NUMBER

7. PERFORMING ORGANIZATION NAME(S) AND ADDRESS(ES)

U.S. Army Engineer Research and Development Center (ERDC)
Cold Regions Research and Engineering Laboratory (CRREL)
72 Lyme Road
Hanover, NH 03755-1290

8. PERFORMING ORGANIZATION REPORT NUMBER

ERDC/CRREL TR-19-17

9. SPONSORING / MONITORING AGENCY NAME(S) AND ADDRESS(ES)

Assistant Secretary of the Army for Acquisition, Logistics, and Technology
103 Army Pentagon
Washington, DC 20314-1000

10. SPONSOR/MONITOR'S ACRONYM(S)
ASA(ALT)

11. SPONSOR/MONITOR'S REPORT NUMBER(S)

12. DISTRIBUTION / AVAILABILITY STATEMENT

Approved for public release; distribution is unlimited.

13. SUPPLEMENTARY NOTES

ERDC 6.2 Boreal Aspects of Ensured Maneuver (BAEM)

14. ABSTRACT

Winter climates present a variety of surfaces that challenge vehicle mobility. Surfaces range from soft, virgin snow, to groomed snow and ice. This study evaluated the capabilities of various testing devices to measure the mechanical properties of winter surfaces. Concurrent satellite imagery supplemented in situ physical testing. The goals were (1) to find tests that most practically evaluate these winter surfaces for vehicle mobility and (2) to determine if imagery analysis correlates with mechanical properties, thus potentially allowing remote assessment of snow physical and mechanical characteristics.

The test methods were typically useful for either virgin snow or groomed snow; no method worked well on all surfaces. Correlations between test devices were generally poor, but there were some important trends identified between (1) tests that measure the near-surface snow strength, (2) tests best suited for stronger snow, (3) the Clegg Impact Hammers and California Bearing Ratio, and (4) the optical imagery and surface drop cones. This study provides a rich dataset for assessing the current state of the art and future research needs for measurement and remote assessment of snow mechanical properties for vehicle mobility prediction.

15. SUBJECT TERMS
Bearing capacity, Mechanical properties, Remote sensing, Snow, Snow mechanics, Snow--Testing, Strength, Trafficability, Vehicle mobility

16. SECURITY CLASSIFICATION OF:			**17. LIMITATION OF ABSTRACT**	**18. NUMBER OF PAGES**	**19a. NAME OF RESPONSIBLE PERSON**
a. REPORT	**b. ABSTRACT**	**c. THIS PAGE**			**19b. TELEPHONE NUMBER** *(include area code)*
Unclassified	Unclassified	Unclassified	SAR	148	